جامعة الإمارات العربية المتحدة
United Arab Emirates University

MASTER THESIS NO. 2023: 65

College of Engineering

Department of Mechanical and Aerospace Engineering

A NUMERICAL INVESTIGATION REALIZING THE FLOW STRUCTURE AND HEAT TRANSFER PERFORMANCE OF THE POTENTIAL IMPINGING JETS

Mohammed Sami Uddin Khan

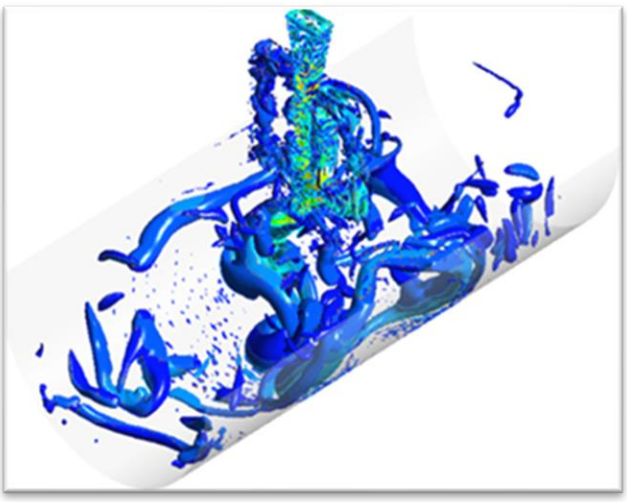

September 2023

United Arab Emirates University

College of Engineering

Department of Mechanical and Aerospace Engineering

A NUMERICAL INVESTIGATION REALIZING THE FLOW STRUCTURE AND HEAT TRANSFER PERFORMANCE OF THE POTENTIAL IMPINGING JETS

Mohammed Sami Uddin Khan

This thesis is submitted in partial fulfilment of the requirements for the degree of Master of Science in Mechanical Engineering

September 2023

United Arab Emirates University Master Thesis
2023: 65

Cover: Iso-surface of Q-criterion for Chevroned Sweeping Jet

(Photo: By Mohammed Sami Uddin Khan)

Print: University Print Service, UAEU 2023

Declaration of Original Work

I, Mohammed Sami Uddin Khan, the undersigned, a graduate student at the United Arab Emirates University (UAEU), and the author of this thesis entitled "*A Numerical Investigation Realizing the Flow Structure and Heat Transfer Performance of the Potential Impinging Jets*", hereby, solemnly declare that this is the original research work done by me under the supervision of Prof. Emad Elnajjar, in the College of Engineering at UAEU. This work has not previously formed the basis for the award of any academic degree, diploma or a similar title at this or any other university. Any materials borrowed from other sources (whether published or unpublished) and relied upon or included in my thesis have been properly cited and acknowledged in accordance with appropriate academic conventions. I further declare that there is no potential conflict of interest with respect to the research, data collection, authorship, presentation and/or publication of this thesis.

Student's Signature: 

Date: September 1st, 2023

Advisory Committee

1) Advisor: Emad Elnajjar

Title: Professor

Department of Mechanical and Aerospace Engineering

College of Engineering, United Arab Emirates University

2) Co-advisor: Mohammad O. Hamdan

Title: Professor

Department of Mechanical Engineering

College of Engineering, American University of Sharjah

3) Co-advisor: Salahaddin Al Omari

Title: Professor

Department of Mechanical and Aerospace Engineering

College of Engineering, United Arab Emirates University

Approval of the Master Thesis

This Master Thesis is approved by the following Examining Committee Members:

1) Advisor (Committee Chair): Emad Elnajjar
   Title: Professor
   Department of Mechanical and Aerospace Engineering
   College of Engineering
   Signature _____ Date: September 4th,2023

2) Member: Fadi Alnaimat
   Title: Associate Professor
   Department of Mechanical and Aerospace Engineering
   College of Engineering
   Signature _____ Date: September 4th,2023

3) Member (External Examiner): Awad Bin Saud AlQuaity
   Title: Assistant Professor
   Department of Mechanical Engineering
   Institution: King Fahd University of Petroleum and Minerals, Saudi Arabia
   Signature _____ Date: September 4th, 2023

This Master Thesis is accepted by:

Dean of the College of Engineering: Professor Mohamed Al-Marzouqi

Signature 

Date September 08, 2023

Dean of the College of Graduate Studies: Professor Ali Al-Marzouqi

Signature 

Date September 08, 2023

Abstract

The demand for improvement in the performance of gas turbines has led to the consideration of flows at increasingly high temperatures, but this introduces challenges in terms of maintaining their structural integrity and preventing overheating. To respond to these challenges, gas turbine manufacturers have turned to internal cooling, and jet impingement provides an effective solution for cooling the leading edge of the blades of gas turbines. In this study, the author numerically simulated the cooling performance of the leading edge of the blades of a gas turbine under constant heat flux by using five configurations of jet impingement: a steady jet, a sweeping jet, a swirling jet, a Chevroned Steady jet, and a Chevroned Sweeping jet. Fluidic oscillators are known for their sweeping behavior and expansive coverage of the cooling surface while swirling jet owing to spiral geometry add tangential velocity component to the fluid which combines with the axial velocity component that generates enhanced momentum transfer area. On other hand by chevron attachment at exit of the nozzle are known to excite the jet downstream by forming coherent vortical structures that increase turbulence and, thus, promote the rates of mixing and heat transfer. These potential jets are compared at stationary and rotatory conditions (3000, 10000, 15000 rpm's) and results showed that at the stationary condition Chevroned Sweeping jet outperformed the steady jet configurations owing to oscillating jet impingement and a higher intensity of turbulence that increased the entrainment of jet flow. Under the configuration involving a Chevroned Sweeping jet, the target surface recorded an average Nusselt number that was 19.23% higher than that with a steady jet without chevrons, along with more uniform distributions of the temperature and the Nusselt number due to oscillations of the sweeping jet and higher turbulence at the exit of the nozzle with chevrons. While for rotation case sweeping jet performed the best as chevroned nozzles due to higher disturbance generated high recirculation regions leading to hotspots formation while swirling jet performed worse of all as swirling strength was negatively impacted due to rotatory motion. It can be concluded that the addition of chevrons and swirling angle improved heat transfer rate for sweeping and steady jet. However, upon rotation sweeping jet predominantly captures the best performance amongst all the jets.

Keywords: Gas turbine blade, Impingement cooling, SST k-ω model, Sweeping jet, Fluidic oscillator.

Title and Abstract (in Arabic)

بحث رقمي لدراسة اشكال التدفق الهوائي وأداء نقل الحرارة للنفاثات الضاربة

الملخص

أدى الطلب على تحسين أداء التوربينات الغازية إلى النظر في التدفقات عند درجات حرارة عالية بشكل متزايد، ولكن هذا يطرح تحديات من حيث الحفاظ على سلامتها الهيكلية ومنع ارتفاع درجة الحرارة. للاستجابة لهذه التحديات، تحول مصنعو توربينات الغاز إلى التبريد الداخلي، ويوفر الاصطدام النفاث حلاً فعالاً لتبريد الحافة الأمامية لشفرات التوربينات الغازية. في هذه الدراسة، قام المؤلف بمحاكاة أداء التبريد للحافة الأمامية لشفرات التوربينات الغازية في ظل تدفق حراري ثابت باستخدام خمسة تكوينات من الاصطدام النفاث: نفاثة ثابتة، ونفاثة كاسحة، ونفاثة دوامة، ونفاثة ثابتة ذات رؤوس مدببة.، ونفاثة كاسحة ذات أداء عالي. تشتهر مذبذبات السوائل بسلوكها الكاسح والتغطية الواسعة لسطح التبريد أثناء الدوران النفاث بسبب الهندسة الحلزونية التي تضيف مكون سرعة عرضية للسائل الذي يتحد مع مكون السرعة المحورية الذي يولد منطقة نقل زخم محسّنة. من ناحية أخرى، من خلال ربط رؤوس مدببة عند الخروج من الفوهة، من المعروف أنه يثير النفاث في اتجاه مجرى التيار من خلال تشكيل هياكل دوامة متماسكة تزيد من الاضطراب، وبالتالي تعزز معدلات الاختلاط ونقل الحرارة. تمت مقارنة هذه النفاثات المحتملة في ظروف ثابتة ودورانية (3000، 10000، 15000 دورة في الدقيقة) وأظهرت النتائج أنه في الحالة الثابتة، تفوقت نفاثة الكنس ذات رؤوس مدببة على التكوينات النفاثة الثابتة بسبب الاصطدام النفاث المتذبذب وارتفاع شدة الاضطراب الذي أدى إلى زيادة استيعاب التدفق النفاث. في ظل التكوين الذي يتضمن نفاثة كنس ذات رؤوس مدببة، سجل السطح المستهدف متوسط رقم نسلت أعلى بنسبة 19.23٪ من ذلك مع نفاثة ثابتة بدون رؤوس مدببة، إلى جانب توزيعات أكثر انتظامًا لدرجة الحرارة ورقم نسلت بسبب اهتزازات النفاثة الكاسحة. واضطراب أعلى عند خروج الفوهة برؤوس مدببة. بينما كان أداء كنس النفاثة النفاث الأفضل بالنسبة لحالة الدوران هو الأفضل حيث أدت الفوهات المزودة بشيفرات بسبب الاضطراب العالي إلى إنشاء مناطق إعادة تدوير عالية تؤدي إلى تكوين النقاط الساخنة بينما كان أداء الدوامات النفاثة أسوأ من كل ذلك حيث تأثرت قوة الدوران سلبًا بسبب الحركة الدورانية. يمكن الاستنتاج أن إضافة رؤوس مدببة وزاوية الدوران أدت إلى تحسين معدل نقل الحرارة للنفاث الكاسح والثابت. ومع ذلك، عند الدوران، تلتقط نفاثة تجتاح في الغالب أفضل أداء بين جميع الطائرات.

مفاهيم البحث الرئيسية: ريش توربينات الغازية، تبريد الاصطدامي، طراز SST k-ω ، نفاثة كنس ، مذبذب مائع.

Author Profile

Mohammed Sami Uddin Khan is currently working as a Research Assistant at the United Arab Emirates University (UAE) for 1.5 years. After graduating, he has worked as CFD (Computational Fluid Dynamics) engineer specializing in Computational Combustion in India. He received his bachelor's degree in mechanical engineering from the Osmania University, India.

Acknowledgments

Firstly, I would like to praise Allah the Almighty, the Most Gracious, and the Most Merciful for his everlasting support throughout the journey of completing this Master's thesis. May Allah’s peace and blessings be upon his final Prophet Muhammad (peace be up on him), his family and his companions. I would like to express my heartfelt gratitude to Prof. Emad Elnajjar for his unwavering support, excellent feedback, and insightful meetings. His expertise, humbleness, and dedication were pivotal in completion of this research work. I extend my appreciation to Prof. Mohammad O. Hamdan and Prof. Salahaddin Al Omari who promptly guided us with their feedbacks creating a supportive learning environment deepening the understanding of subject. My deepest gratitude goes to these co-authors and scholars whose reviews and collaboration for journal publications helped me shape my thesis. I am thankful to all my friends particularly my fellow colleague Eng. Mohammed Qasem and dear friend Eng. Abubakar Khan for their encouragement and belief in my skills who rightly provided any kind of support throughout my master’s work and I’m grateful for their willingness to provide their time and knowledge. Also, I am obliged to the United Arab Emirates University for providing with the facilities and opportunities necessary to conduct research and appreciative of the Lab engineer’s assistance during the tenure. Lastly, my deepest gratitude goes to my dear family for the enduring support throughout my life.

Dedication

To my beloved parents, adored wife, dear sister, wonderful in laws, all my dedicated teachers and family

Table of Contents

List of Tables

List of Figures

List of Abbreviations

3D	Three Dimension
CFD	Computational Fluid Dynamics
LE	Leading-Edge
SST	Shear Stress Transport

List of Symbols

A	Area
D	Diameter of Impinging Jet
d	Leading-Edge Diameter
K	Kelvin
k	Turbulent Kinetic Energy
L	Length
$\dot{m}$	Mass Flow Rate
R	Gas Constant
Re	Reynolds Number
Roj	Jet Rotation Number, Roj = (Ω . dj / vj)
RPM	Rotation Per Minute
T	Temperature
v	Velocity

Greek Symbols

θ	Twist Angle
μ	Molecular Viscosity
μ_t	Turbulent Viscosity
ρ	Density
σ	Stress Transport

Γ_k	Effective Diffusivity of k
Γ_ω	Effective Diffusivity of ω
ω	Dissipation

Chapter 1: Introduction

1.1 Overview

Gas turbines offer efficient and reliable energy conversion that play a significant role in sectors such as land-based power generation and aircraft propulsion along with other industrial applications. A continuous demand for higher power generation has led to the development of advanced gas turbines operating at higher pressure and temperatures. This meant that the material structure of these turbines had to advance parallelly in order to meet the standards required to withstand such high temperatures. Although the material used for gas turbines has improved over the years still efficient cooling plays a pivotal role in maintaining the structural integrity of gas turbines. From the cooling of components related to gas turbines, cooling of the leading edge of gas turbine blades is critical as it experiences the highest heat flux due to its proximity to the combustor. Traditionally, the cooling technique of internal jet impingement is employed to cool the front edge of a blade. This is because it is effective in achieving a high rate of heat transfer, as it allows the cooling air to be directed straight onto the heated surface [1,2] along with its compact design especially considering that the leading-edge blade is subjected to rotation.

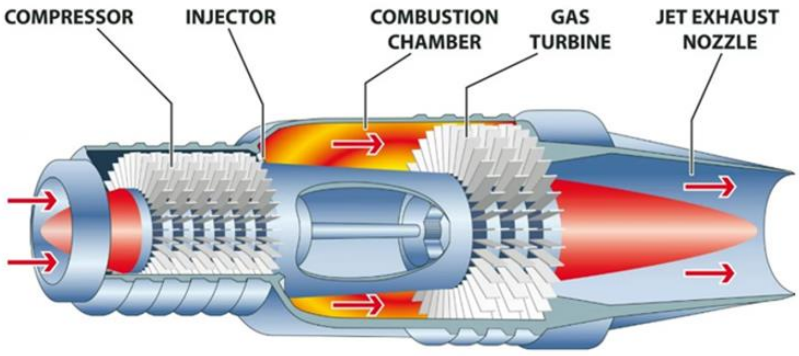

Figure 1: Working principle of gas turbine [2]

1.2 Problem Statement

Traditionally, the leading edge of a gas turbine blade has been cooled using constant impinging nozzles due to their capability to achieve high rates of heat transfer. These nozzles offer localized cooling and allow for the reuse of coolant. However, the

cooling effectiveness of continuous jet impingement declines as one moves away from the stagnation point. This decrease in efficiency results from the quadratic decrease in flow velocity as distance from the stagnation point increases. This causes the formation of a thick boundary layer over the uncooled region, negatively impacting heat transfer. To address this challenge, the study proposes an innovative approach involving chaotic and more turbulent impinging downstream flow from the nozzle. The research primarily focuses on the design and evaluation of different contoured nozzles that can produce a more turbulent impingement effect compared to steady nozzles. This enhanced turbulence is expected to provide greater cooling coverage over the blade surface. The core objective of this thesis is to conduct a comprehensive numerical investigation that aims to compare various impinging jet configurations. The study will delve into understanding the distinct flow characteristics of these jets, ultimately leading to a detailed understanding of their respective heat transfer performances.

1.3 Research Objectives

Jet impingement symbolizes epitome of efficient cooling method over a gas turbine blade. As the study focuses on increasing its efficiency further by replacing the steady impinging jet by promising contoured impinging jets as per the literature, the primary objective of this thesis will be to realize the potential of sweeping jet, swirling jets and chevroned jets over the conventional steady jets on a leading-edge turbine blade by performing a comparative study focusing on understanding the fluidic behavior of each jet. The study will be mainly analyzing the vortex behavior along with shredding and paring of each jet respectively which will lead to a better understanding of heat transfer performance of each jet on how they interact with target surface in removal of high heat fluxes immediately and effectively from the target surface. The secondary aim of this study is also to study how blade rotation affects the cooling capabilities of each jet. As turbine blades operate in a rotating environment, it is important to understand the effect of rotation on each jet to realize their potential in actual working conditions. Furthermore, jet to target distance, jet length, crossflow, different Reynolds number, sweeping angle for sweeping jet etc., influence the impact of impingement cooling performance. However, as this thesis will set a foundation for further research on

various promising contoured impinging jets, the influence of these parameters is beyond the scope of this study. The thesis will be a numerical investigation using ANSYS 20.0 following successful validation over the same case, the numerical study is preferred over the experimental investigation here as the level of intricate fluid details can be best understood through CFD analysis via an Unsteady RANS SST k-ω model.

1.4 Relevant Literature

Advanced gas turbines currently operate at high temperatures (~2000 K) to generate high power output. As the use of turbines with increased efficiency has become essential due to an increase in the demand for power, the only possibility for achieving this feat is by raising the turbine inlet temperature (TIT). Effective turbine blade cooling is significant as it aids in achieving a higher TIT by keeping in check with the metallurgical boundary limitations of the turbine blade material. To cool the blades, air is sucked from the engine's compressor. This extraction of air influences the thermal efficiency and therefore, it is important to comprehend and improve the cooling method of gas turbine which is conventionally performed utilizing both internal and external cooling techniques.

1.4.1 Internal Cooling Technique

The internal cooling approach involves channeling cooling air extracted from the compressor stages into a network of serpentine channels. According to the amount of heat transmission required in the blade’s region (leading edge, middle portion and trailing edge) the internal cooling can be divided into three primary sections [3,4]. Impingement, Pin-fin, Rib turbulated cooling etc. are a few different methods of internal cooling.

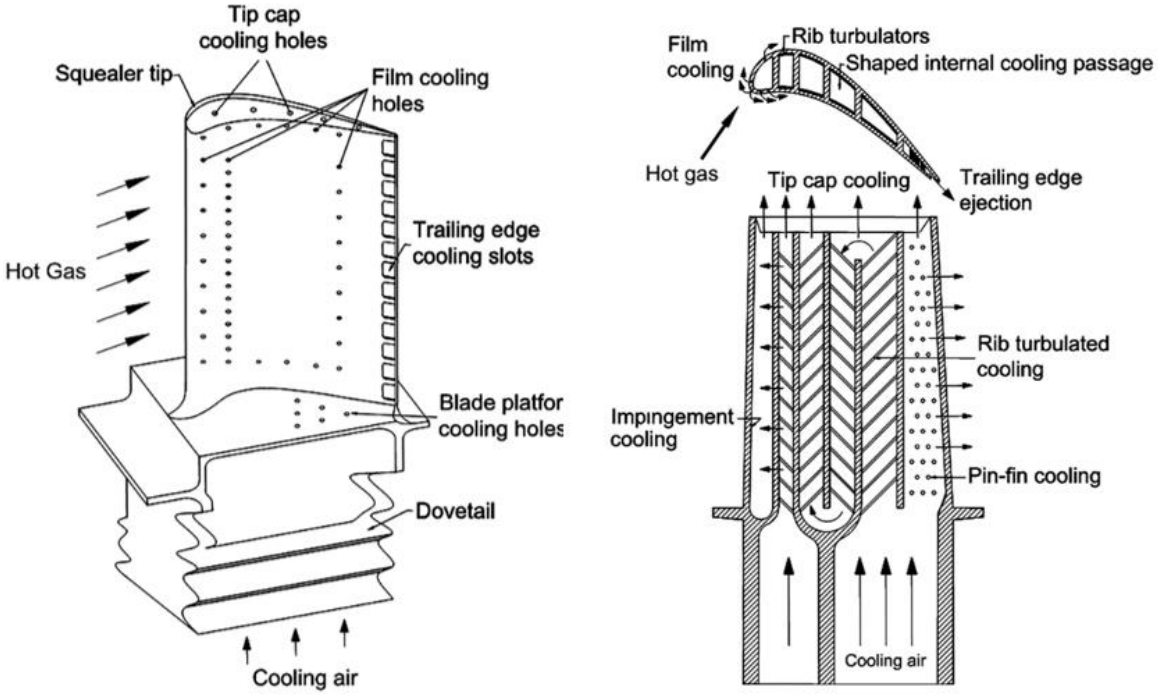

Figure 2: Different cooling methods employed for gas turbine blades [4]

1.4.1.1 Impingement Cooling

Owing to the manufacturing complexity of the leading-edge blade, serpentine channels cannot be installed and jet impingement technique considering its simple structure and the unstable moving stagnation flow generated by the impinging jets can remove high heat load significantly which fits it aptly into this segment. This method involves directing cooling fluid onto the target surface by forcing it through small diameter nozzles that generates a high-velocity cooling fluid impinging on the hot target surface and effectively cools it down by development of a thin boundary layer enhancing the heat transfer as depicted in the Figure 3. A highly chaotic flow is generated as the downstream impinging flow has higher mass flow rate than ambient surroundings inducing a higher entrainment of the cooling fluid. Upon impingement over the target surface generates a stagnation region at the striking point and this region due to lower convection effects and no velocity spreads within a specified boundary [4].

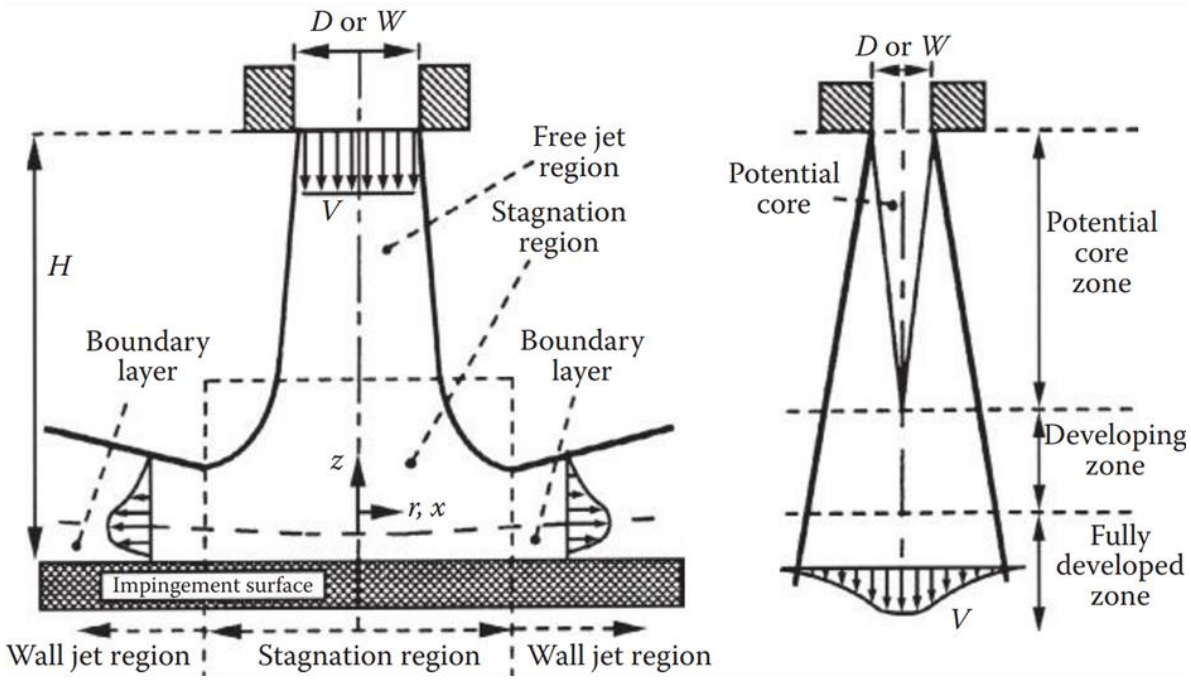

Figure 3: Flow development along the downstream of impinging jet [4]

1.4.1.2 Pin Fin Cooling

Pin fins are utilized to enhance the efficiency of heat transfer by enlarging the interface between the cooling fluid and the heat-receiving surface. These cylindrical pins, protruding from the surface, find applications in cooling electronic components, compact heat exchangers, and gas turbines [5]. Internal cooling channel with a pin fin corresponds to a channel fabricated with array of cylindrical fins. As the flow downstream hits the pin, development of stagnation region near the front surface of pins is observed followed by acceleration before separation. This unsteady flow separation is responsible for the shredding phenomenon of fluid leading to horseshoe vortex formation [6] at the end wall near the pin front producing high shear stress regions resulting in high heat transfer rates. This type of cooling is affected by the pattern arrangement (in-line, staggered) of fins, number of fins and pin shape.

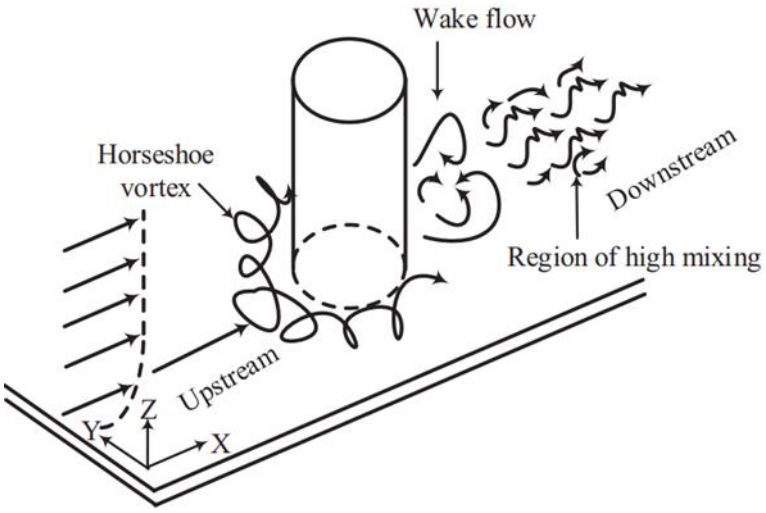

Figure 4: Flow development along the downstream of pin-fin cooling [6]

1.4.1.3 Rib Turbulator Cooling

Rib turbulators increase the heat transfer rates like pin fins by increasing the surface contact area between cooling fluid and heated surface. Serpentine channels contain ribs that result in flow separation at the upper part of the rib. Subsequently, the flow reattaches, enhancing flow turbulence.

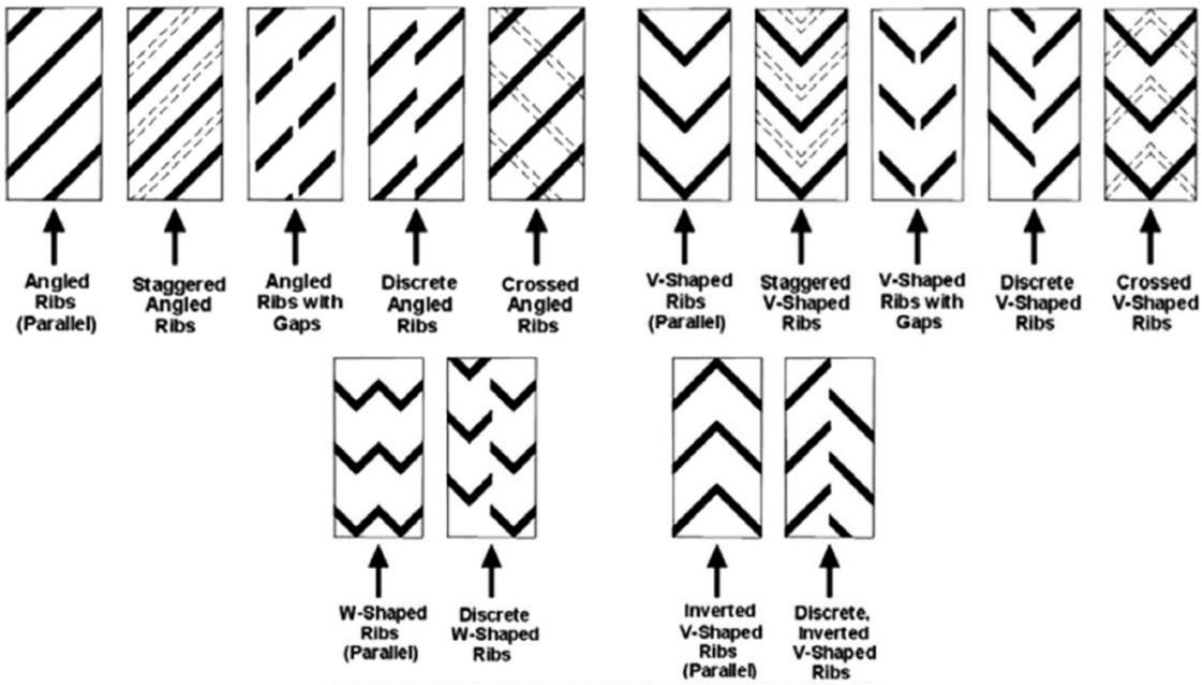

Figure 5: Flow downstream along the ribs of different configurations [7]

This cooling method is commonly favored close to the blade's trailing edge due to spatial constraints in that area. There are various shapes of installing a rib turbulator in the trailing edge as shown in Figure 5 [7]. However, studies have shown that V-shaped ribs outperform angled ribs in given flow conditions [8,9].

1.4.2 External (Film) Cooling

Film cooling provides efficient heat transfer between the cooling fluid and a heated solid surface by forced convection majorly. Here, cooling fluid i.e., extracted from the compressor, is then injected at a certain angle through tiny holes that are drilled in surface of blade as shown in Figure 6. In this manner, a slender layer of comparably cooler air is formed, providing a shield to the blade against the heat of external gases. The introduced air ascends and exits through specific holes that have been incorporated into the surface. The flow pattern wherein interaction of cooling fluid and ambient air generates horse-shoe vortex near the jet exit alike in pin-fin cooling and an addition counter rotating vortex pair is also formed along the crossflow. Efficiency of film cooling is dependent on configuration of hole, inclination angle of it along with blowing ratio [10].

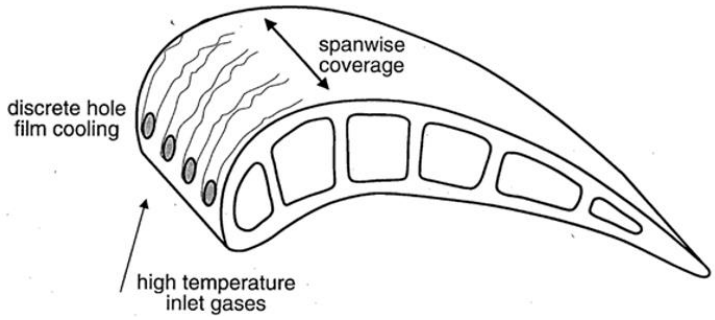

Figure 6: Film cooling over gas turbine blade [10]

1.4.3 Jet Impingement Technique

As we have already discussed that leading-edge blade has fabrication restraints due to its structure complexity. Jet impingement technique has resulted as one of the efficient cooling methods owing to its uncomplicated geometry that fits in effectively as an internal cooling system for leading-edge blade displayed in Figure 7 [11]. With reference to section 1.4.1.1, it is well understood that impingement technique leaves the

jet-nozzle with a high velocity generating a thin boundary layer resulting in high turbulent region near the stagnation area.

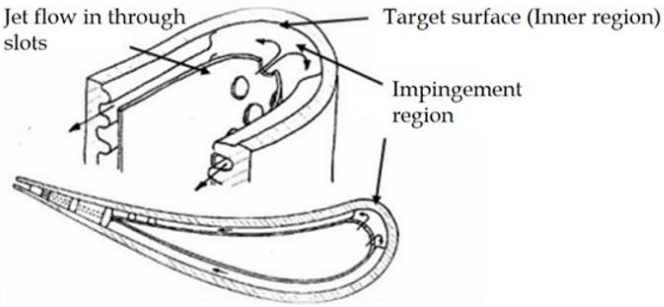

Figure 7: Slot jet Impingement Cooling in Leading Edge of Turbine Blade [11]

In quest to increase the heat transfer rate related to jet impingement technique studies have focused on excitation of jets as the flow characteristics and heat transfer of impinging jets can be controlled by managing vortices that are formed due to Kelvin Helmholtz instabilities which eventually merge in the developing region at the target surface by using active or passive means. These detailed studies involving increment of heat transfer performance have been much focused on performing investigations on jet hydraulic diameter (d_j), Reynolds number (Re_j), target surface roughness and geometry of it (concave, flat, circular), jet to target distance (l/d_j), blade rotation [-]. However, in recent years, studies have been focusing on the impact of jet nozzle geometry on heat transfer performance of jet impingement that have been quite successful. A detailed exploration of the same topic forms the basis of our study.

1.4.3.1 Sweeping Jet Impingement Technique

The fluctuating behavior and efficacy of fluidic oscillators have expanded their utilization across various engineering applications, encompassing the reduction of skin friction [12,13], noise mitigation [14] and transformation of laminar regimen into turbulent regimen. Two categories of fluidic oscillators exist based on their design: those attached to walls and those involving jet interaction [15]. In this research, the wall-attached type proved more proficient and included a power nozzle, mixing zone, two feedback channels, and an exit throat. Under high pressure, fluid is ejected through the power nozzle, directed from the source, and adheres to one of the walls due to the

turbulent jet drawing in the surrounding fluid – a phenomenon referred to as the Coanda effect [16]. This effect propels a portion of the fluid into the neighboring feedback channel via separator walls. The inclination of the fluid to cling to a wall prompts lateral fluctuations in pressure and mass flow, leading to the detachment of the main jet flow from the primary sidewall due to inherent dynamic instabilities. Consequently, the Coanda effect dictates the flow pattern, fastening the jet to the opposite sidewall, generating an oscillating jet periodically [17], as depicted in Figure 8 owing to the symmetrical attributes of the fluidic oscillator.

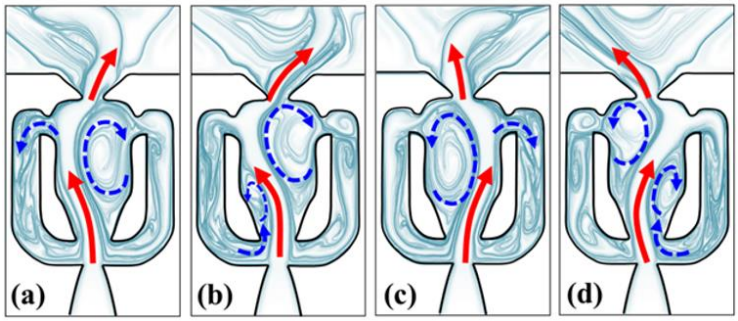

Figure 8: Oscillating flow mechanism of sweeping jet at different time steps [17]

1.4.3.2 Chevroned Jet Impingement technique

The chevron or saw-toothed pattern extrusion is capable of enhancement of jet flow mixture promoting heat transfer rate. The vortex ring structure could be destroyed by streamwise vortices that are excited by the chevrons at nozzle exit leading to vortical coherent structures formation that increases turbulence and thereby promoting mixing rate and enhanced heat transfer rate [18]. Initially chevrons were attached at the nozzle exit of jet engines as it efficiently reduced the noise level by shifting it to higher frequencies [19]. In recent years, chevrons have started to be employed in areas to achieve higher heat transfer rates. The principle was the same as noise reduction technique i.e., chevrons initiated large and small scale vortical motion that excited the near-field jet thereby providing between co-axial flow structure an aggravated entrainment rate [20]. This promoted better mixing of cooling fluid leading to an enhanced heat transfer rate.

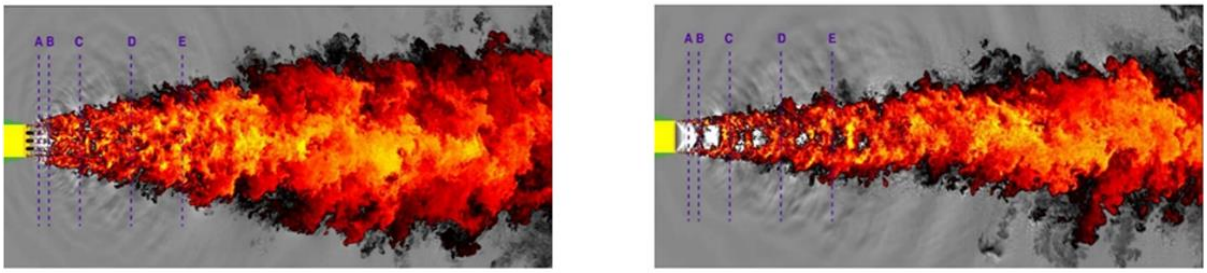

Figure 9: Instantaneous temperature field of the jet flow from chevron jet (left) vs no chevron jet (right) [19]

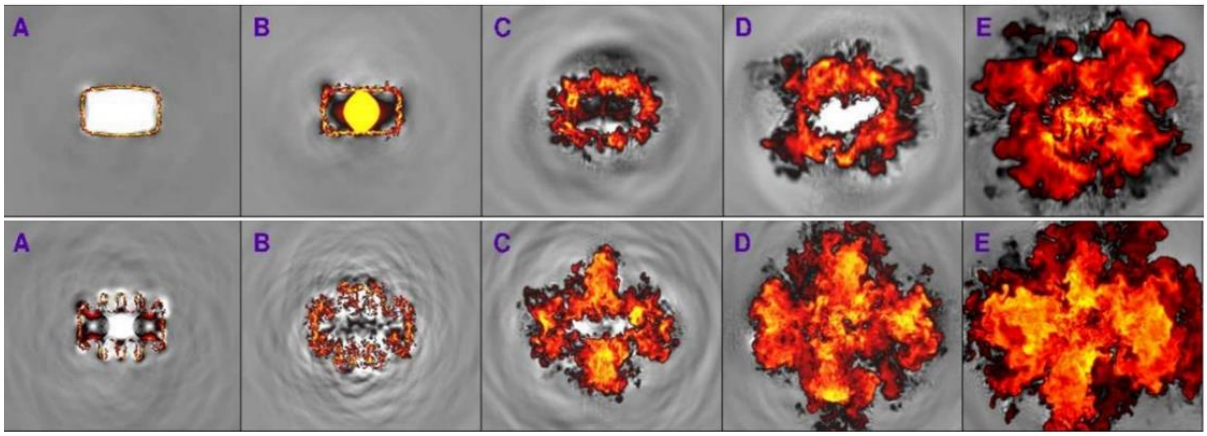

Figure 10: Cross-section at different locations colored with instantaneous temperature field of the jet flow from chevron jet (top) vs no chevron jet (bottom) [19]

1.4.3.3 Swirling Jet Impingement technique

This technique attains enhanced heat transfer rate by introducing swirl flow which can introduced via twisted tapes, spirals, or screw rods throughout the length of the impinging jet. These spirals add tangential velocity component to the fluid which combines with the axial velocity component that generates enhanced momentum transfer area particularly near the stagnation point. The impinging area therefore covered is larger due to generation of toroidal flow reversed zones near the central impinging region. by broadening [21]. Thus, creating localized pressure gradients leading to increased flow entrainment and turbulent characteristics as the jet impinges over the target surface. The flow behavior and heat transfer efficiency of these rotating jets are influenced by the angle of rotation of the tapes.

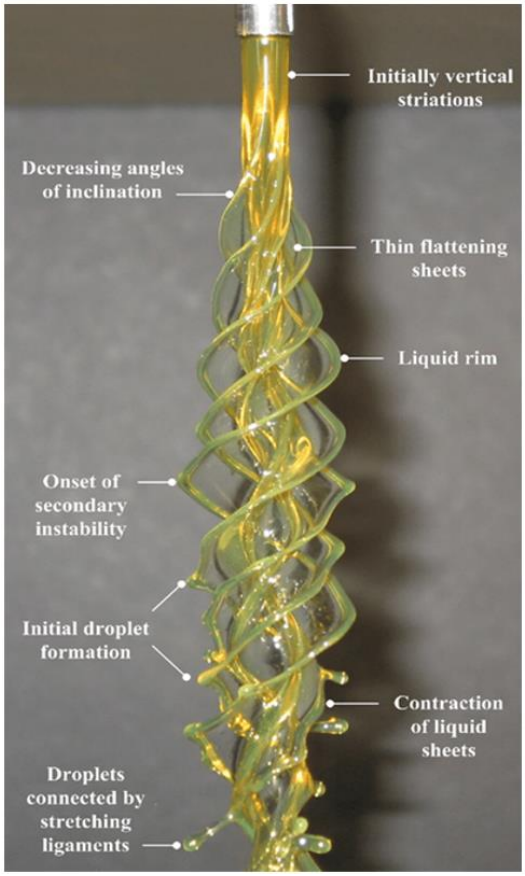

Figure 11: Vortex structure of Swirling jet [21]

1.4.4 Jet Impingement Cooling Review

The curved front portion of turbine blades, known as the leading edge, holds significant importance in gas turbines due to the exposure to extremely high temperatures resulting from the combustion process. Traditionally, internal jet impingement cooling is employed to cool the leading edge of these blades. This method is favored for its ability to achieve a high rate of heat transfer, as it allows cooling air to be directed onto the hot surface directly [22]. Various studies have been conducted to explore the effectiveness of jet impingement cooling on the leading edge of turbine blades. Metzger et al. [23] were pioneers in experimenting with circular jet impingement cooling on concave surfaces. They established a correlation between maximum heat transfer and arc length, as well as maximum and local Stanton numbers. Chupp et al. [24] carried out experiments on jet impingement cooling at the blade's leading edge and developed correlations for stagnation and average Nusselt numbers in relation to parameters such as Reynolds number (Re), leading edge diameter, distance

between jet nozzle and surface, jet nozzle pitch, and jet nozzle diameter. Tabakoff et al. [25] explored the effects of different jet configurations (circular, round, and slot nozzles) on impingement cooling performance at the leading edge, finding that circular nozzles exhibited the highest heat transfer among the configurations tested. Yang et al. [26] examined three jet configurations' impact on heat transfer, concluding that circular jets outperformed rectangular and 2D contoured jets at various Reynolds numbers. Han and Goldstein [27] reviewed experiential studies on gas turbine impingement cooling, comparing single and multiple jet heat transfer characteristics. They also investigated parameters like rotation and curvature effects on heat transfer and jet impingement. For rotating systems, they observed distinctions from crossflow due to a thin wall boundary layer formed by the rotation, and for curvature, they noted how the positioning of film cooling holes influenced leading-edge heat transfer.

Taslim et al. [28] conducted experimental studies on impingement cooling, considering factors like surface texture, jet spacing, presence of film holes, and crossflow. Elnajjar et al. [29,30] explored varying Reynolds numbers on semicircular surfaces using central and side jet configurations, finding higher local and average Nusselt numbers for the central-jet case. With advances in Computational Fluid Dynamics (CFD) technology, studies on impingement cooling have integrated numerical simulations since the early 2000s. Kayansayan and Kucuka [31] numerically investigated jet impingement on a concave surface, showing good agreement at low Reynolds numbers but deviations at higher Reynolds numbers. Taslim et al. [32] numerically studied different target surfaces and reported enhanced cooling performance with increased surface complexity. Jia et al. [33] compared turbulence models in numerical simulations and found V2F models better represented the fluid flow. Kumar et al. [34] numerically investigated the same case as Chupp et al. [23], favoring the k–ω SST turbulence model. Liu et al. [35] concluded that the k–ω SST model performed better for jet impingement cooling simulations. Hamdan et al. [36] investigated heat transfer enhancement in a semicircular cavity using numerical and experimental methods. Sharif et al. [37] studied the impact of jet inclination angle on heat transfer using numerical simulations. Yang et al. [38] and Wang et al. [39] compared experimental and numerical results for single-row jet impingement cooling,

with each study favoring different turbulence models. Safi et al. [22] explored central jet impingement cooling on a semicircular surface, highlighting the significance of entrance length on heat transfer performance.

1.4.5 Jet Impingement Excitation Technique Review

Research on increasing the rate of heat transfer by using jet impingement have focused on the excitation of jets, as the characteristics of flow and heat transfer of impinging jets can be controlled by managing the vortices that are formed due to Kelvin–Helmholtz instabilities, and eventually merge in the developing region on the target surface through active or passive means. Ghadi et al. [40] classified the manipulation of the shape of the nozzle, the distance between the nozzle and the target surface, the shape of the target surface, and the Reynolds number of the fluid used for impingement into the passive category of the methods of merging of the vortices, and regarded the features of flow that can be dynamically controlled as belonging to the active category of such methods. Similarly, Maghrabie et al. [41] presented different methods of exciting the jet, including passive self-excitation, active excitation, and hybrid techniques. Passive self-excitation was further classified into annular, swirling, and sweeping jets. Kalinina et al. [42] experimentally compared round and annular jets by using a Particle Image Velocimetry system (PIV) and observed that the latter kind of jet created a turbulent outlet that intensified the rate of heat transfer. Xu et al. [43] designed a swirler and used numerical simulations to show that it was superior to the traditional, multi-channel impinging jet in terms of the radial uniformity of heat transfer. A 60° swirl in the jet resulted in a turbulent impinging jet and increased the local Nusselt number (Nu) when the spacing between jets was h/Dj = 3. Khan et al. [44] numerically analyzed an array of sweeping and steady jets over the leading edge of the blades of a turbine. They concluded that the impingement of the sweeping jet led to a wider area of cooling than that of the steady jet due to a reduction in crossflow, and an increase in the turbulence and the region of stagnating oscillation in heat transfer. Shakouchi et al. [45] examined the characteristics of the exits of a nozzle with a pipe, one with an orifice, and quadrant nozzles. The jet with the nozzle featuring an orifice yielded a local Nusselt number that was higher by 17% and 33% at the point of stagnation compared with its

counterparts. This can be attributed to its high velocity of exit from the outlet of the nozzle. Brignoni et al. [46] experimentally investigated chamfered and non-chamfered nozzles under Reynolds numbers ranging from 5000–20000 by using chamfers with different angles and lengths as well as varying nozzle-to target spacing. They found that heat transfer increased by 20%–30% when chamfered nozzles were used, and narrow chamfers yielded the best performance. Stevens et al. [47] compared the flow fields of the impinging jets generated by a pipe-type nozzle, nozzles with sharp-edged orifices with and without turbulence damping, and a nozzle with a contoured orifice. They observed that the rate of heat transfer was the highest close to the plate when nozzles with sharp-edged orifices were used.

The acoustic excitation of the jet is a commonly used active method to increase the rate of heat transfer by introducing time-dependent disturbances to the incoming flow. Mladin and Zumbrunnen [48] concluded that a critical Strouhal number of St = 0.26 is required for external excitation, and no significant change in the rate of heat transfer occurs below this value. Uddin et al. [49] claimed that passive excitation at the nozzle of the jet improved the rate of heat transfer to a greater extent than active excitation and swirl. Kim et al. [50] conducted large eddy simulations (LES) to investigate the changes in heat transfer when single-frequency excitation was applied at the exit of the jet at a Strouhal number of 0.017 and concluded that effect of excitation was the greatest at l/Dj=6 because the maximum turbulence occurred at this value. Rakhsha et al. [51] experimentally and numerically investigated the active excitation of impinging jets in comparison with steady jets and reported an increase in heat transfer of up to 36% when the frequency of the pulsating jet was 100 Hz. Bilsky et al. [52] performed an experimental study on a submerged, round, water jet impinging on a flat heated surface by using IR thermography at a Strouhal number of 0.5 as the velocity of flow underwent periodic pulsations. The results showed that heat transfer at the point of stagnation could be enhanced through excitation at a low amplitude with a small spacing between the nozzle and the plate (l/Dj).

Kataoka et al. [53] demonstrated that enhancing the breakdown of vortical ring structures that are formed due to the instability of the laminar shear layer [54], which

arises from the edge of the nozzle, can increase mixing in the jet and enhance heat transfer over the target surface. The extent of mixing is enhanced in relation to active/passive excitation in impingement-induced cooling by using chevrons with a particular geometry or a nozzle with a zig-zag-shaped outlet. The chevron, or an extrusion with a saw-toothed pattern, can enhance the mixing of jet flow and increase the rate of heat transfer. The vortical ring structure can be broken down by streamwise vortices that are excited by chevrons at exit of the nozzle, and form coherent vortical structures that increase turbulence and, thus, promote the rates of mixing and heat transfer [55]. The use of chevrons for jet impingement involves modifying the 4 geometries of the nozzle, and thus can be classified as a passive method according to the standard of delineation provided by Violato et al. [56]. However, it can also be classified as an active method of excitation [57] because chevron nozzles were originally designed to reduce the intensity of noise by using vortical flow. This can smoothen the mixture of flows with different velocities and reduce the noise resulting from their interaction.

Few studies have sought to improve the rate of heat transfer through impingement based on a nozzle with chevrons. Reeder et al. [58] performed experiments on round jet impingement by using delta shaped tabs at the exit of the nozzle. The tabs generated a pair of counter-rotating vortices that increased mixing in the shear layer of the jet. Gao et al. [59] subsequently performed experiments by using a nozzle with a circular orifice and triangular tabs to better understand the increase in heat transfer induced by the tabs. Their results showed that the use of triangular tabs enhanced heat transfer by 25%. Yu et al. [60] investigated the heat transfer-related performance of a single row of round, impinging jets with triangular tabs with different orientations at the exit. They tested this setup under Reynolds numbers ranging from 10,000 to 20,000 as well as different jet-to-target spacings (l/Dj). They observed the formation of pairs of vortices that increased the velocity of the jet and, thus, heat transfer over the target surface. Yu et al. [61] also investigated the initial cross-flow and found that it reduced the rate of heat transfer by 15% compared with the case in which no cross-flow was formed. Guan et al. [62,63] experimentally and numerically investigated a chevroned jet on a conical leading edge and found that it increased heat transfer on

the target surface by 20% compared with a jet with a conventional nozzle. Heat transfer increased due to large fluctuations of the jet caused by the chevron nozzle.

Lyu et al. [64] recently performed experiments on single row chevroned jet impingement on concave surfaces. Their results showed that the Nusselt number at the leading line increased by about 20%–30% at small nozzle-to-surface distances and by 10%–15% at large nozzle-to-surface distances. They also observed that the curvature of the surface had a clear impact on the rate of heat transfer. That is, a surface with a high curvature reduced the average Nusselt number of leading line of the concave surface at large Reynolds numbers. Lyu et al. [65,66] also experimentally and numerically investigated pulsed chevron-based heat transfer to better understand the regime of flow involved. A key finding was that the coupling of pulsed excitation and the chevroned jet reduced the rate of heat transfer by 21% compared with that in case of a Chevroned Steady jet. While the study provides minute details of fluid flow, it was ultimately an unsuccessful attempt to couple two methods of excitation.

1.4.6 Effect of Rotation on Jet Impingement Review

Parsons et al. [67] investigated rotation at an extremely low rotation number of 0.0028 and a Reynolds number of 10,000. The study focused on a single arrangement of impinging jets that flowed radially outward. They concluded that heat transfer performance decreased up to 20% compared to stationary case. Hsieh et al. [68] examined experimentally using TLC technique the effect on heat transfer with respect to various jet positions over ribbed channels with Reynolds number in range of 5000–9000 and at low rotational speed of 600 RPM. They observed that heat transfer performance was lower stationary case. It increased up to 20-30% and was highest for square rib roughened type as compared to the semi-circular roughened type. Hong et al. [69] investigated heat and mass transfer characteristics of impinging jet cooling on the concave surface with rotation compared to a flat surface at a Reynolds number of 5000 and a rotation number of 0.075. They found that heat and mass transfer performance slightly enhanced due to better mixing by rotational effect. Also compared to flat surface, the heat and mass transfer on the concave surface is enhanced due to the curvature effect, providing the higher averaged Sherwood value.

Elston et al. [70] The effect of rotation on single row jet impingement cooling over semicircular concave surface is experimentally investigated in their study at an average jet Reynolds number between 6000 – 24000 along with jet rotation number varied from 0 – 0.13. They observed that deflection of the impinging jet along with the rotation induced secondary flows leading to better mixing promoting enhanced heat transfer**.** Yang et al. [71] studied effect of rotation on turbine blade internal cooling and concluded it as important factor in gas turbine cooling systems. They studied impingement design in a two-pass channel to reduce impact of rotational forces experimentally using TLC method for channel Reynolds number between 25,000 to 100,000 while rotation number ranging from 0 to 0.14. To gain insight of flow behavior a series of computational simulations with SST model was performed that impacted the heat transfer distributions on the walls. Their results indicated that rotation reduces the heat transfer on both sides of the impingement due to the Coriolis force and the pressure redistribution. Another finding of this study is the impingement channel has advantages in the upstream channel and the end region when compared to U-bended two pass channel, but its performance deteriorates on the leading side of the downstream channel.

Lamont et al. [72] studied single row of jets impinging on smooth target surface (leading and trailing edge included) subjected to crossflow condition experimentally using TLC. They reported that when the flow was radially outward, the Coriolis force promotes the heat transfer rate for trailing edge while offering a contrasting case i.e., reduction of heat transfer rate over the leading-edge blade. Singh et al. [73] performed a rotational study comparing dimpled target surface and smooth surface at Reynolds jet number of 2500 at rotational number of 0.00274. They found that dimpled target surface at no rotational condition exhibited higher heat transfer performance compared to smooth surface. However, at rotating conditions both leading and trailing edges heat transfer performance was enhanced as compared to the indented patterned surface. Craft et al. [74] investigated computationally for flow and heat transfer performance for an array of five round impinging jets onto a concave surface subjected to both stationary and rotating conditions. They performed using k-epsilon linear and non-linear eddy-viscosity model with wall-functions to cover the near-wall layer. Their study captured overall flow characteristics under stationary conditions, however it failed to achieve so

in rotating conditions while compared to experimental case. Iacovides et al. [75] performed an experimental study of water impingement cooling via a row of five jet holes in a rotating passage of about 250 RPM (both clockwise and anti-clockwise) of concave surface at a Reynolds number of 15000. Under stationary conditions, via liquid-crystal technique, a high Nusselt number region develops around each impingement point along with secondary peaks half-way between impingement points. For rotating condition, reduction in heat transfer parameter is observed with disappearance of all secondary peaks along with few absences of primary peaks due to spreading rate of the jets.

Jung et al. [76] conducted an experimental exploration of heat transfer traits utilizing the naphthalene sublimation technique. They studied an array of impinging jets over a concave surface while considering the influence of rotation. The jet Reynolds number was set at 3000, and the rotation number was 0.032. The flow structure was studied using numerical methods. It was observed that rotation increased the flow mixing compared with the stationary case and there was overall averaged heat transfer values enhancement for this case. In separate but coordinated works, Burberi and Massini et al. [77,78] simultaneously conducted numerical and experimental inquiries with the objective of evaluating the impact of rotation on the distribution of heat transfer within an internal cooling system situated along the leading edge of a high-pressure gas turbine blade. The experiments were conducted under both stationary and rotating conditions, with jet Reynolds numbers (Rej) ranging from 10000 to 40000, and Rotation numbers (Roj) reaching up to 0.05. To attain a more precise understanding of flow dynamics during rotation, hybrid RANS-LES models were employed for the numerical simulations. These simulations aimed to align closely with experimental observations of flow behavior and heat transfer, which were captured using Particle Image Velocimetry (PIV) and Thermochromic Liquid Crystal (TLC) techniques, respectively. The researchers revealed that rotational effects are more pronounced in instances of slight cross-flow jet deflection, while exerting a relatively subdued influence on both the core velocity of the jet and the area-averaged Nusselt number. Interestingly, the pattern of heat transfer distribution was determined to be independent of Reynolds number. For the numerical investigation of flow patterns and heat transfer alterations

due to rotation in the context of turbine blade cooling, a three-dimensional k-ω SST model was employed. The analysis maintained a constant heat flux application to the leading edge, with internal cooling achieved through the utilization of seven jets. The numerical findings aligned with the experimental outcomes, reinforcing their validity. Safi et al. [22] performed a 3D numerical simulation for array of seven impinging jets over a rotational gas turbine blade leading edge using the turbulent SST k–ω model to study its flow field characteristics and heat transfer performance. Their study was exhaustive covering a range of jet Reynolds numbers from 7500 to 30,000 with rotational number ranging between 0-0.04. It was observed that effect of rotation is diminished on the heat transfer performance as the Reynolds number increases and they developed a mathematical correlation between Nusselt number to jet Rotation and jet Reynolds number for a leading-edge blade of gas turbine.

As discussed in the initial statements of introduction all the aforementioned studies have been investigation for rotational effect over leading edge using conventional steady jet impinging jets and to best awareness of authors there has been only a single investigation performed on rotational effect of sweeping jet by Hossain et al. [79] at three rotational numbers of 0.013, 0.026 and 0.039. Numerical simulation was performed using URANS models that demonstrated oscillation frequency of sweeping jet drops with rotational speed due to a drop in averaged velocity inside the feedback channel and also observed that the internal flow has been moderately affected by rotation while a significant change in the external flow was observed. Both on and off axis rotation was applied for sweeping jet where they observed out-of-plane motion induced by the Coriolis force for former case and for the latter case the local pressure gradient in the radial direction formed an asymmetric jet trajectory both for streamwise and spanwise direction.

Chapter 2: Methods

The computational approach provides deeper insight into flow physics and heat transfer characteristics of impinging jet nozzle over leading-edge blade. Different impinging nozzles used in the study namely sweeping jet, steady jet, swirling jet, Chevroned Sweeping jet and Chevroned Steady jet as shown in Figure 12. are performed numerically for both stationary and rotational condition. Numerical approach presents an advantage, primarily for rotational case, as rotation condition presents a challenging situation to capture the flow behavior during experimental approach. The computational tool in this study utilized was ANSYS Fluent Workbench version 20.0. A detailed step wise process carried out during the computational study is discussed accordingly.

2.1. Research Design

This section is dedicated to understanding the geometry and the dimensions of various impinging nozzles shown in Figure 12. For this computational analysis, the dimensions of the sweeping jets were taken from the research conducted by Khan et al. [44]. As for the steady jet it is rectangular shaped jet designed consistently to align with sweeping jet geometrical details. The design of swirling jet is adopted from study of Amini et al. [80] where the nozzles equipped with twisted tapes are employed to produce swirls. In our study twists of 45 degrees are applied to above mentioned steady jet as the particular twist angle achieves the highest heat transfer performance confirmed by Xu et al. [81]. For the Chevroned Sweeping jet and Chevroned Steady jet includes addition of triangular tabs/zig-zag shaped nozzle exit outlets i.e., the rectangular base exit of sweeping jet is attached with triangular chevrons [82] with its configurations as an isosceles triangle are chosen [83,84] as shown in the Figure 13. Detailed dimensions of the impinging jets are described in Table 1. The novelty in the investigation lies in performing a comparative study for all the exciting and conventional steady jet adapted in the similar category within same set of operating conditions, primarily to test these jets subjected to rotational condition of gas turbine. Another novel feature of thesis study is analyzing the overall performance of unique Chevroned Sweeping jet geometry ever presented in the literature.

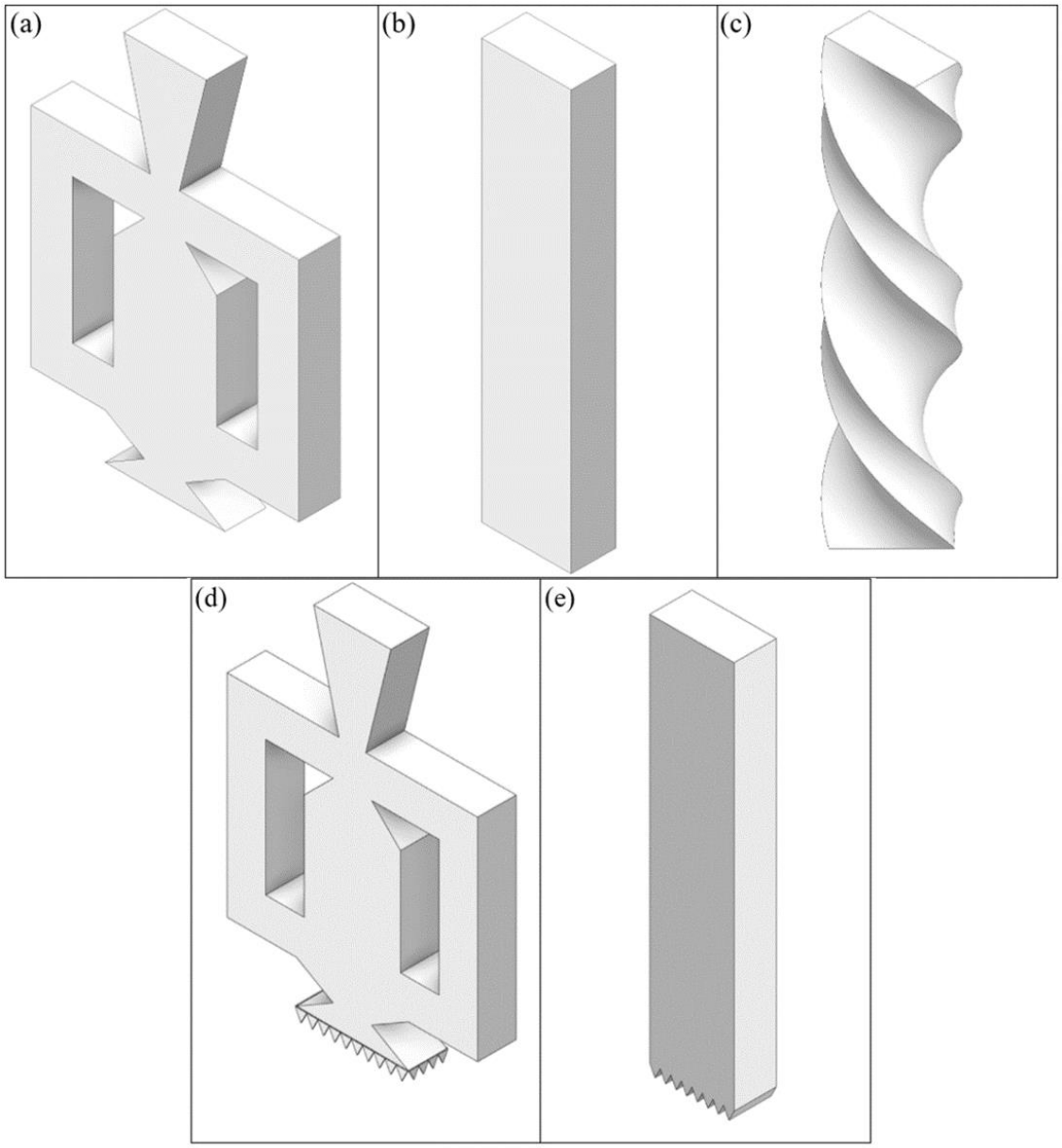

Figure 12: 3D view of impinging jets (a) Sweeping jet (b) Steady jet (c) Swirling jet (d) Chevroned Sweeping jet (e) Chevroned Steady jet

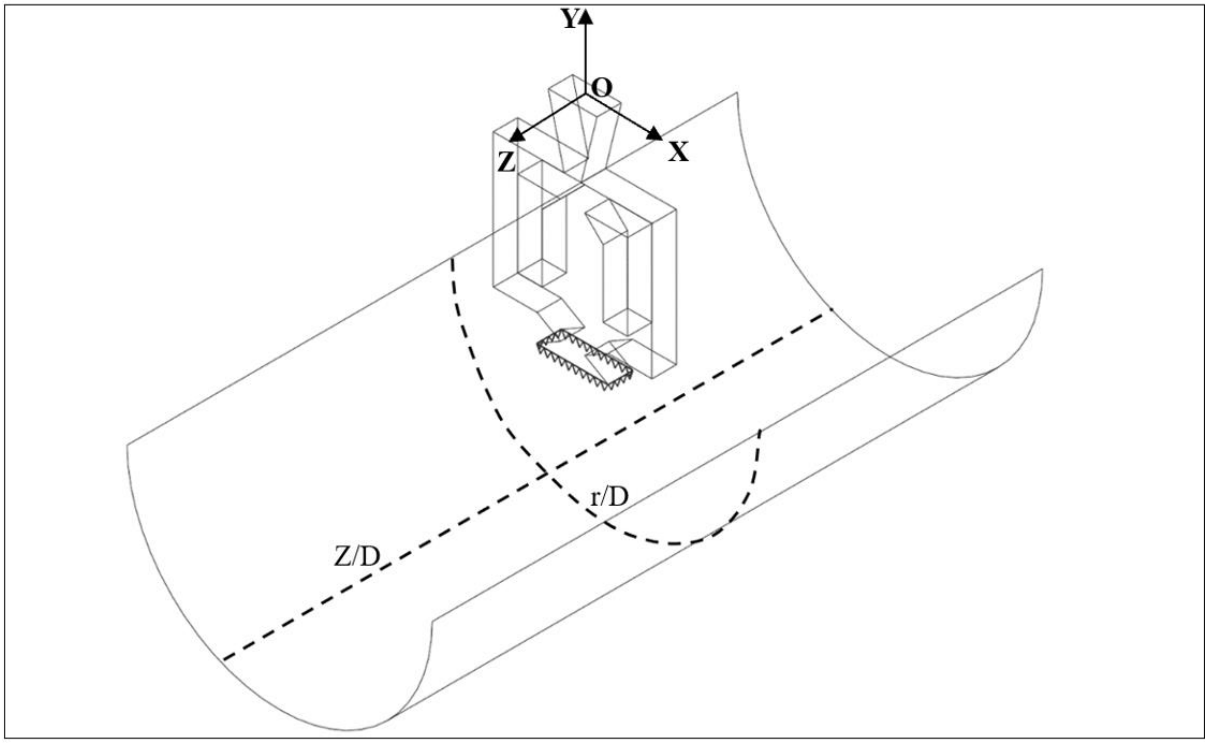

Figure 13: Isometric view of Chevroned Sweeping jet along with leading-edge blade

2.2 Description of Physical Setup

This section attempts to briefly explain the computational setup of impingement flow over leading-edge blade. A controlled amount of cooling air gushes through restricted passage of nozzles unsteadily (for excitation jets) which impinges on the leading-edge blade and can escape through only one outlet at the top. A model with zero wall thickness is utilized. The length of the leading-edge blade is extended sufficiently to allow the coolant to exit, ensuring improved convergence. A detailed physical description of the problem statement is described through Figure 14 i.e., Chevroned Sweeping impinging jet over the leading-edge blade. Similar setup conditions are applied for all other impinging jets, that are designed using Space Claim ANSYS 20.

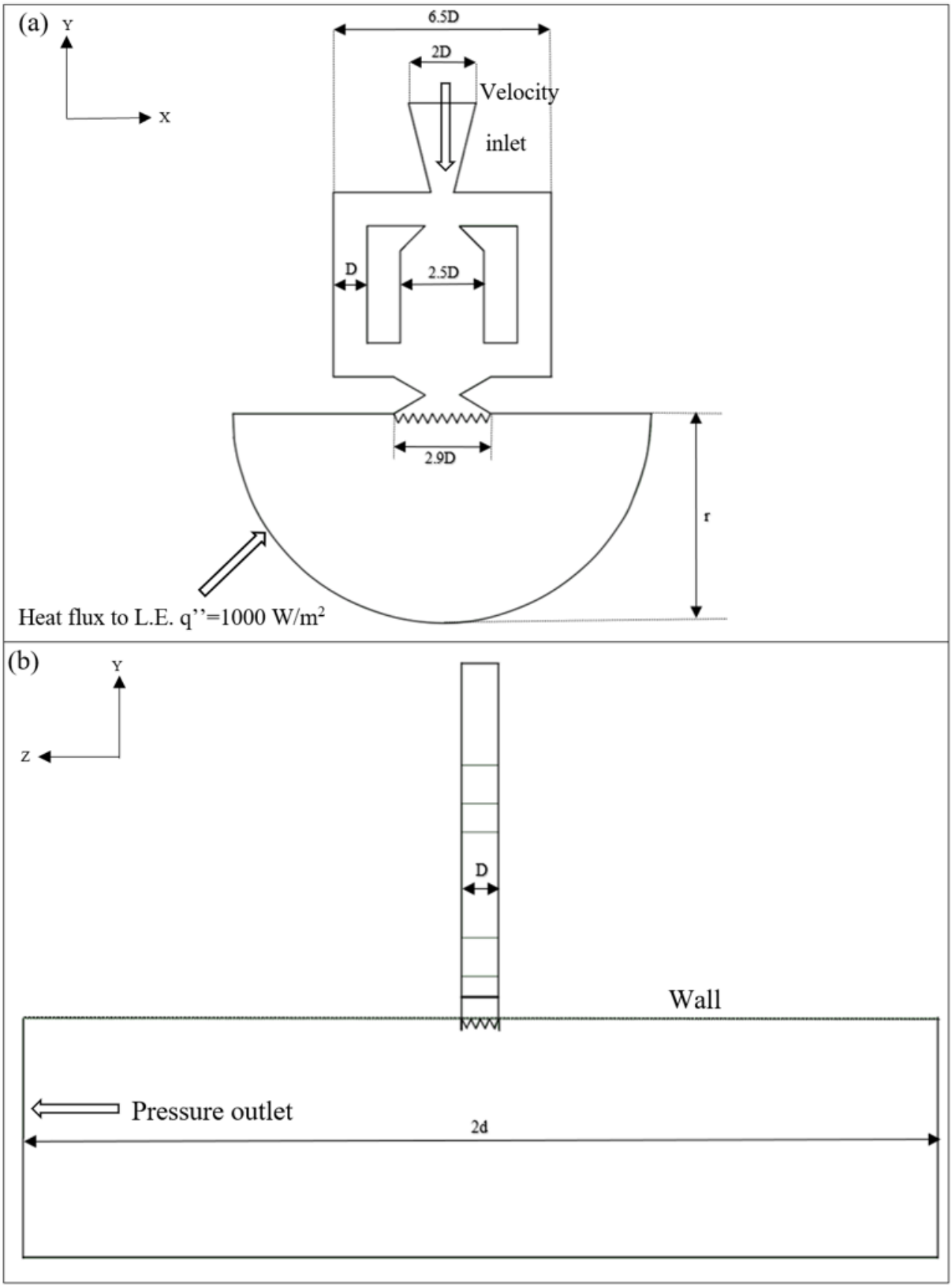

Figure 14: Computational domain and boundary conditions of the Chevroned Sweeping jet (a) Front view (b) Side view

Table 1: Dimensions and geometric details of the model [44]

Parameter	Value
Jet initial supply *2D*	8 mm
Mixing chamber width *2.5D*	10 mm
Power nozzle *0.7D*	2.8 mm
Feedback channel width *D*	4 mm
Throat of nozzle *D*	4 mm
Exit of nozzle *2.9D*	11.6 mm
Triangular chevron base transverse side of nozzle exit *0.29D*	1.16 mm
Jet thickness D_j	4 mm
Triangular chevron base at height of rectangular base exit *0.25D*	1 mm
Twist angle for swirling jet θ	45°
L.E. diameter *d* and radius *r*	*d*=50 mm and *r*=25 mm
Leading edge length L_{LE}	100 mm
Jet-to-wall distance *l*	25 mm
Thickness of chevrons	0.1 mm

2.2.1 Mesh Description

The fluid dynamic analysis for the present numerical study was carried out using FLUENT Mosaic poly-hexcore Meshing 20.0 technology. The poly-hexcore mesh is a highly efficient meshing technology that results in reduction of total element count by 20 to 50% when compared to the traditional hexcore mesh [85]. It works by generating isotropic poly-prisms in boundary layer region and top-quality octree hexahedrons in the fluid region which are connected with Mosaic polyhedral elements by the Mosaic poly-hexcore technology as it is capable to connect any different types of mesh elements conformally and automatically shown in Figure 15. Mosaic meshing uses a “bottom-up” technique in contrast to the conventional “top-down” technique. The “Bottom-Up” approach provides freedom to generate high quality thick prism layers, while respecting

geometric fidelity, which is very challenging in cartesian based cut/snapped "Top-Down" meshing approaches. The grid numbers chosen for all the geometric configurations were 2 million elements respectively and the dimensionless $y+$ wall distance is ensured to be less than 1 throughout the analysis. An excellent grid quality as shown in Figure 15 was generated utilizing the Mosaic poly-hexcore technique that converged for every time steps with residuals set to 10^{-5} for all the equations and 10^{-7} in the energy equation.

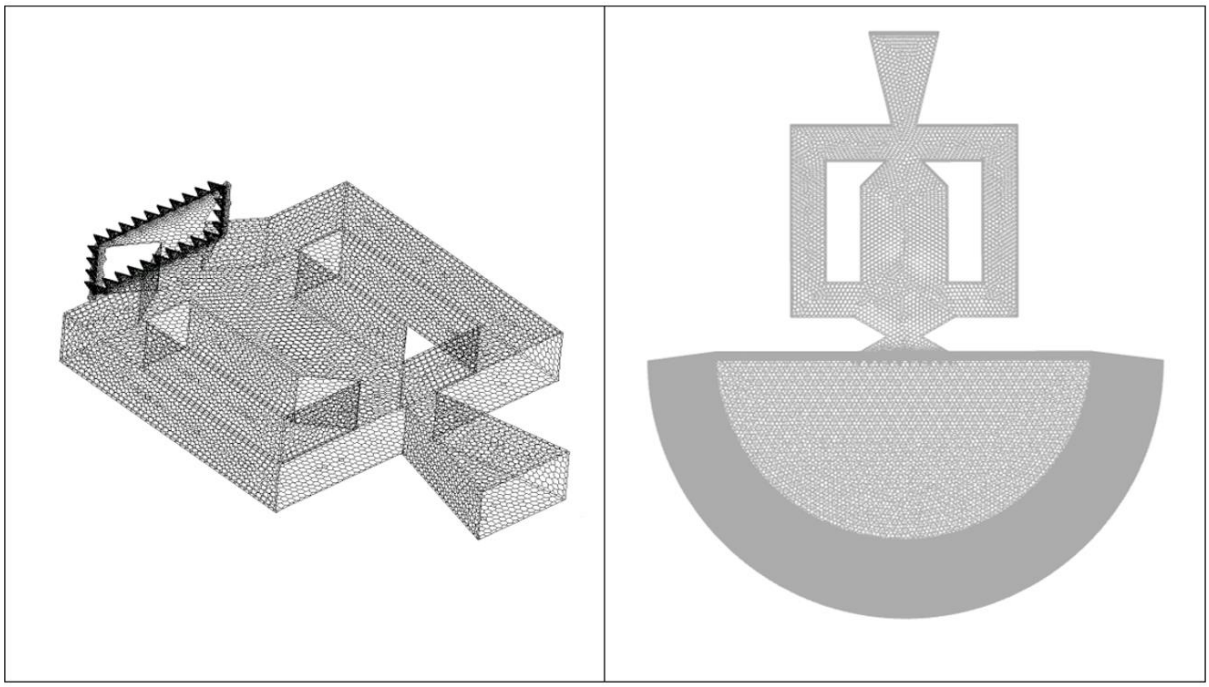

Figure 15: Surface mesh resolution of the geometry focused near the jet

2.2.1.1 Grid Independence Study

To establish our mesh to be truly grid independent, we have performed analysis of 7 million elements on polyhexcore mesh which correspond to nearly 14-15 million elements of conventional meshing case and obtained deviation less than 1% of Nusselt number as described in Figure 2 and are said to be grid independent when Nusselt values of 2, 5 and 7 million elements of poly-hexcore are compared as shown in Figure 16.

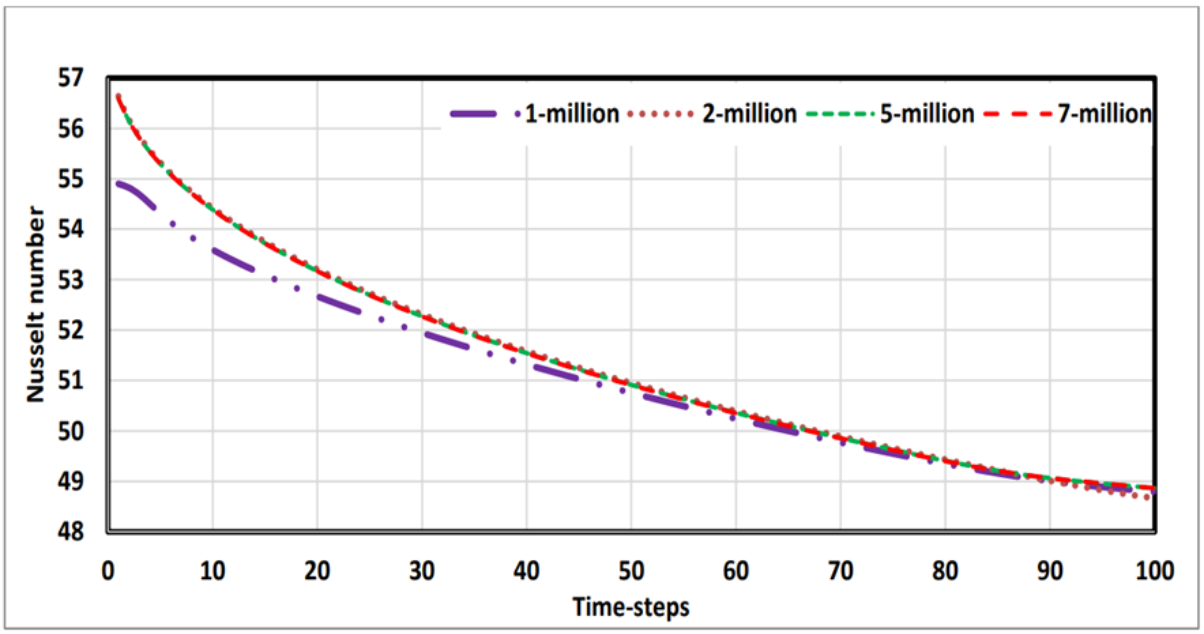

Figure 16: Mesh independent study performed for sweeping jet nozzle

2.2.2 Numerical model

To capture the flow phenomenon of impinging jets, numerical model selected must be able to better predict the turbulent length scale capturing the physics of impinging flow. The unsteady RANS turbulence model predicted the flow well when compared to the ELES model as stated by Wu et al. [86]. Thus, URANS model can provide a time efficient way modelling the complex physics of turbulent impinging flow without compromising the accuracy. The basic governing equations are as follows:

Continuity Equation:

$$\frac{\partial(\rho)}{\partial t} + \frac{\partial(\rho u_j)}{\partial x_j} = 0 \tag{1}$$

Momentum Equations:

(*Stationary condition*)

$$\frac{\partial(\rho u_i)}{\partial t} + \frac{\partial(\rho u_i u_j)}{\partial x_j} = -\frac{\partial p}{\partial x_i} + \frac{\partial \tau_{ij}}{\partial x_j} + \frac{\partial}{\partial x_j}\left(\mu \frac{\partial u_i}{\partial x_j}\right) \tag{2}$$

(*Rotatory condition*)

$$\frac{\partial(\rho \vec{v}_r)}{\partial t} + \frac{\partial(\rho \vec{v}_r \vec{v}_r)}{\partial x_j} = -\frac{\partial p}{\partial x_i} + \frac{\partial \tau_{ij}}{\partial x_j} + \frac{\partial}{\partial x_j}\left(\mu \frac{\partial u_i}{\partial x_j}\right) - \rho(2\vec{\omega} \times \vec{v}_r + \vec{\omega} \times \vec{\omega} \times \vec{r}) \tag{3}$$

Energy Equation

$$\frac{\partial(\rho u_i)}{\partial t} + \frac{\partial(\rho u_i u_j)}{\partial x_j} = -\frac{\partial p}{\partial x_i} + \frac{\partial}{\partial x_j}\left(\mu \frac{\partial u_i}{x_j} - \rho \overline{u_i' u_j'}\right) \quad (4)$$

2.2.2.1 Turbulence model

Impinging flows create adverse pressure gradients and damping functions used in *k–ε* model doesn't provide accurate results. Contrarily, the *k–ω* model doesn't need these damping functions to solve the flow physics and provides better accuracy for impinging flows. One main weak point of *k–ω* model is dependency on freestream turbulent conditions where small changes in it leads to large changes in turbulent viscosity and skin friction coefficient as well. Menter et al. [87] provided a solution for the above by blending two different models *k–ε* and *k–ω*, where *k–ε* model handles the freestream turbulence problems faced by the latter model. In this way *k–ω* SST model was developed where flow near the boundary layer was dealt with the *k–ω* model and the flow in the outer region of boundary layer was solved by the *k–ε* model.

k- Equation:

$$\frac{\partial(\rho k)}{\partial t} + \frac{\partial}{\partial x_j}(\rho U_j k) = \frac{\partial}{\partial x_j}\left[\left(\mu + \frac{\mu_t}{\sigma_{k3}}\right)\frac{\partial k}{\partial x_j}\right] + P_k - \beta' \rho k \omega + P_{kb} \quad (5)$$

ω- Equation:

$$\frac{\partial(\rho \omega)}{\partial t} + \frac{\partial}{\partial x_j}(\rho U_j \omega) = \frac{\partial}{\partial x_j}\left[\left(\mu + \frac{\mu_t}{\sigma_{\omega 3}}\right)\frac{\partial \omega}{\partial x_j}\right] + (1 - F_1)\, 2\rho \frac{\sigma_{\omega 2}}{\omega}\left(\frac{\partial k}{\partial x_j}\right)\left(\frac{\partial \omega}{\partial x_j}\right) + \alpha_3 \frac{\omega}{k} P_k - \beta_3 \rho \omega^2 + P_{\omega b} \quad (6)$$

Turbulent Kinetic energy- Equation:

$$\frac{\partial k}{\partial t} + U_j \frac{\partial k}{\partial x_j} = P_k - \beta^* k \omega + \frac{\partial}{\partial x_j}\left[(\nu + \sigma_k \nu_T)\frac{\partial k}{\partial x_j}\right] \quad (7)$$

Specific dissipation rate Equation:

$$\frac{\partial \omega}{\partial t} + U_j \frac{\partial \omega}{\partial x_j} = \alpha S^2 - \beta \omega^2 + \frac{\partial}{\partial x_j}\left[(\nu + \sigma_\omega \nu_T)\frac{\partial \omega}{\partial x_j}\right] + 2(1 - F_1)\sigma_{\omega 2} \frac{1}{\omega}\frac{\partial k}{\partial x_i}\frac{\partial \omega}{\partial x_i} \quad (8)$$

Here, $\tau_{ij} = 2\mu_t S_{ij}$, S_{ij} is the mean rate strain tensor, and σ_{k1} =2, σ_{k2} = 1, $\sigma_{\omega 1}$ =2, $\sigma_{\omega 2}$ =1.1682, $\beta*$=0.09. β_1 =0.075, β_2 =0.0828, α_1 =0.55 and α_2 =0.44 are revised factors in the k−ω model. For the k and ω equations, μ_t and $\sigma_{\omega 1}$ are related to the blending functions where μ_t is the viscosity limiter.

The additional term in the *k–ε* model $2\rho\frac{\sigma_{\omega 2}}{\omega}\left(\frac{\partial k}{\partial x_j}\right)\left(\frac{\partial \omega}{\partial x_j}\right)$ is blended between models *k–ε* and *k–ω* by multiplying with $(1 - F_1)$ factor. When F_1 = 0 (away from the wall) the model will be solved as *k–ε* and when F_1 = 1 (near the wall) the model is *k–ω*. The blending function F_1 is given by following equation below and tanh is used to smoothen the transition between two models.

$$F_1 = \tanh\left(\min\left(\max\left(\frac{\sqrt{k}}{\beta' \omega\, y}, \frac{500}{y^2\, \omega}\right), \frac{4\,\rho\, k}{CD_{kw}\sigma_{\omega 2} y^2}\right)^4\right) \quad (9)$$

This function is used to blend between two constants Φ_1 and Φ_2 which are model constants for *k–ε* and *k–ω* models respectively.

$$\Phi = F_1\Phi_1 + (1 - F_1)\Phi_2 \quad (10)$$

In the SST k–ω model, the eddy viscosity is not constant for finding the transport of the turbulent shear stress and this limiter results in accurate results for separated flow measurements which is presented as

$$\mu_t = \frac{a_1 k}{max(a_1\omega, SF_2)} \quad (11)$$

Here F_2 is another blending function similar to F_1. Both blending functions are dependent on *'y'* which is the distance to closest wall, If *'y'* is small then F_2 is larger which limits the viscosity

$$F_2 = \tanh\left(\max\left(\frac{2\sqrt{k}}{\beta' \omega\, y}, \frac{500\,\nu}{y^2\,\omega}\right)^2\right) \quad (12)$$

2.2.3 Solution Scheme and Boundary Conditions

The SIMPLE algorithm was used to solve pressure–velocity coupling by using the least-square cell to discretize the pressure. Convergence was easily achieved by using the first-order implicit method for transient formulations, with a time step of 10-

5 s used to obtain the detailed time-averaged physics of flow and values of heat transfer. Such a selection ensured that the Courant number was smaller than one during the computational runs. The flow was incompressible, with a rate of mass flow of 0.0008 kg/s supplied directly to the inlet of the impinging jets, accounting for a Reynolds number of around 12,000 based on the hydraulic diameter of the sweeping jet when the working fluid was air. The numerical study was grid independent, with grids containing 1, 2, and 5 million elements used for the system. This yielded a deviation smaller than 2%, and 2 million elements were considered appropriate for the base mesh. The boundary conditions of note are shown in Figure 3. For instance, the incoming air was supplied at a uniform velocity and a temperature of 300 K to the power nozzle, while the only outlet was open to the atmosphere. The concave face was assumed to be the surface of the leading edge of the blade of a turbine exposed to a uniform heat flux of 1000 W/m^2. 10 The other walls along with the chevron tabs were assumed to be adiabatic, with no-slip conditions. The working principle was that the cool air supplied passed through the nozzles and impinged on the concave surface that was exposed to a constant heat flux of 1000 W/m^2. The impinged hot air then moved through the top of the test section, which was exposed to the atmospheric outlet as mentioned in Table 2. The Reynolds number and Nusselt number of the jet were calculated as follows:

$$Re_j = \frac{\dot{m}}{D\mu} \tag{13}$$

$$Nu = \frac{q'' \, d_j}{k_f(T_j - T_w)} \tag{14}$$

Table 2: Properties of air (cooling fluid)

Parameter	**Value**
Inlet temperature of coolant (T_{inlet})	308 K
Thermal conductivity (k)	0.02625 *(W/m.K)*
Dynamic viscosity (μ)	1.895e-5 *(kg/m.s)*
Density (ρ)	1.145 *(kg/m3)*

2.3 Thesis Case Study

The study as briefed earlier will involve studying around five different impinging nozzles essentially examining their heat transfer performance behavior when subjected to rotational conditions. Numerous studies as addressed in the literature have presented that Coriolis force induced due to rotation has an impact (both positive and negative) over the flow physics of impinging jet. This thesis study, therefore, realizes the importance of investigating the impact of rotational effect over the potential impinging jets and compares individual performance of each potential jet at both stationary and rotating conditions. Table 3 lists all the cases performed in this study.

Table 3: Case study table

Case number	**Nozzle configuration**	**Mass flow inlet (kg/s) corresponding to $Re_{sweeping\ jet}$=12,000**	**Rotation (rpm)**
1	Steady jet	0.0008	0
2	Steady jet	0.0008	3000
3	Steady jet	0.0008	10000
4	Steady jet	0.0008	15000
5	Sweeping jet	0.0008	0
6	Sweeping jet	0.0008	3000
7	Sweeping jet	0.0008	10000
8	Sweeping jet	0.0008	15000
9	Swirling jet	0.0008	0
10	Swirling jet	0.0008	3000
11	Swirling jet	0.0008	10000
12	Swirling jet	0.0008	15000
13	Steady jet with chevron	0.0008	0

Table 3: Case study table (Continued)

14	Steady jet with chevron	0.0008	3000
15	Steady jet with chevron	0.0008	10000
16	Steady jet with chevron	0.0008	15000
17	Sweeping jet with chevron	0.0008	0
18	Sweeping jet with chevron	0.0008	3000
19	Sweeping jet with chevron	0.0008	10000
20	Sweeping jet with chevron	0.0008	15000

Chapter 3: Results and Discussions

This chapter delves into the discussion of numerical outcomes achieved through Fluent ANSYS Workbench version 20.0 for the analysis of potential impinging jets. The current investigation involved conducting transient simulations for both Sweeping jet and Chevroned Sweeping jet configurations, with a time step of 1e-5 seconds selected to maintain a Courant number near unity. This approach aimed at accurately capturing the flow pattern. On the other hand, for the Swirling jet configuration, steady-state simulations were employed, taking into consideration the findings of Amini et al. [80], which demonstrated the credibility of steady-state results through comparison with experimental investigations. This choice was made to conserve computational resources.

The transient simulation for stationary case did not present any challenges and the results for both Sweeping jet and Chevroned Sweeping jet converged at 1e-5 residual for momentum residual and other residuals as well. While the additional term of angular velocity to the Navier stokes equation for the rotational case adds complexity to the equation. However, the mosaic mesh takes care of it by meeting minimum convergence of 1e-3 for the momentum residuals with other residuals converging duly. The convergence criterion is also monitored for Surface Nusselt number over the leading-edge blade. Here, extra attention to rotational case is allotted and data is taken after a minimum of 20 oscillating cycles for Sweeping Jet and Chevroned Sweeping Jet are performed.

3.1 Validation

Initially, the numerical results were validated by comparing them to the numerical code developed by Safi et al. [22], using their prescribed boundary conditions. They had previously established their code by aligning it with experimental data from various rotating conditions, spanning from 0 to 200 RPM. By verifying our numerical approach against their well-established investigation, we could establish the robustness of our study.

The validation process was conducted at a jet Reynolds number (Rej) of 7,500 as shown in Figure 17. We applied their geometry on our mosaic grid and utilized the setup adopted in our own study. A noteworthy outcome emerged from this validation, as the comparison of Surface Nusselt numbers indicated a deviation of less than 2%. This alignment was achieved by comparing the original Safi et al. [22] code, employing 8 million elements, with our code that utilized 2 million elements and employed the Mosaic polyhexcore mesh.

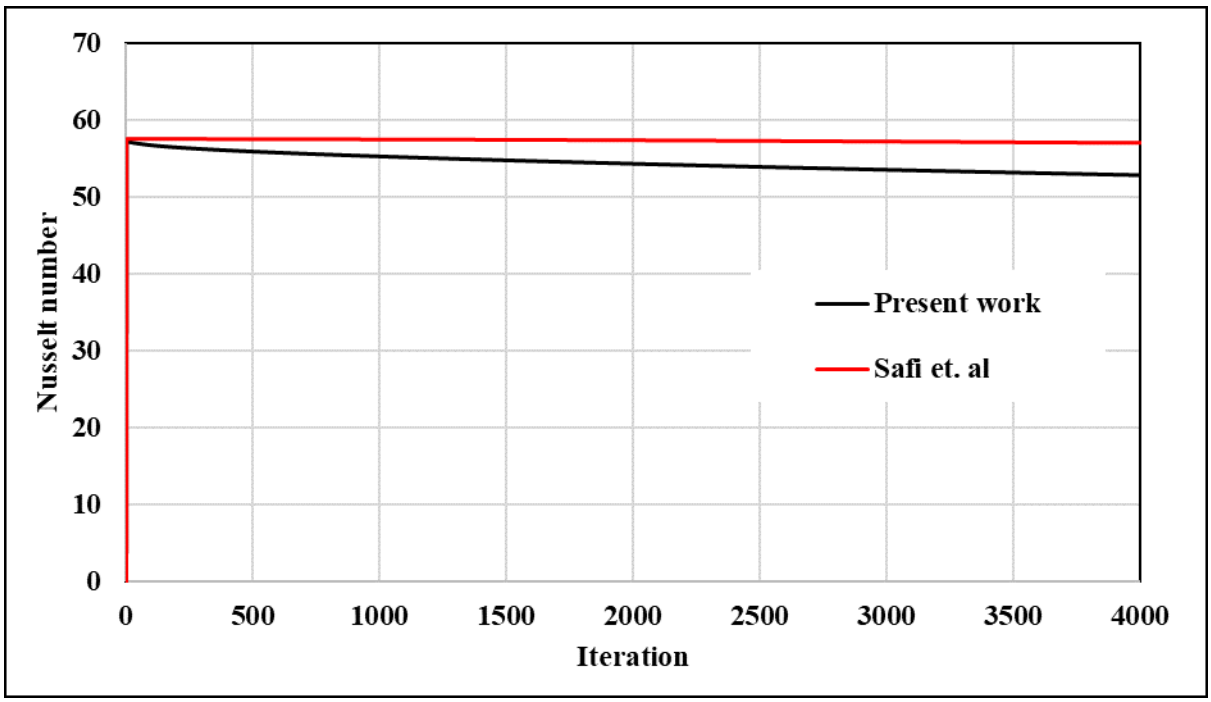

Figure 17: Validation of the numerical code used in thesis study with literature results

Furthermore, an observation was made regarding the convergence behavior of the original Safi et al. [22] code when compared to our present code. The original code, as reported by Safi and colleagues, required a higher number of iterations to achieve convergence, even though similar residuals were maintained. Specifically, the Nusselt value at convergence was recorded as 52.1 for Safi et al. [22], whereas our code achieved a Nusselt value of 52.8 upon convergence. Notably, the Mosaic polyhexcore mesh in our code contributed to a quicker convergence, a finding corroborated by Zore et al. [85].

3.2 Impingement Flow Behavior at Stationary Condition

This section addresses the flow physics of each impinging jets through different data quantities such as Entrainment ratio, Turbulent kinetic energy, Q-criterion, Vorticity. The results are discussed for both stationary and rotating conditions separately.

3.2.1 Entrainment Ratio

The flow characteristics of the potentially impinging jets will be studied in this section. At stationary condition, the Chevroned Sweeping performance dominates to sweeping jet right from the onset, due to higher entrainment of fluid leading to generation of increased hair pin vortex structures which spreads better than sweeping jet and mixes with its primary vortex ring and has overall better mixing efficiency. This could be well illustrated by Figure 18 that describes Entrainment Ratio (ER) along axial length of the leading-edge blade. Nozzle configurations play a significant role in the flow characterization and entrainment of impinging jet i.e., when the fluid (coolant) mixes with the atmospheric air in jet area, it generates a shear layer responsible for higher amount of entrained air resulting in higher turbulent fluid impinging the target area. As described by Yadav et al. [88] the entrainment ratio for jets is defined as

$$\mathrm{ER} = \frac{\dot{m}_y - \dot{m}_j}{\dot{m}_j} \tag{15}$$

Here $\dot{m}_y$ and $\dot{m}_j$ are mass flow rate at defined axial location of impinging jet and mass flow rate at the exit of nozzle, respectively. Note that exit nozzle here is considered at the end of nozzle configuration excluding the tabs of chevrons to be consistent with the mass flow rate value. Also, for the sweeping jet and Chevroned Sweeping jet mass flow rate at any location is calculated based on the time averaged velocity.

While the sweeping jet downstream near the exit of the nozzle is almost like the steady jet in terms of entrainment of fluid, higher turbulence is created due to sweeping effects results in a better entrainment of fluid with the ambient air along the axial length. The addition of swirl angle to steady jet adds tangential velocity as compared to steady jet observed from Figure 26. The flow from the rectangular channel produces vertical

impingement like the steady jet impingement. The spiral channels produce rotating flow infusing with the vertical impingement. This leads its transition to turbulent nature right from the onset of swirls, increasing the entrainment rate due to higher diffusivity of fluid expelling from jet nozzle as seen in Figure 28. Thus, swirling jet creates more spread of fluid radially over the leading-edge blade and improves the heat transfer performance The effect of chevron augmentation to both sweeping jet and steady jet demonstrated by an increment of entrainment of fluid i.e., due to increased hair pin vortical structures resulting in an enhanced mixing and is vividly observed in Figure 27, wherein the overall highest entrainment ratio is manifested by Chevroned Sweeping jet. This is well supported by the fact that Nu number was highest for Chevroned Sweeping jet followed by sweeping jet, Chevroned Steady jet, swirling jet and steady jet.

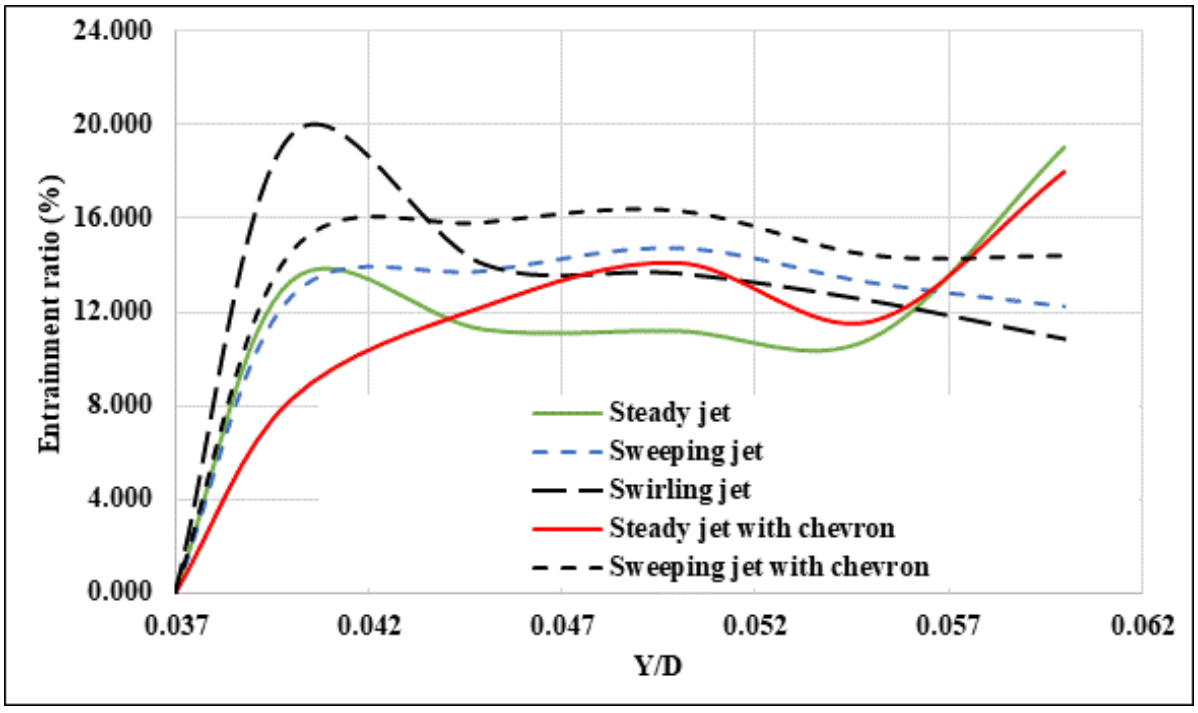

Figure 18: Entrainment ratio in percentage of all jets along the axial impinging direction over L.E.

3.2.2 Turbulent Behavior of Impinging Jets

Figures 19-24 depict the Turbulent Kinetic Energy (TKE) and the Nusselt Number distribution on the target surface for all studied configurations, respectively. It displays the behavior of the sweeping jet with and without chevron for half period reported for 0τ, τ/6, τ/3 and τ/2 where (0-τ) represents one full cycle of sweeping span.

The area with elevated Turbulent Kinetic Energy (TKE) is identified within the oscillating jet impingement zone, and notably, this region encompasses a larger expanse for the sweeping jet configuration with chevron as compared to the sweeping jet configuration without chevron, and the steady jet configuration. This disparity in behavior significantly impacts the cooling efficiency on the surface of interest, and the assessment of cooling efficiency is carried out by mapping the Nusselt number across the surface. Among the alternatives considered, the Chevroned Sweeping jet configuration outperforms the others both in terms of numerical values and the extent of coverage across the target surface. As for swirling jet the turbulent kinetic energy is higher than the conventional steady jet. The swirling effect created due to spiral structure forms an ‘S’ shaped pattern also seen in Figure 23 covers a larger area due to tangential velocity increasing the mixing rate with surrounding stationary fluid resulting in higher Nusselt number.

The Chevroned Sweeping jet case has a 19.23% Nusselt number percentage increase over the steady jet, a 2.73% increase over the sweeping jet without the chevron and 15.4% increase over the swirling jet. Furthermore, in the situation of Chevroned Sweeping jet, the target surface has lower temperatures than in the other arrangements as observed from Figure 46. This result supports the overall finding reported in Figure 18. and agrees with another studies of Tu et al. [89]. Figures 23 and 24 show the jet flow development for the steady jet without and with chevron along with swirling jet, two pairs of side vortex are very clear and are observed for this case.

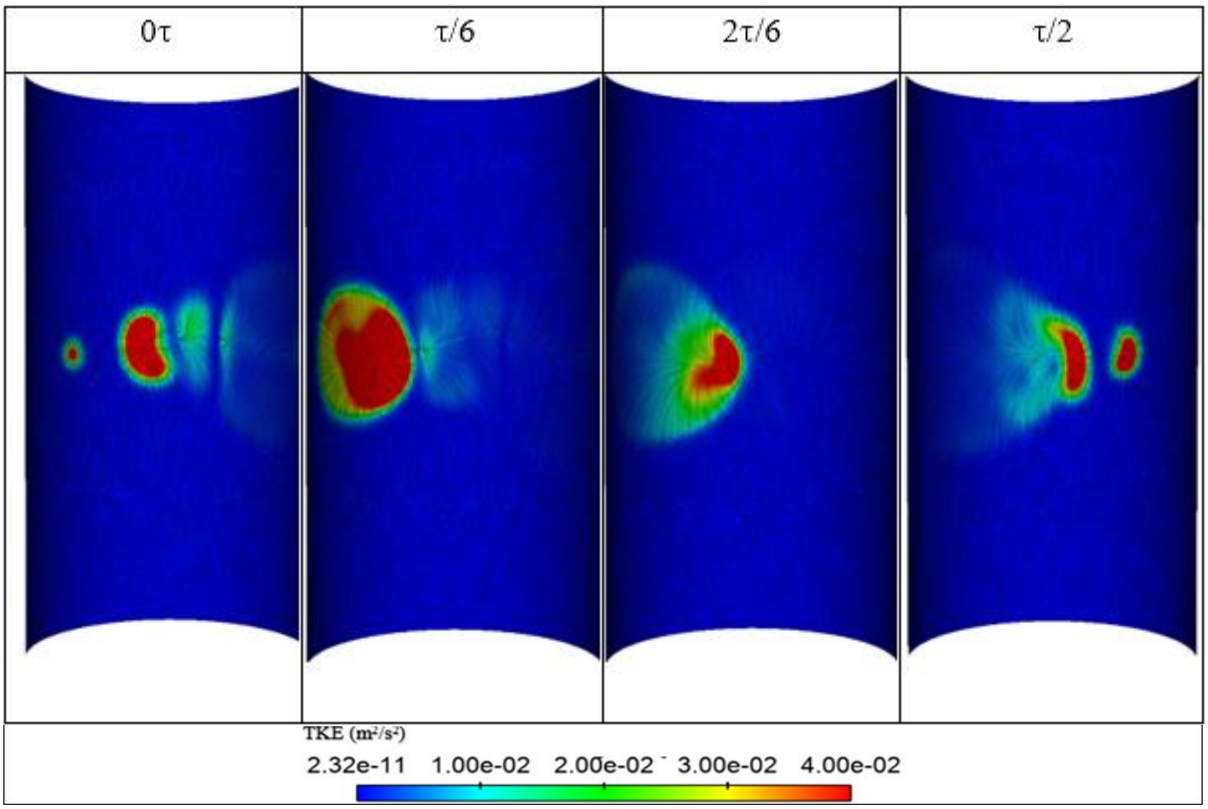

Figure 19: Turbulent Kinetic Energy contours on target surface for Sweeping jet

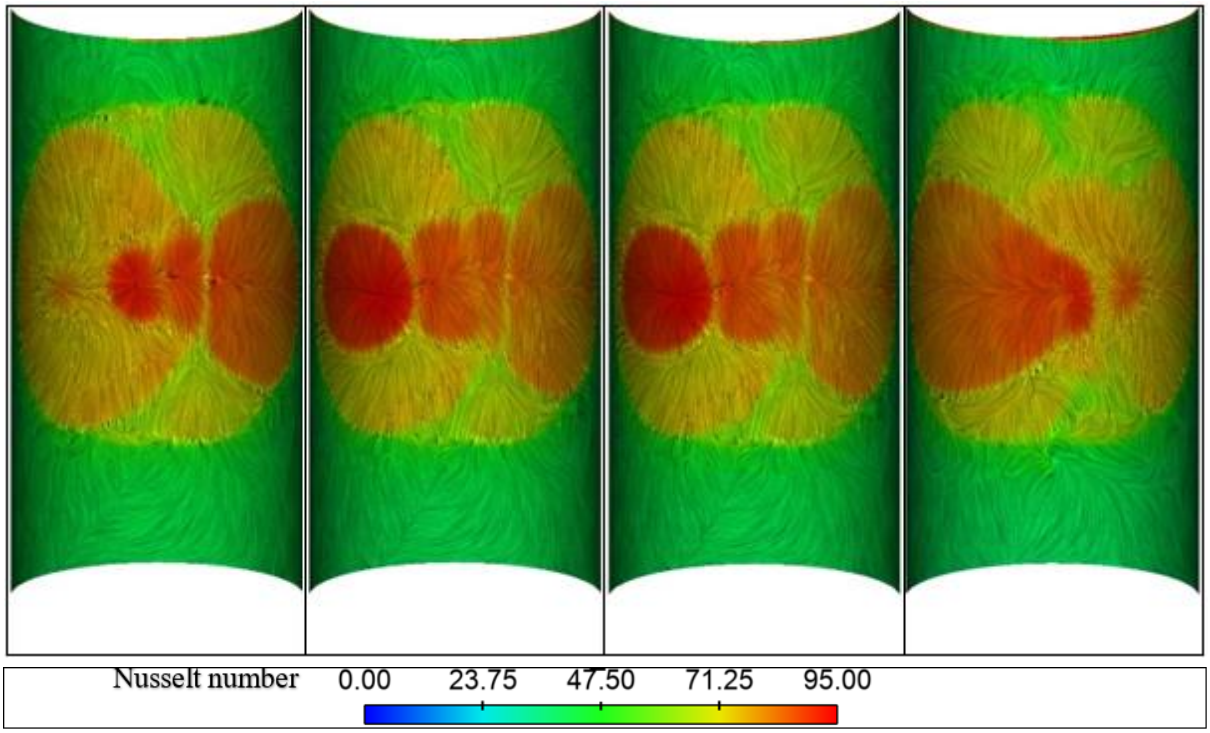

Figure 20: Nusselt number contours on target surface for Sweeping jet

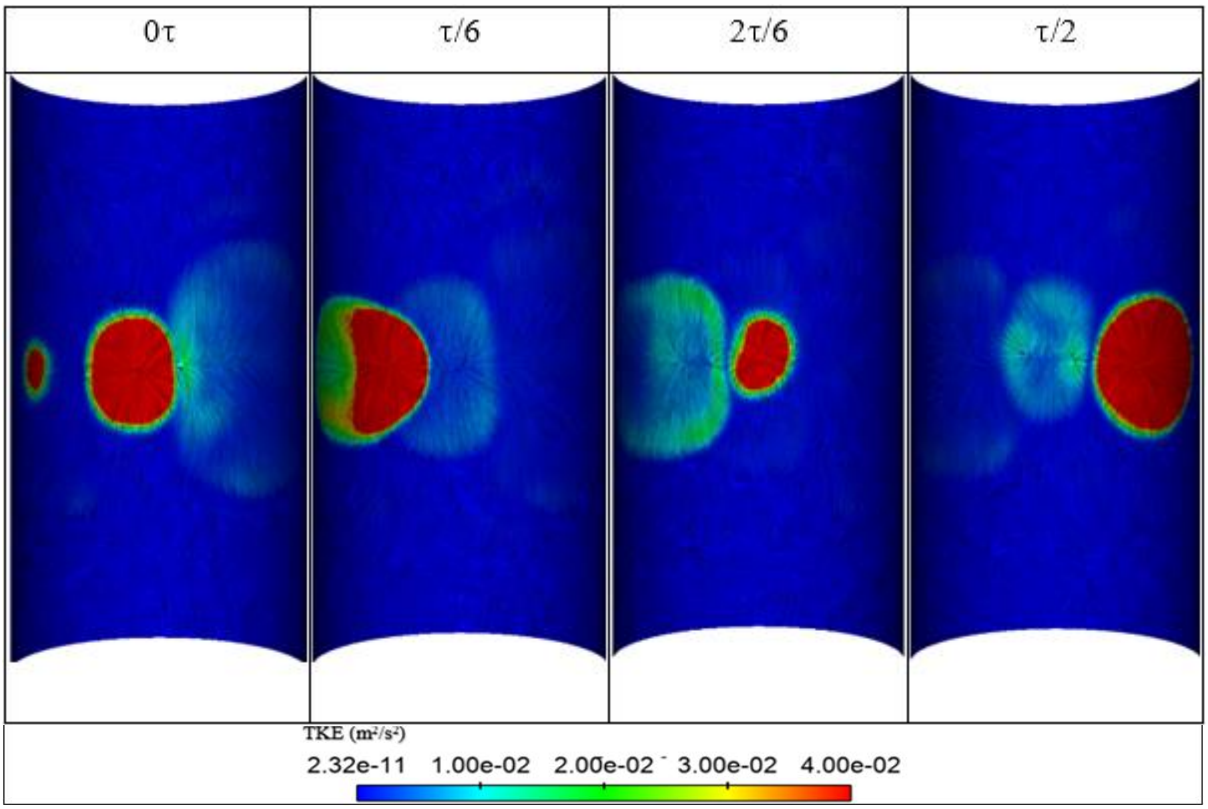

Figure 21: Turbulent Kinetic Energy contours on target surface for Chevroned Sweeping jet

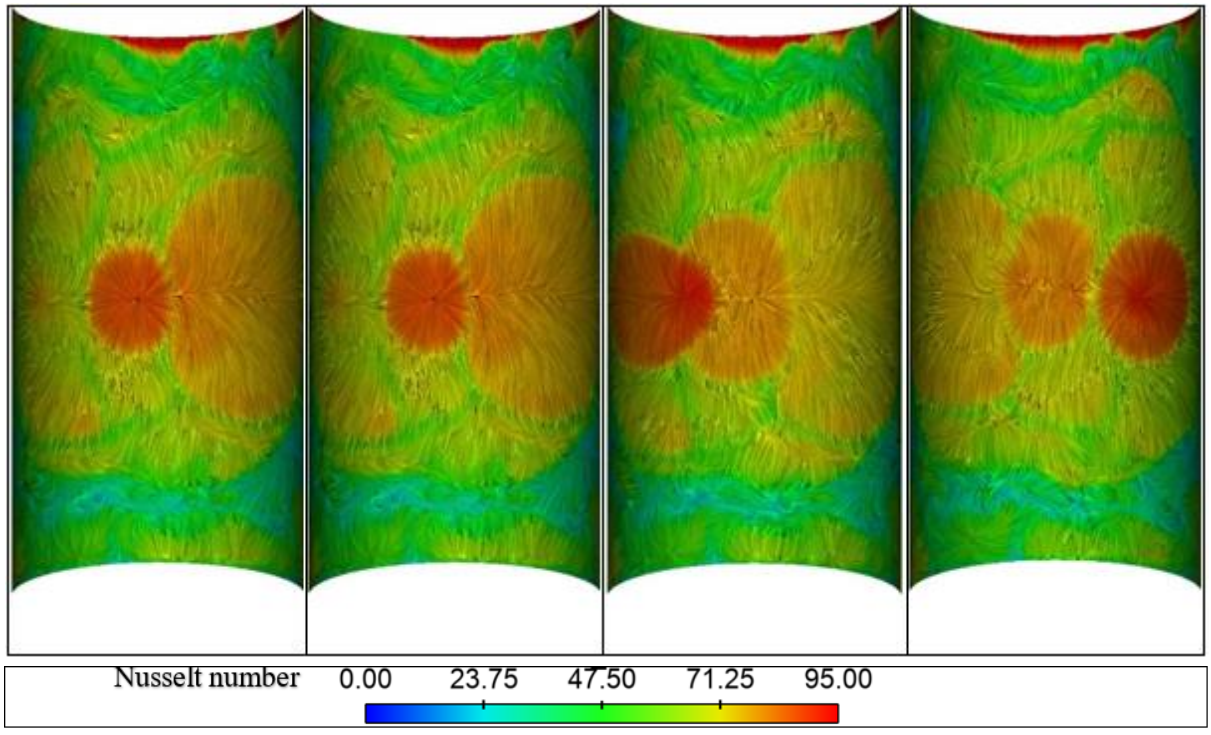

Figure 22: Nusselt number contours on target surface for Chevroned Sweeping jet

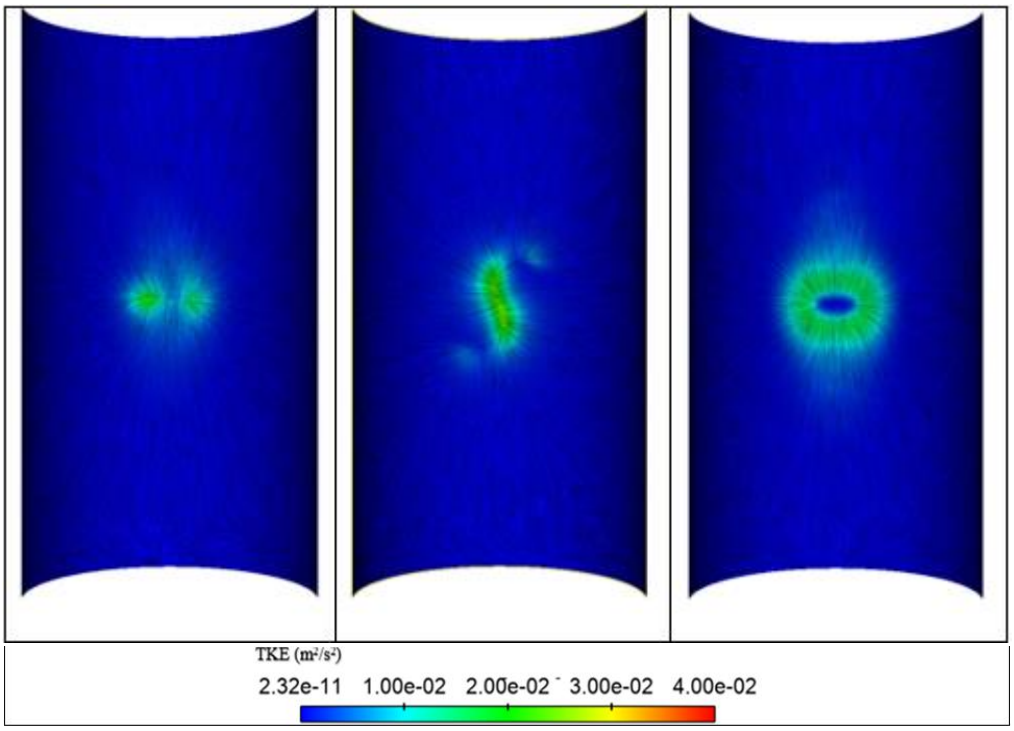

Figure 23: Turbulent Kinetic Energy contours for (a) Steady Jet (b) Swirling jet and (c) Chevroned Steady Jet

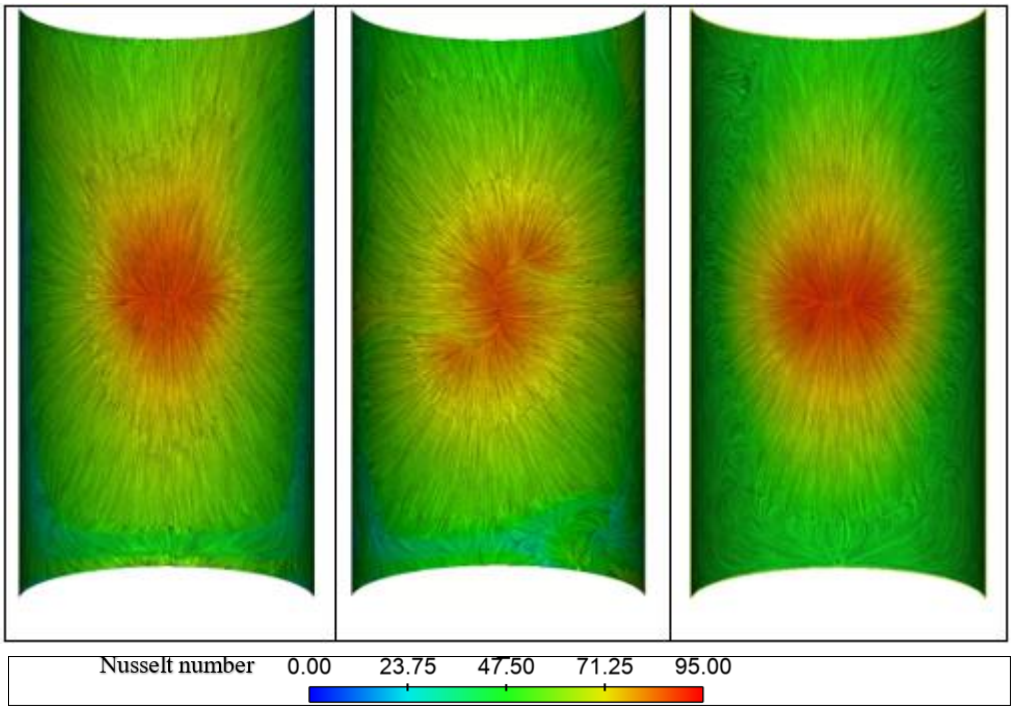

Figure 24: Nusselt number contour for (a) Steady Jet, (b) Swirling jet, (c) Chevroned Steady Jet

3.2.3 Flow Structure of Impinging Jets

This section attempts to grasp a better understanding of flow characteristics of all the jets., the “Q-Criterion” describing the vortex intensity of the flow field is introduced along with velocity contours with flow texture adapted from ENSIGHT 20 post-processor.

3.2.3.1 Velocity Contours

Figure 25 displays the velocity contours depicting a quasi-steady oscillating flow pattern for all four configurations. Specifically, cases (a) and (b) exhibit the sweeping jet and Chevroned Sweeping jet at time steps 0, $\tau/6$, $\tau/3$, and $\tau/2$. The oscillations observed in the sweeping jet operation stem from the Coanda effect, where the pressurized fluid from the power nozzle causes the jet to adhere to the adjacent side wall. This enables the fluid to enter the connected feedback loop through the feedback legs. Subsequently, the fluid initiates pressure waves that drive the power jet away from the sidewall, leading to its redirection towards the opposite wall. This cyclical process triggers oscillatory fluid motion at the throat exit [52].

At period 0τ, The jet impacts the right-hand-side corner of the leading edge, generating an imbalanced pressure situation in the feedback channel. Consequently, the left feedback channel experiences elevated pressure, leading to pressurization of the channel's flow and subsequent restriction of flow in the right feedback channel. Consequently, the jet impingement occurs primarily on the right-hand-side corner of the leading edge. In response, the flow within the mixing chamber starts adapting to the heightened pressure in the right feedback channel while simultaneously reducing the pressure in the left feedback channel at $\tau/6$ and $\tau/3$, this alteration in pressure dynamics prompts the jet's impingement to shift towards the left side of the leading edge due to the influence of inertia. In the $\tau/2$ period, a reverse flow pattern materialized, resulting in heightened pressure within the right feedback channel, obstructing the flow from the left feedback channel. Consequently, the jet's impingement shifted to the left-hand corner of the leading edge. The Chevroned Sweeping jet exhibited a similar behavior to the sweeping jet but demonstrated a higher degree of turbulence in the jet entrainment

region due to the intricate flow field. It's important to note that the swirling flow is not depicted in this view since the visualization only captures the vertical axial jet flow. The comprehensive perspective of the swirl effect is introduced in the subsequent section through the Q-criterion parameter, presenting a more comprehensive depiction of the swirl effect.

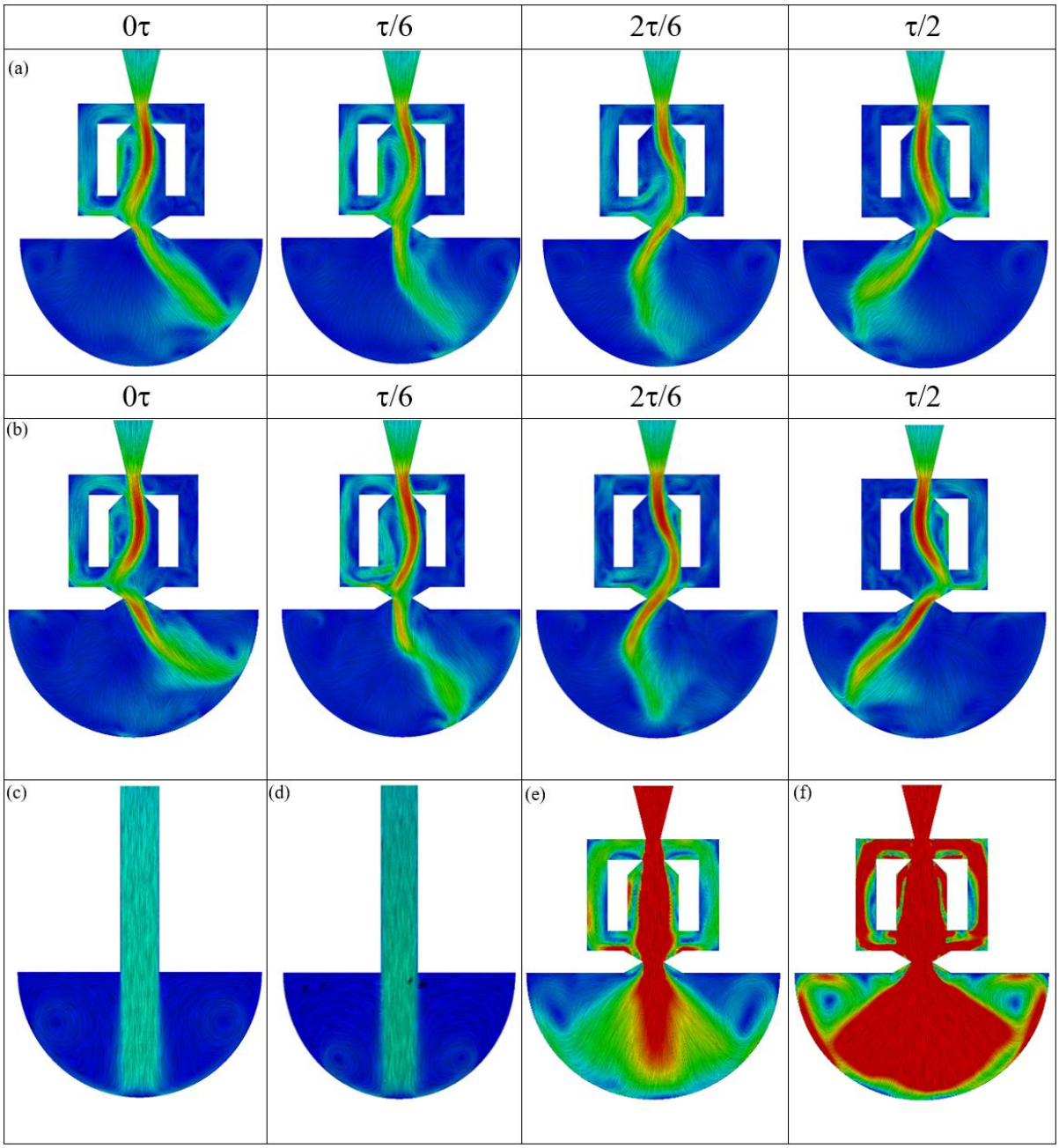

Figure 25: Flow depicted by velocity contours at different timesteps (half-cycle) with surface flow textures for (a) Sweeping jet (b) Chevroned Sweeping jet (c) Steady jet (d) Chevroned Steady jet (e) Mean velocity for Sweeping jet (f) Mean velocity for Sweeping jet

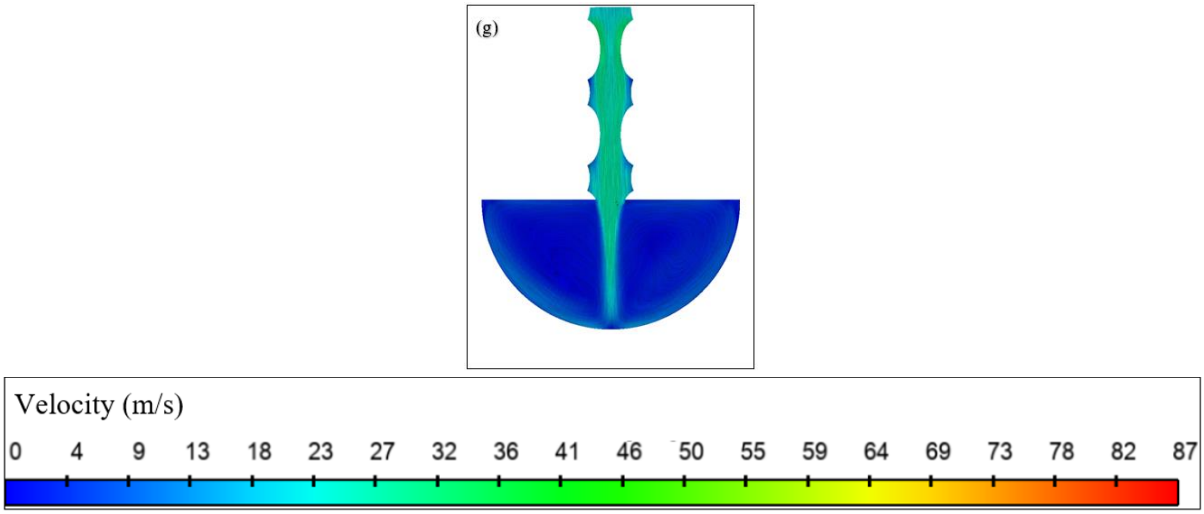

Figure 25: Flow depicted by velocity contours at different timesteps (half-cycle) with surface flow textures for (a) Sweeping jet (b) Chevroned Sweeping jet (c) Steady jet (d) Chevroned Steady jet (e) Mean velocity for Sweeping jet (f) Mean velocity for Sweeping jet (Continued)

3.2.3.2 Analyzing the Flow by Q-criterion Parameter

The vortex structure in the flow field is quantified by using axial vorticity rendering Q-criterion parameter. The parameter is used to describe the flow field vorticial structure within the jet flow and the target surface. The Q-criterion parameter is defined as follow:

$$Q = \frac{1}{2}\left(\bar{\Omega}_{ij}\bar{\Omega}_{ij} - \bar{S}_{ij}\bar{S}_{ij}\right) \tag{16}$$

$$\bar{\Omega}_{ij} = \frac{1}{2}\left(\bar{u}_{i,j} - \bar{u}_{j,i}\right) \tag{16a}$$

$$\bar{S}_{ij} = \frac{1}{2}\left(\bar{u}_{i,j} + \bar{u}_{j,i}\right) \tag{16b}$$

Where $\bar{\Omega}_{ij}$ *and* $\bar{S}_{ij}$ are the vorticity and the strain tensors respectively.

The flow structure for chevroned and non-chevroned jet mainly differs in the type of vortex that is produced. The development of vortex structures is quite complex for sweeping jet as compared to a steady impinging jet, as the steady jet offers a more stable and predictable behavior for shredding and paring phenomenon, while sweeping jet impingement generates variances in both shredding and paring. The addition of

chevrons to sweeping jet altered its flow structure significantly as observed from Figure 26 (b) and Figure 26 (e), the fluid when it is initially expelling from the Chevroned Sweeping jet, a striped shaped structure to the flow is added from the zig zag edges of chevron. A bell-shaped mushroom-like structure flows out from the Chevroned Sweeping jet while an elliptical coherence structure flows from the onset of sweeping jet at t= 0.0005s observed in Figure 26 (b) and Figure 26 (e). After impinging at the target surface at t=0.0053s in Figure 27 (b) and Figure 27 (e) the coherent structures involve shredding phenomenon which was observed to be more enhanced in Chevroned Sweeping jet due to altered flow dynamics caused by staggered nozzles. This could be also explained by obvious hair pin vortex formations in Figure 27 (e) for Chevroned Sweeping jet as compared to sweeping jet in Figure 27 (b). As the sweeping jet oscillates the primary vortex ring reaches along the lateral section of target surface. Shredding of the primary vortex adds to hair pain vortex structures and as the Coanda effect kicks in and switches the fluid from one feedback channel to the adjacent, flow is diverted to an opposite direction which involves mixing up of primary vortex with hair pin vortex structures of previous flow direction leading to better mixing of fluid for sweeping impinging jet over the target surface as compared to steady impinging jet. As discussed by Lyu et al. [66], the Chevroned Steady jet is similar in formation of primary toroidal vortex and paring of hair pin vortex over the leading-edge blade observed in Figure 27 (a) and Figure 27 (d) to the steady jet. The difference is vivid in downstream flow after impingement due initiation of striped structures by chevrons which leading to a more turbulent structure as seen in Figure 27 (a) and Figure 27 (d).

Figures 26 and Figure 27 display the flow structure onset at the jet exit and the at the moment of impingement over the target surface, respectively, for all studied jet configurations. The flow structure is depicted by the Iso surface with Q-criterion of $4x10^6$ s^{-1}. Regarding the onset of the jet exit flow structure, a more defined structure is observed for the sweeping jet in comparison to the steady jet. And as the jet flow progresses towards the target surface, the sweeping jet exhibits a significantly enhanced vorticial structure due to its higher level of entrainment caused by the elevated turbulent levels. This contrasts with the steady jet, where a less pronounced vorticial structure is observed at the target surface.

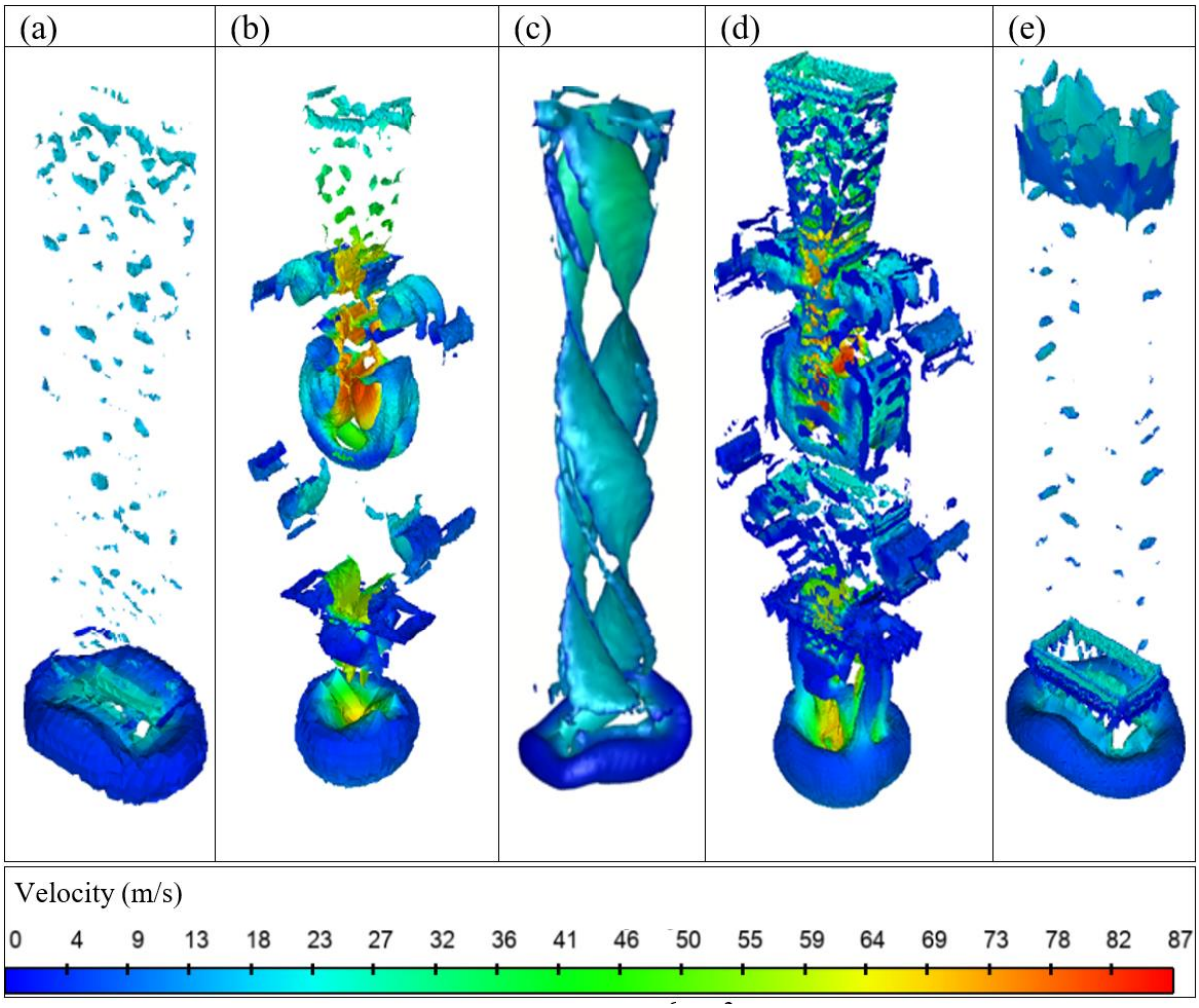

Figure 26: Iso-surface with Q-criterion at $4x10^6$ $1/s^2$ for velocity contours at equal initial time-steps before impinging the curved plate (a) Steady jet (b) Sweeping jet (c) Swirling jet (d) Steady jet with chevrons (e) Sweeping jet with chevrons

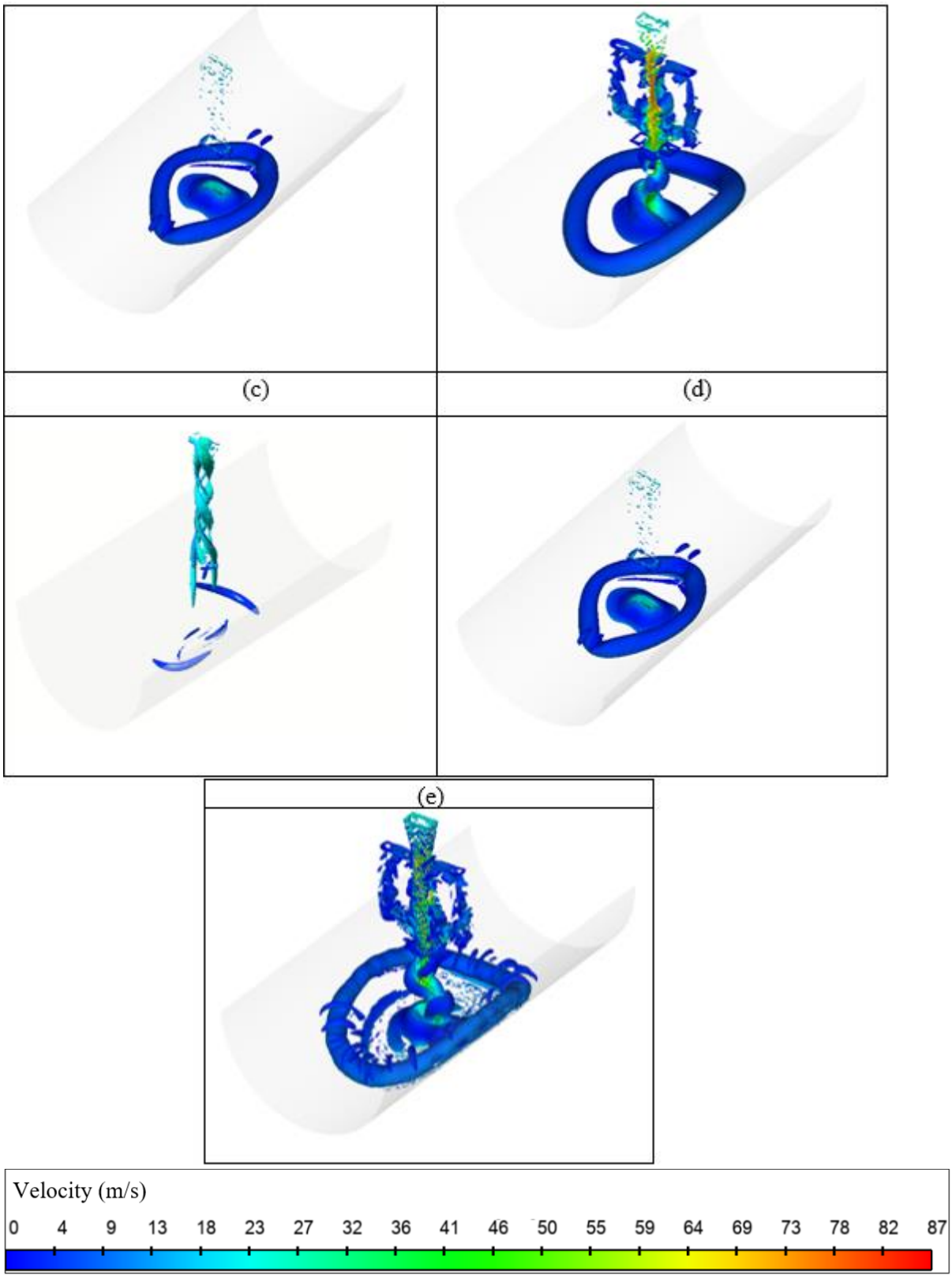

Figure 27: Iso-surface with Q-criterion at $4x10^6$ $1/s^2$ for velocity contours at equal time-steps during impinging the curved plate (a) Steady jet (b) Sweeping jet (c) Swirling jet (d) Chevroned Steady jet

Referring to Figure 28, for the steady jet case, with and without chevrons, the main and secondary vorticial structures are displayed with a lower turbulence intensity level at the target surface. This intensity of vortex of the steady jet is verily low when compared to swirling jet while the vortex structure of Chevroned Steady jet and swirling jet is contrasting, however the heat transfer enhancement is close enough which will be introduced in heat performance section. The spiral channel for swirling jet creates vortex flow with higher intensity which along with the axial flow ejects from the nozzle forming a chaotic vortical structure that effectively enhances the heat transfer rate as compared to steady jet.

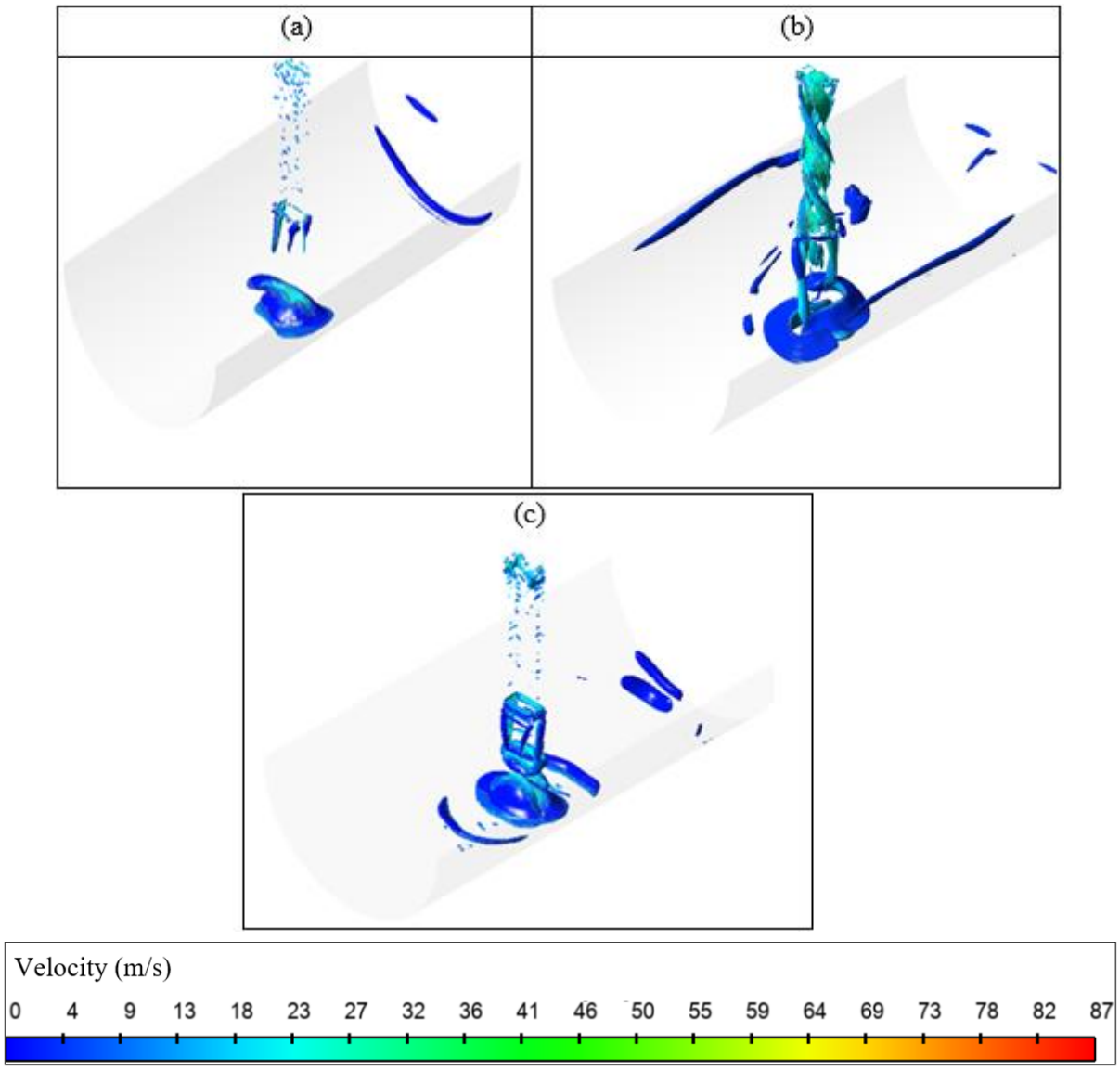

Figure 28: Iso-surface with Q-criterion at $4x10^6$ $1/s^2$ for velocity contours after attaining convergence for (a) Steady jet (b) Swirling jet (c) Chevroned Steady jet

As observed from Figure 29 and Figure 30, the Q-criterion of velocity demonstrates the splashing effect of sweeping and Chevroned Sweeping jets. As in the sweeping jet, fluid spends it's much time span being attached to either wall of mixing chamber and as the fluid detaches and attaches to adjacent wall this creates a splashing oscillating fluid. The splashing effect is quite stable in the sweeping jet until any disturbance is induced. The serrated trailing edge geometry induces vortices along the longitudinal span of chevron/tabs for Chevroned Sweeping jet enabling better mixing of fluid to cover much larger area for Chevroned Sweeping jet than sweeping jet as shown in Figure 30. Thereby a pattern of temperature and Nu contours which is evenly spreading through the curvature of the leading-edge is observed for Chevroned Sweeping jet. In summary, the Chevroned Sweeping jet owing to higher turbulence fluctuations introduced extra energy fluxes affecting the overall heat transfer process exhibiting highest average Nu value and minimum average temperature value of the leading-edge blade. In the case of the sweeping jet, Figure 29 and Figure 30 illustrates four periods representing a half cycle of oscillation at 0, $\tau/6$, $\tau/3$ and $\tau/2$ respectively. The reported results demonstrate the existence of a clear main vortex at the centerline along axis Z/D of the target surface. This vorticial structure is more pronounced for the cases at $\tau/3$ and $\tau/2$. Along the sweeping jet path curvature axis S/D, a secondary vortex is observed moving with sweeping jet path. A similar behavior is observed for the Chevroned Sweeping jet, as shown in Figure 30 due to the turbulence generated by the chevron nozzle exit, a busier vorticial structure is noticed.

Overall, when comparing the sweeping jet, especially with a Chevroned Sweeping jet with the other jets, a much more complex flow field is observed. Consequently, because of this complex flow field structure being sprayed over the centerline and in the direction of the oscillation arc, a more uniform cooling effect and a lower occurrence of hot spots are expected over the target surface, as compared to the steady jet.

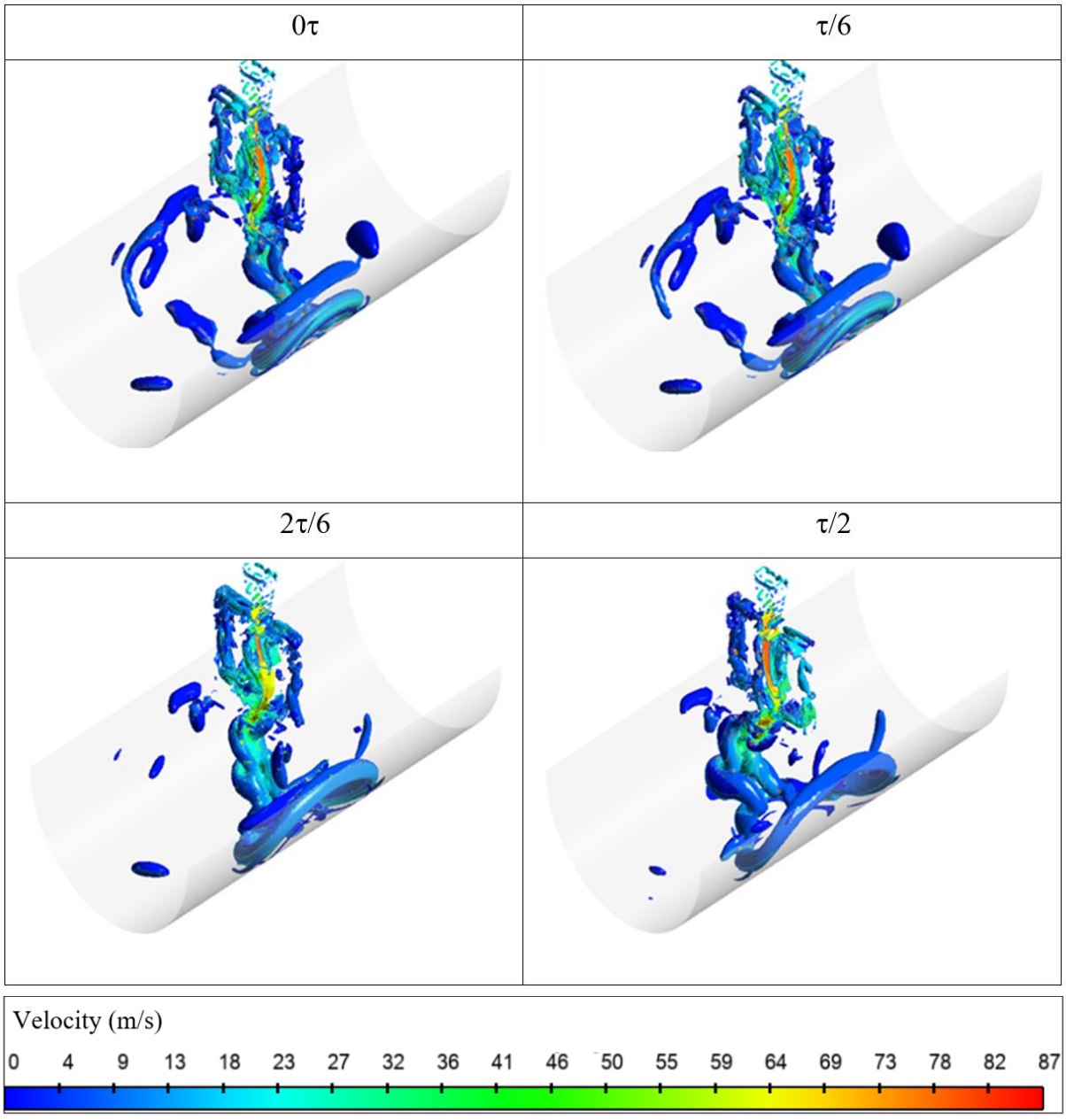

Figure 29: Iso-surface with Q-criterion at $4x10^6$ $1/s^2$ for velocity contours after attaining stable oscillating nature for Sweeping jet for half cycle

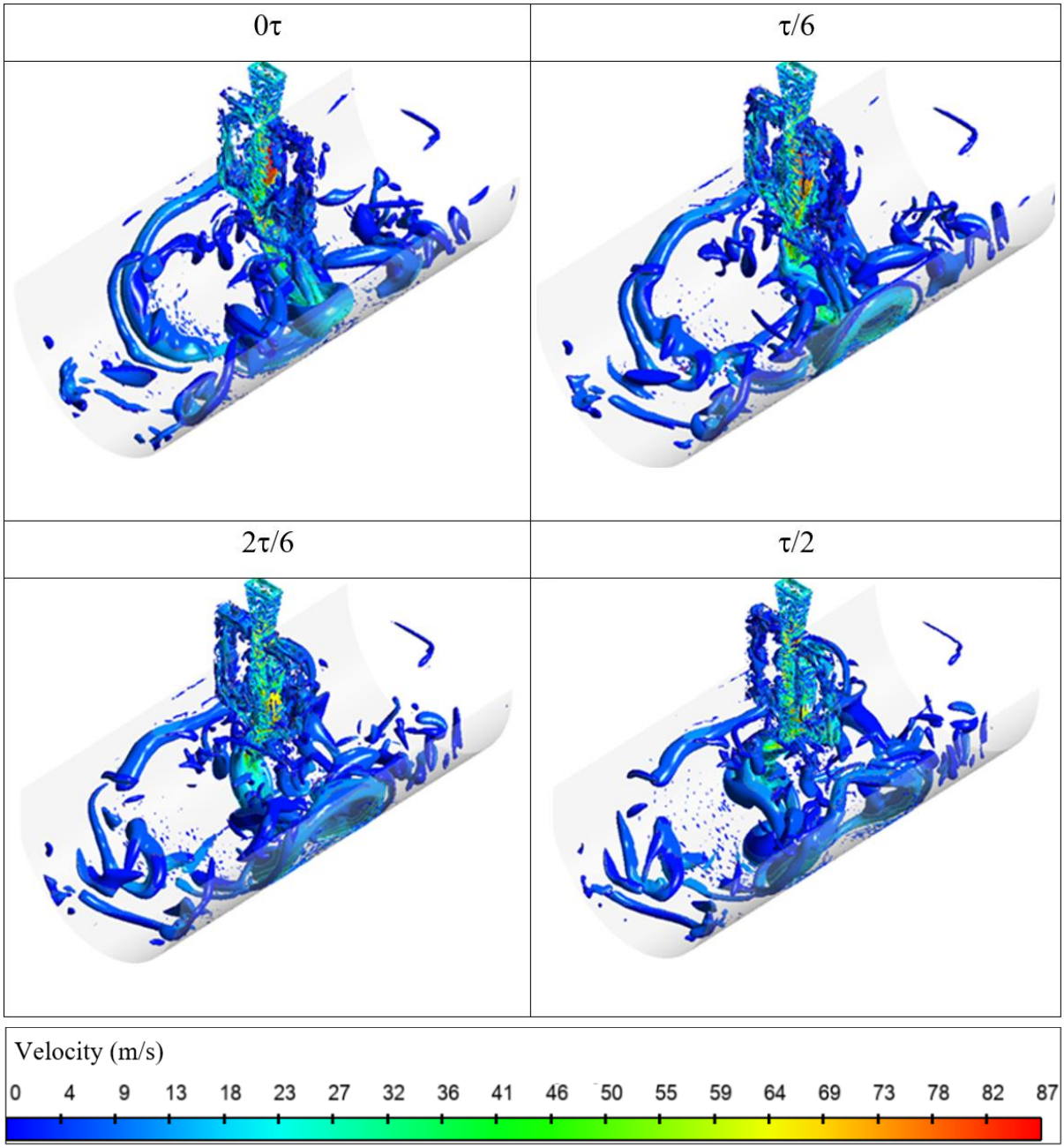

Figure 30: Iso-surface with Q-criterion at $4x10^6$ $1/s^2$ for velocity contours after attaining stable oscillating nature for Chevroned Sweeping jet for half cycle

3.3 Impingement Flow behavior of Impinging Jet at Rotatory Conditions

The leading-edge turbine blade component is operated in a rotating environment, understanding how rotation affects the heat transfer performance of these potential jets is crucial as the centrifugal force and the Coriolis force induced by rotation influences the flow field. The jet deflection or bending is the significant flow alteration observed due to the interaction between the pressurized downstream flow and strong Coriolis force.

The flow behavior of CSJ is as predicted i.e., when the rotational condition is applied flow moves toward the pressure side due to high squeezing of jet flow impinging toward the pressure side. At a lower rotational condition of 3000 RPM, the vortex formed inside the internal flow isn't strong enough to squeeze the jet flow towards pressure side as observed from Figure 31 (b). The flow is more pronounced towards the suction side. As the rotational condition is increased to 10,000 and 15,000 RPM, this vortex intensifies and squeezes the internal jet flow such that the impinging action is now directed towards the center line and pressure side seen in Figure 32 (c) and Figure 32 (d). A note must also be taken here to better grasp the heat transfer performance of steady jet in upcoming section when its rotational condition increases i.e., the peak velocity of jet increases due to squeezing and the flow is more pronounced towards pressure side of the leading-edge blade as observed from Figure 32.

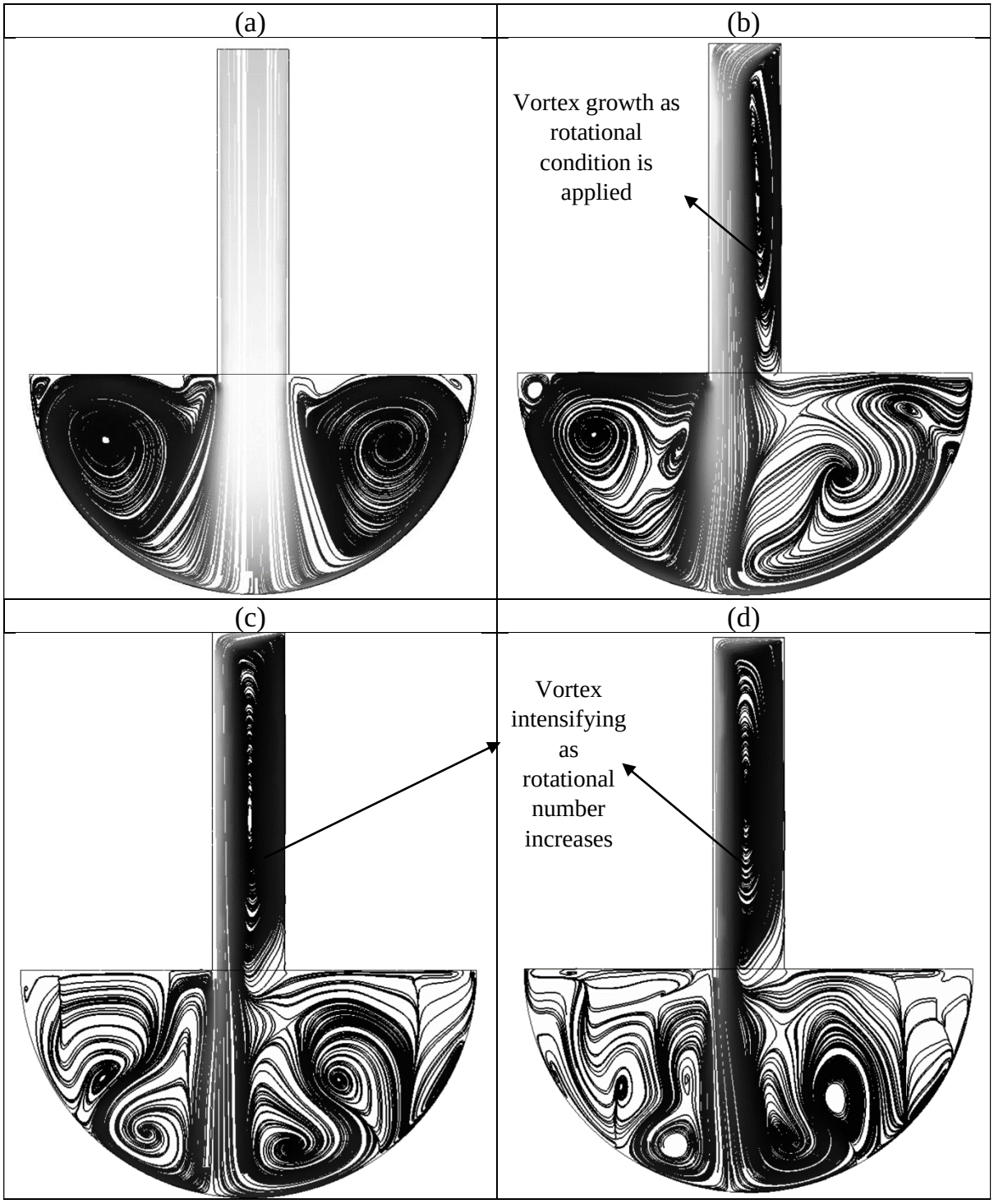

Figure 31: Streamlines depicting development of vortex near the internal flow in Steady jet at (a) Stationary condition (b) 3000 RPM (c) 10000 RPM (d) 15000 RPM

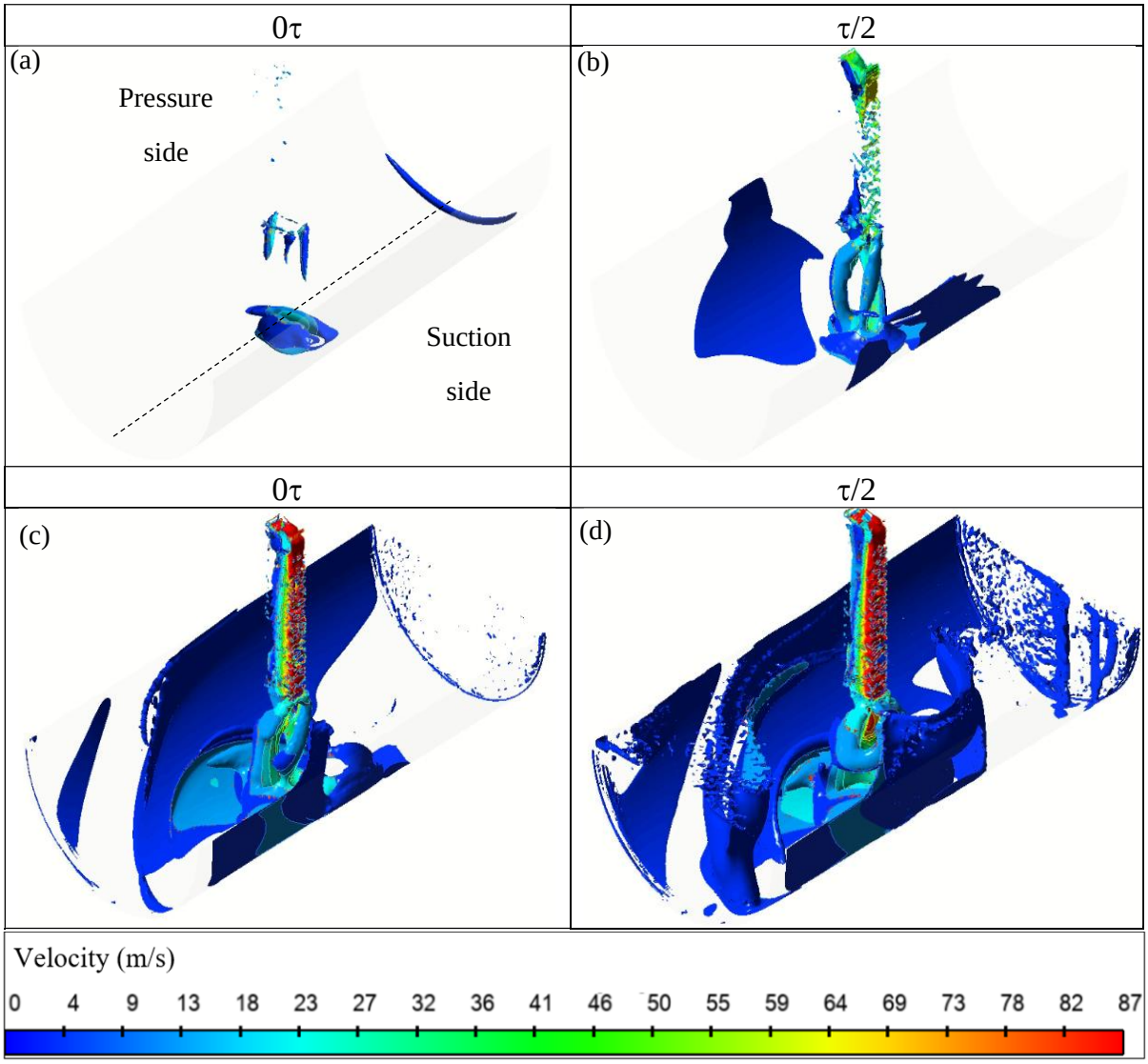

Figure 32: Iso-surface with Q-criterion at $7x10^6$ $1/s^2$ for velocity contours related to Steady jet at (a) Stationary condition (b) 3000 RPM (c) 10000 RPM (d) 15000 RPM

For sweeping jet the Coriolis force causes secondary recirculation region near the inlet of the jet as shown in Figure 34 i.e., confirmed by similar investigations by Hossain et al. [79] and Deng et al. [90]. A resemblance in our study and Deng et al. [90] report was observed that as the rotational number increases the strength of secondary vortex growing in the internal flow field of sweeping jet. The growth region of secondary vortex contrasted with Hossain et al investigation where they reported this vortex to be appearing in the feedback channels only and further stated no discernible difference between the stationary and rotating cases. They concluded that inherently oscillating nature of sweeping jet cancels out the unstable effect Coriolis forces produces. The only viable explanation for this discrepancy although our study is

working on a similar mass flow rate and rotational condition, could be the difference in geometrical structure and dimensions that contributes to higher Reynolds number for Hossain et al. [79] case. This could be also supported by Safi et al. study [22] in their investigation on rotational effect at different Reynolds number values. They stated that rotation had a clear effect on heat transfer rate at lower Reynolds number, that diminished as the Reynolds number increased that was evidently supported by the observed flow and produced pressure fields.

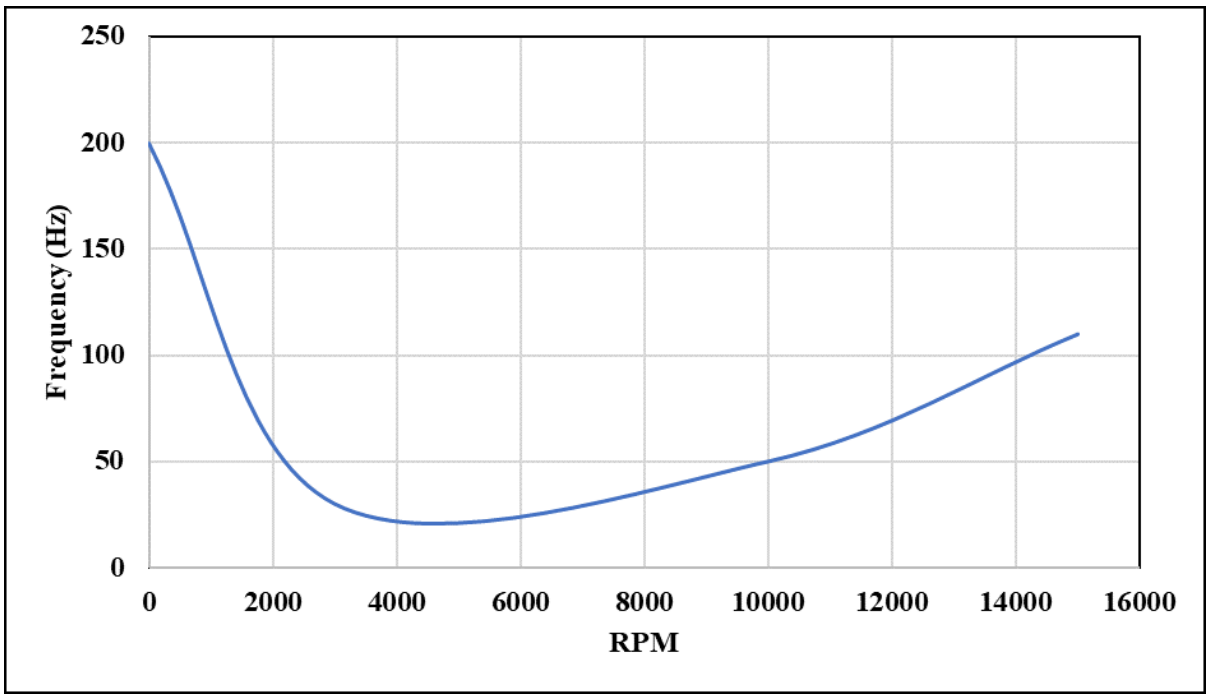

Figure 33: Peak oscillation frequency for Sweeping jet measured at throat of nozzle as function of RPM.

Nevertheless, our study at jet hydraulic Reynolds number of 12000 for sweeping jet indicates presents of strong vortex right near the inlet region. This causes jet deflection near the converging section of inlet. At rotational condition of 3000 RPM this force is strong enough to squeeze the incoming fluid thereby pressurizing it more and increasing the peak velocity of incoming fluid. For this rotational condition, the frequency of the jet drops to the minimum value of nearly 30 Hz while the spreading angle ‘θ’ almost remains the same. As discussed, upon increasing the rotational number strength of the secondary vortex further increases impacting on incoming fluid. For a sweeping jet, the primary vortex is already formed due to the Coanda effect owing to

its design, responsible for driving the flow into feedback channel. This intensifies along with the secondary vortex and pressurizes the incoming fluid such that its flow is directed towards the inner section of feedback channel near the pressure side of the turbine blade. It allows fluid to flow into feedback channel near the suction side and causes the flow output from sweeping jet nozzle only towards the suction edge of the leading-edge blade. This behavior is contrary to the steady jet and swirling jet where rotation causes the fluid flow directed towards the pressure side of leading-edge blade. The sweeping jet has similar behavior but due to presence of feedback legs, the flow is directed towards the opposite channel causing the flow to be oriented towards the suction side of leading-edge blade. The impact on spreading angle 'θ' as the rotational number increases is severed as the flow is now restricted to going through only one of the channels that restricts the spreading span. The frequency calculated at the exit of throat, however, starts to rise as now the spreading area is decreased with increased peak velocity of the fluid as shown in Figure 33. The direct impact of impingement is reduced as the rotational condition is raised. This could be observed vividly from Figure 34.

For comparative understanding Figure 34 and Figure 35 describe then streamlines and Q-criterion iso-surface parameter for sweeping jet at stationary condition and at 3000 RPM for half cycle. As for 10000 RPM and 15000 RPM, the spreading area is sparse and therefore only extreme end of sweeping is displayed. A key observation for sweeping jet at 10000 and 15000 RPM is that it behaves as tangential/side impinging jet due to flow directed towards one end of the leading-edge which is leaving from angled end of exit of sweeping jet nozzle.

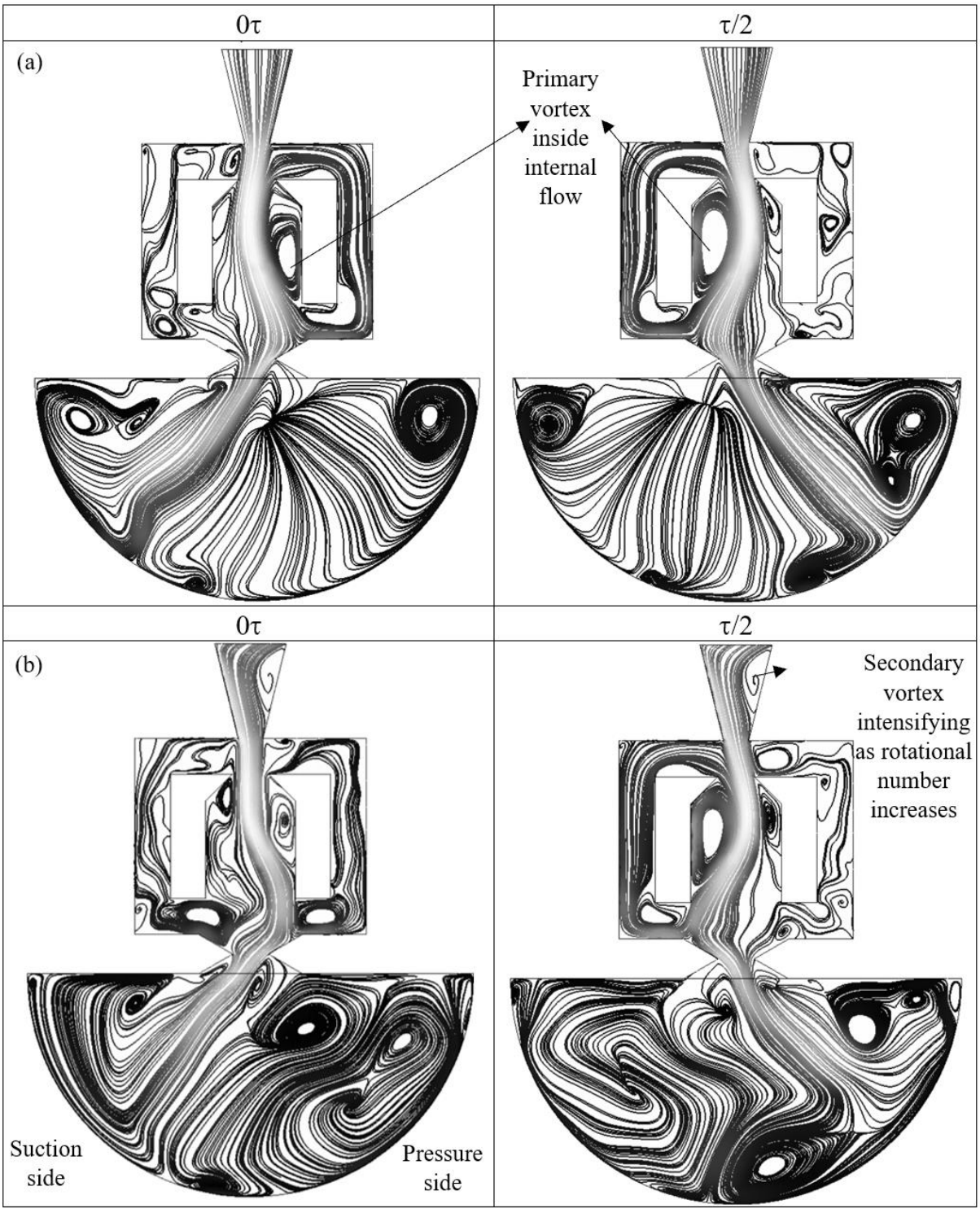

Figure 34: Streamlines depicting primary and secondary vortex of internal flow in Sweeping jet at (a) Stationary condition (d) 3000 RPM (c) 10000 RPM (d) 15000 RPM

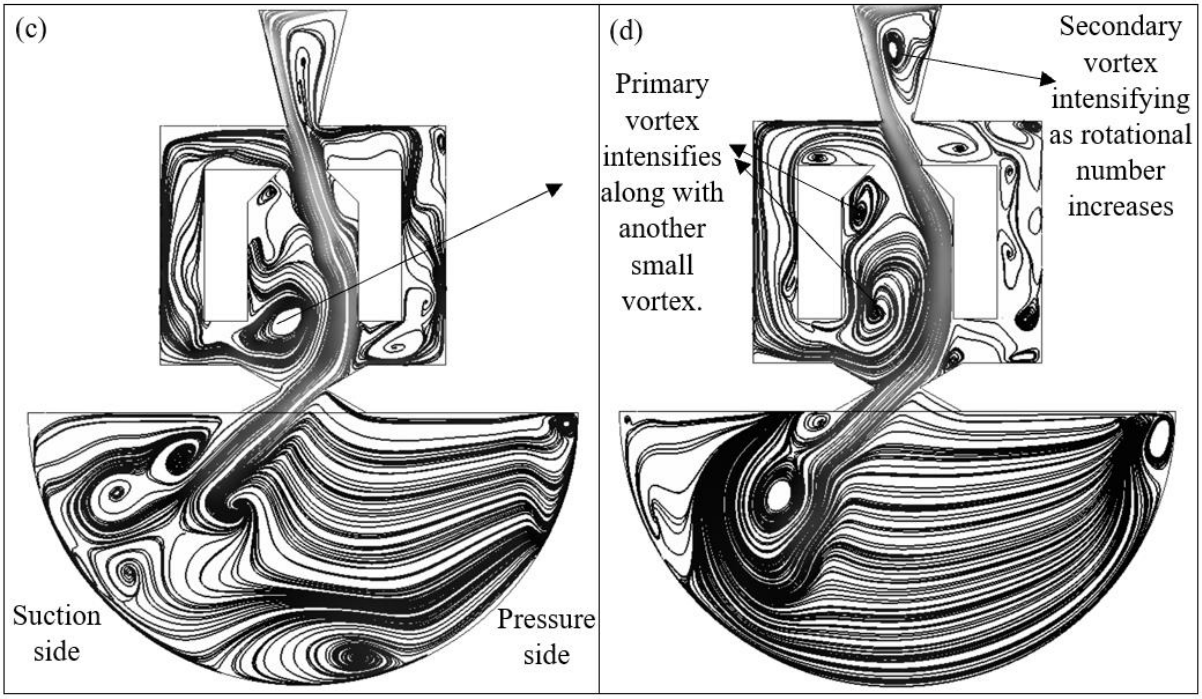

Figure 34: Streamlines depicting primary and secondary vortex of internal flow in Sweeping jet at (a) Stationary condition (d) 3000 RPM (c) 10000 RPM (d) 15000 RPM (Continued)

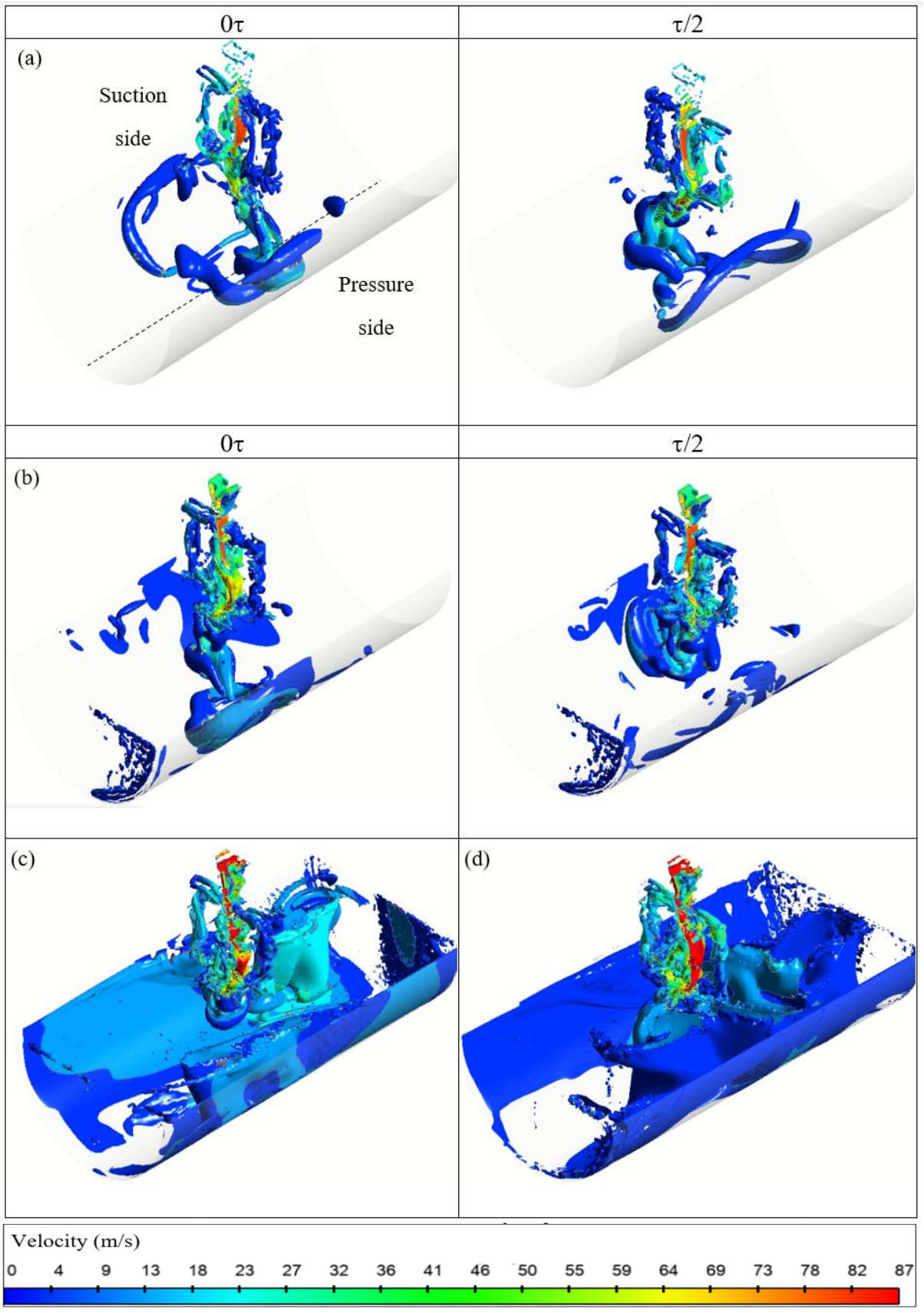

Figure 35: Iso-surface with Q-criterion at $7x10^6$ $1/s^2$ for velocity contours after attaining stable sweeping for Sweeping jet at (a) Stationary condition (b) 3000 RPM (c) 10000 RPM (d) 15000 RPM

The swirling jet performs the weakest of all the jets when subjected to rotational condition. Downstream the channel it is carried away by the Coriolis force towards the pressure side of the leading-edge blade and it underperforms even when compared to steady jet as seen in Figure 36 and Figure 37. The reason for the sharp decline in the performance of swirling jet could be attributed to low axial velocity and high swirl velocity. The rotating swirls can't withstand the strong Coriolis force and are swayed away towards the rotational direction i.e., towards the pressure side.

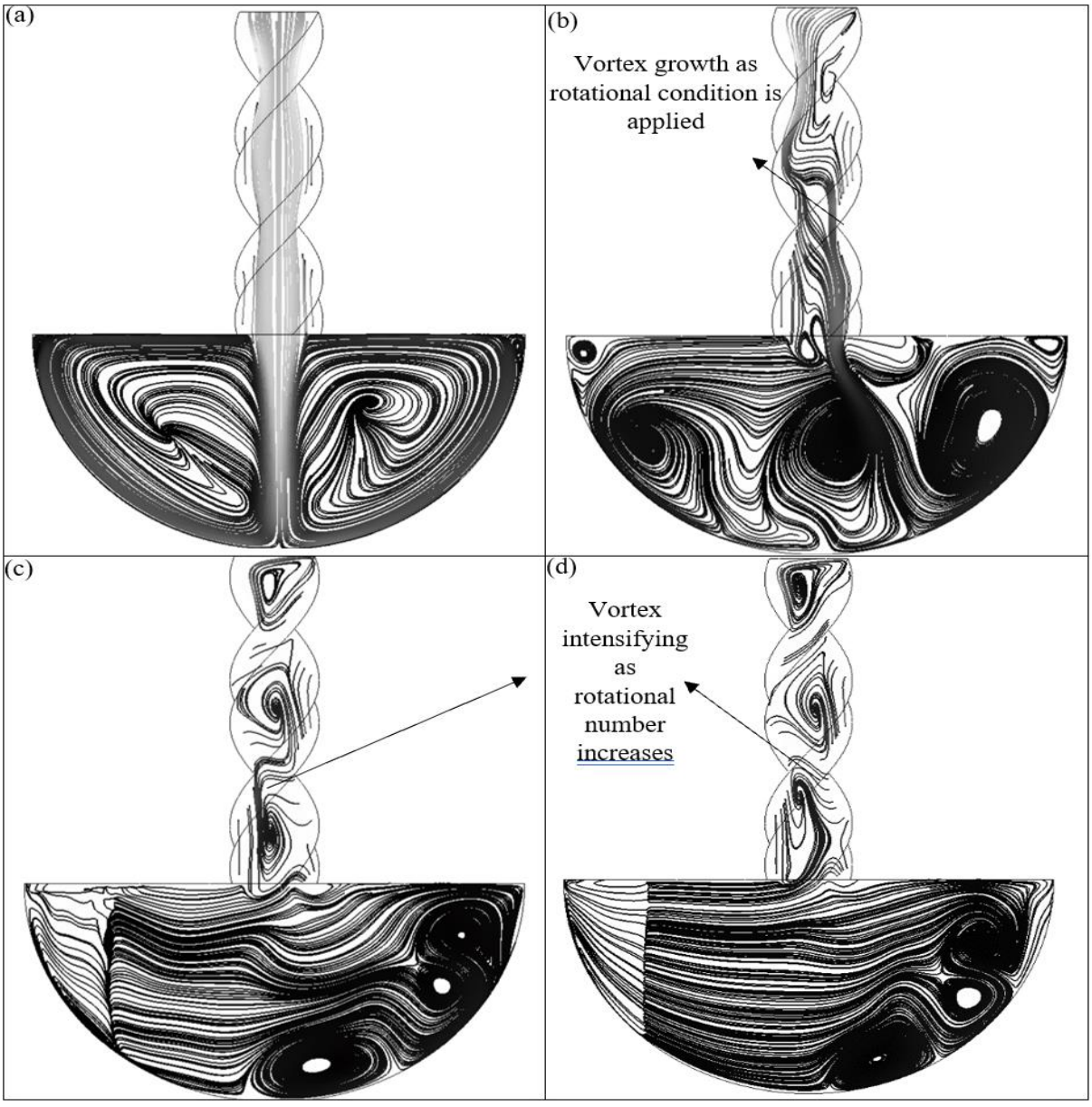

Figure 36: Streamlines depicting vortex development in Swirling jet at (a) Stationary condition (b) 3000 RPM (c) 10000 RPM (d) 15000 RPM

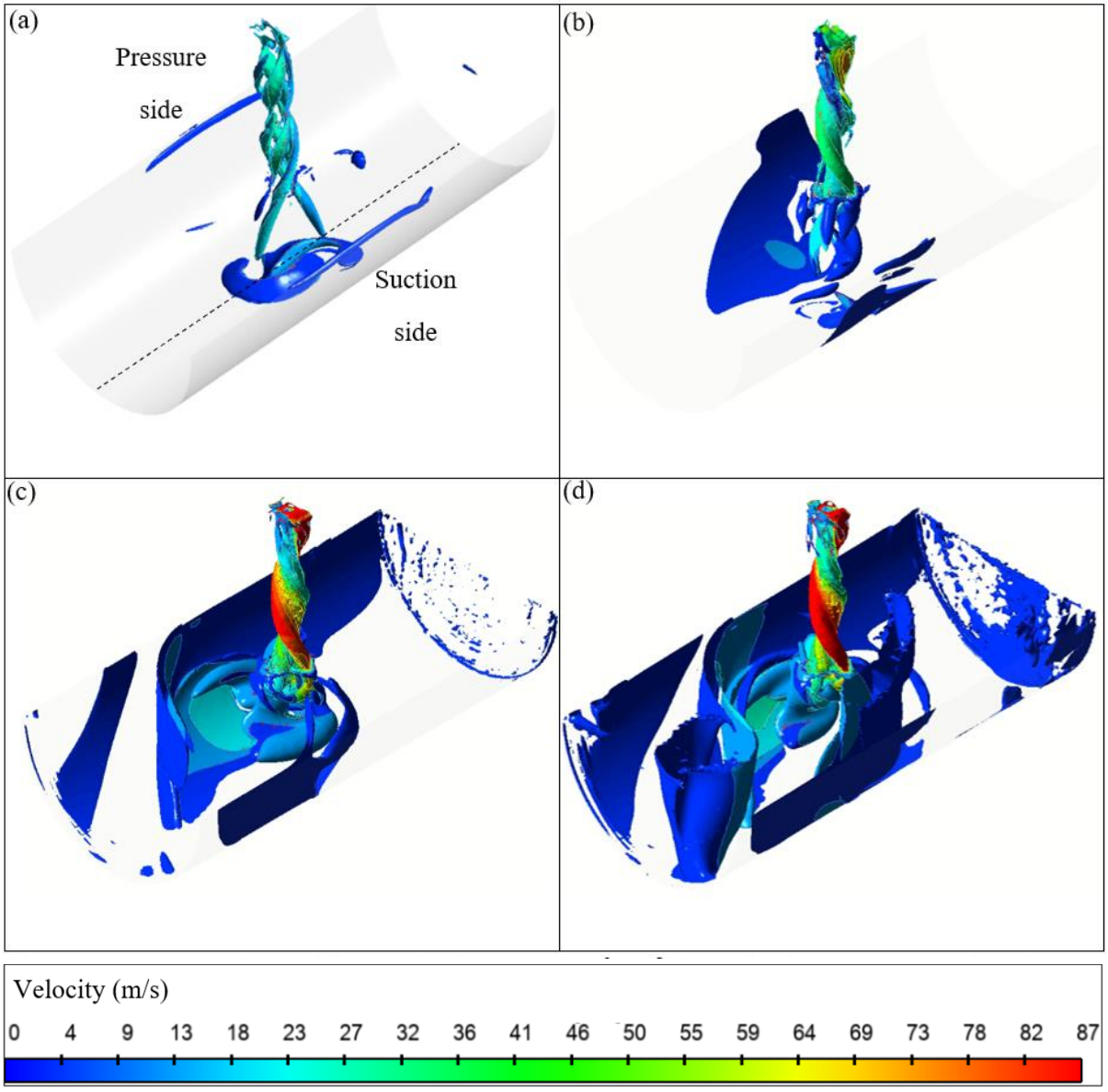

Figure 37: Iso-surface with Q-criterion at $7x10^6$ $1/s^2$ for velocity contours related to Swirling jet at (a) Stationary condition (b) 3000 RPM (c) 10000 RPM (d) 15000 RPM

The development of vortex characteristics for Chevroned Steady jet upon subjected to rotational conditions is like the steady jet. However, the recirculation region near the impinging area is strengthened upon discharge downstream from the nozzle when subjected to rotation. The disturbance created for the Chevroned Steady jet is incremented due to the presence of tabs/chevrons for Chevroned Steady jet depicted in Figure 38 (c) and Figure 38 (d) also compared to steady jet in Figure 31 (c) and Figure 31 (d). The excessive recirculation leads to the formation of stagnation points on the surface, where the flow velocity is nearly zero. This results in inefficient

cooling at these points since there is minimal convective heat transfer leading to uneven cooling across the surface due to localized hotspots and cold spots, leading to an uneven temperature distribution as shown in Figure 39. Hence, the heat transfer performance decreases as the rotational condition are applied for Chevroned Steady jet.

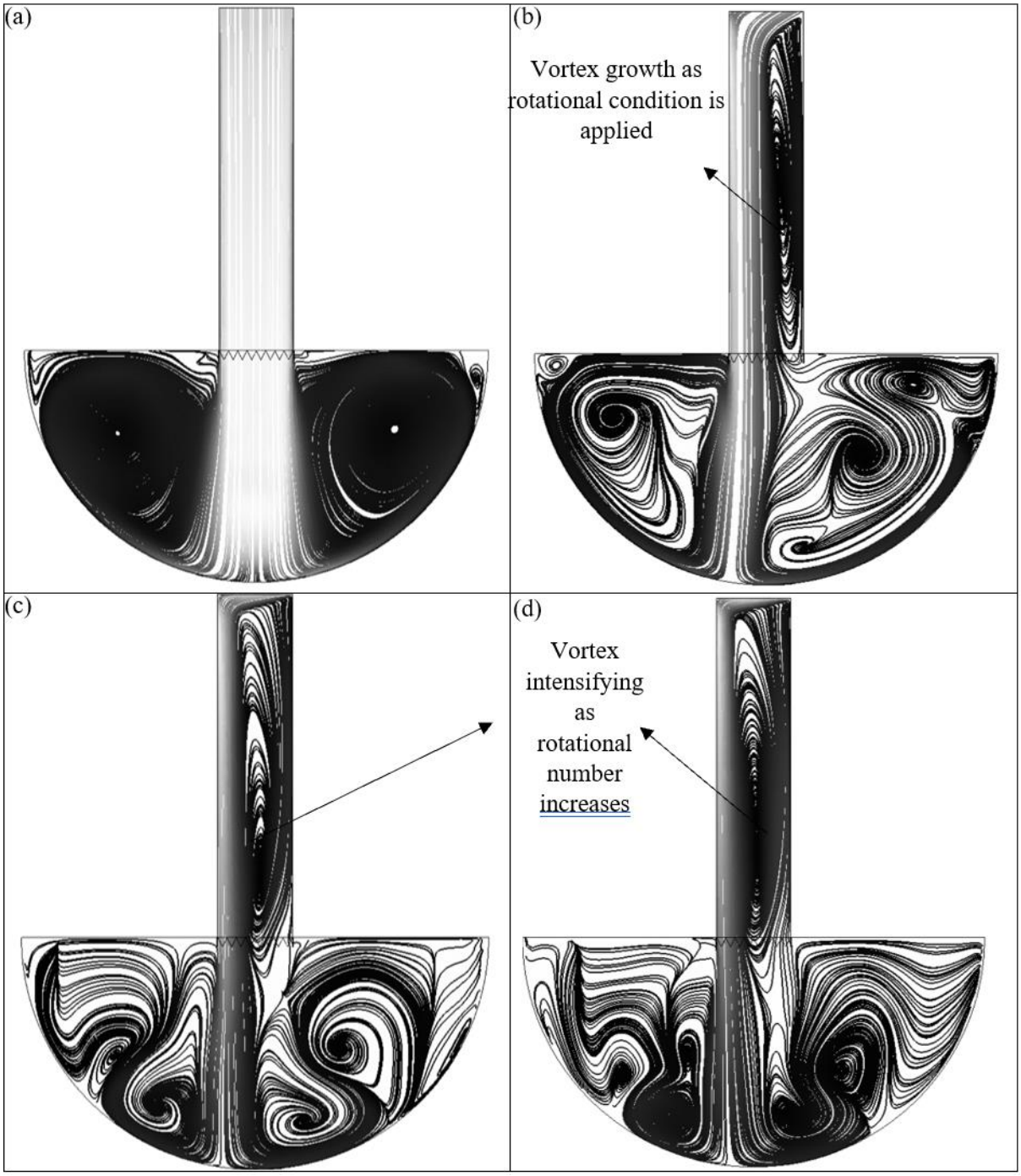

Figure 38: Streamlines depicting vortex development in internal flow region for Chevroned Steady jet at (a) Stationary condition (b) 3000 RPM (c) 10000 RPM (d) 15000 RPM

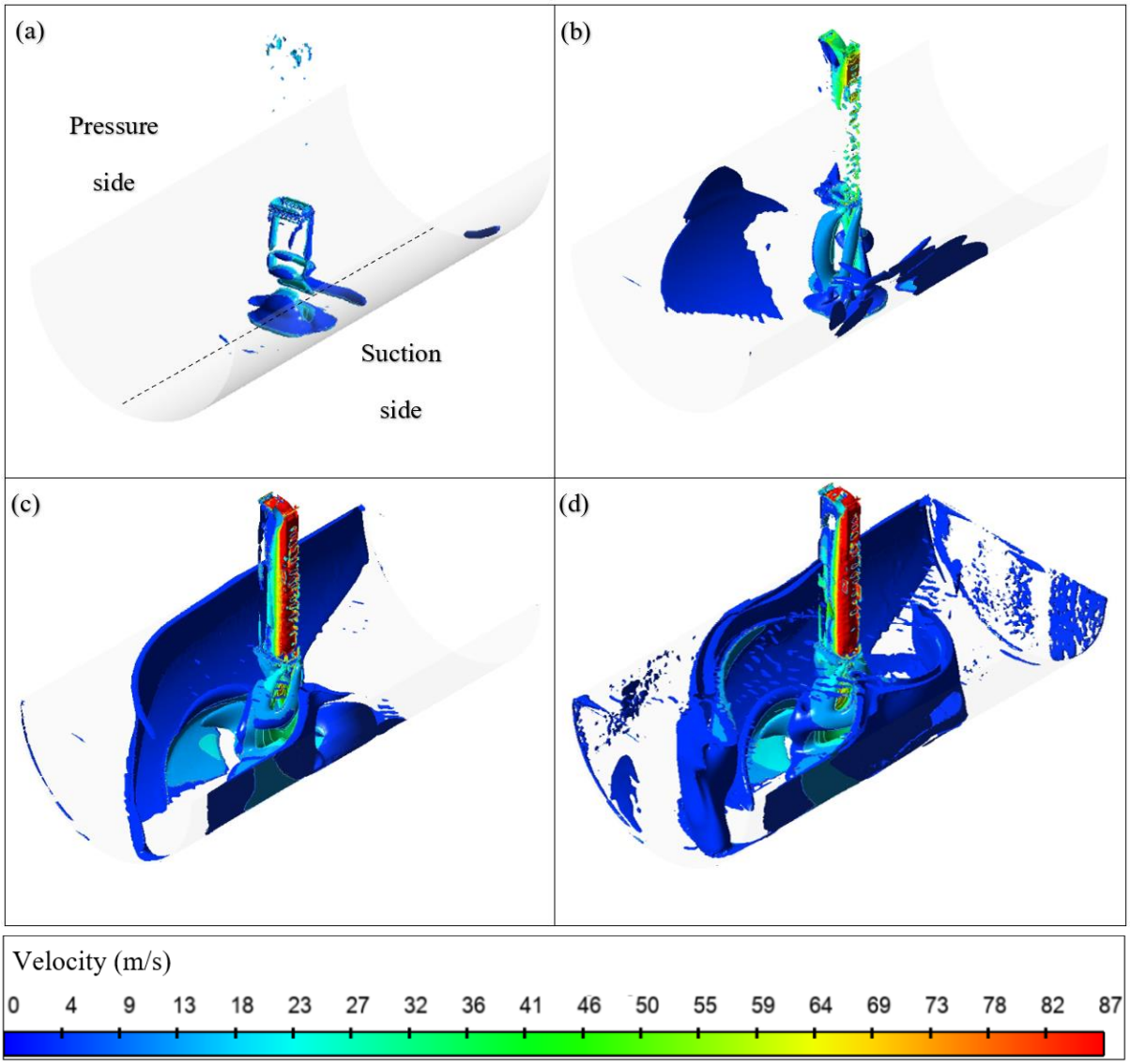

Figure 39: Iso-surface with Q-criterion at $7x10^6$ $1/s^2$ for velocity contours related to Chevroned Steady jet at (a) Stationary condition (b) 3000 RPM (c) 10000 RPM (d) 15000 RPM

As discussed, the presence of chevrons affects the discharge downstream from the nozzle. The rotational condition has a strong impact on the direct impingement over target surface for a Chevroned Sweeping jet as compared to sweeping jet. This is due to the elevated strength of recirculation region seen in Figure 40 (c) and Figure 40 (d). These recirculation regions lead to formation of vortices shown in Figure 41 (c) that hinders the spread of the coolant further. Recirculation zones for Chevroned Sweeping jet leads to growth of stagnant or slow-moving fluid regions. This comparatively reduces the effective heat transfer between the jet and the surface in contrast to

sweeping jet under rotational condition resulting in uneven cooling leading to hot spots that is discussed in upcoming heat transfer performance section.

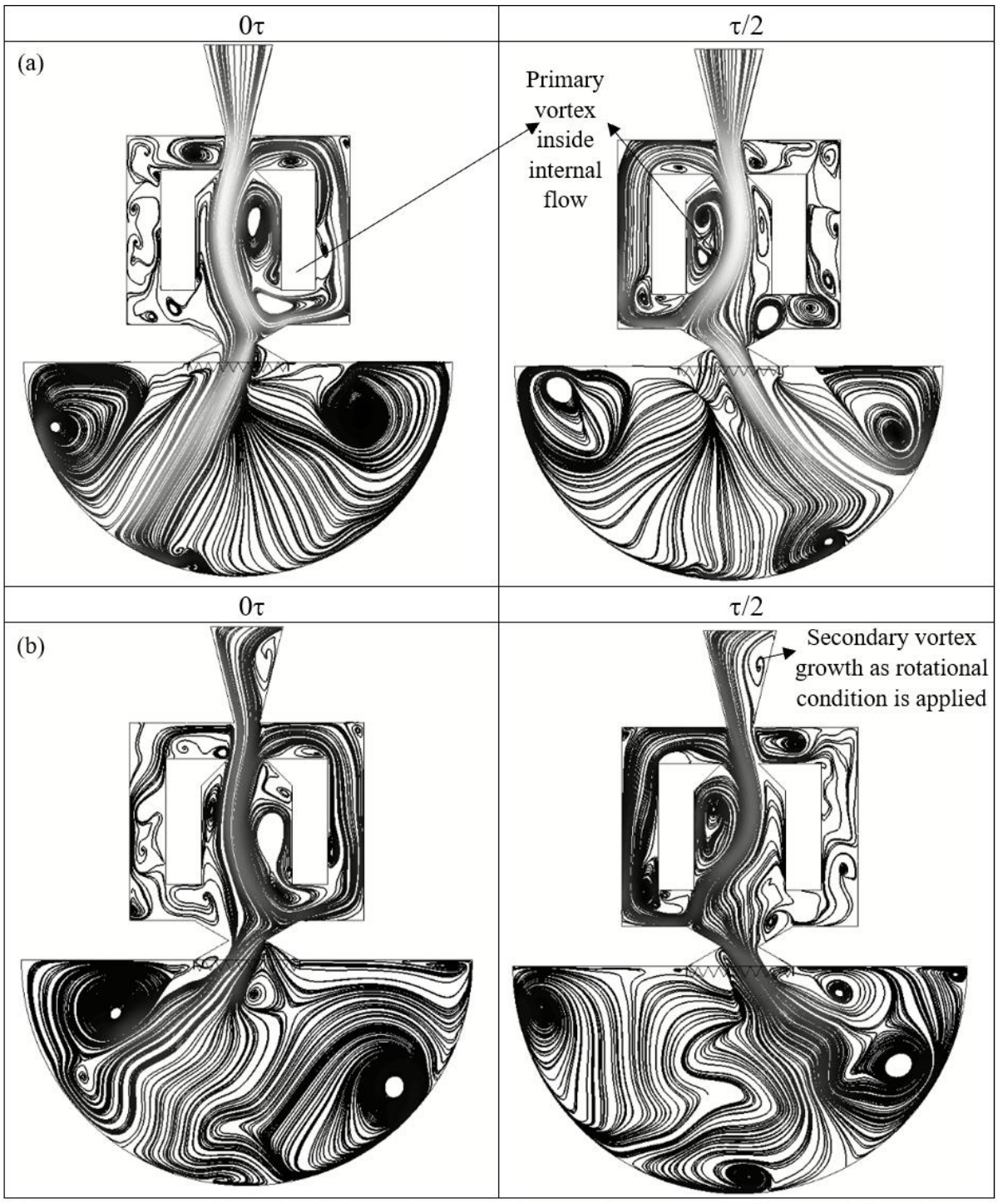

Figure 40: Streamlines depicting primary and secondary vortex of internal flow in Chevroned Sweeping jet at (a) Stationary condition (b) 3000 RPM (c) 10000 RPM (d) 15000 RPM

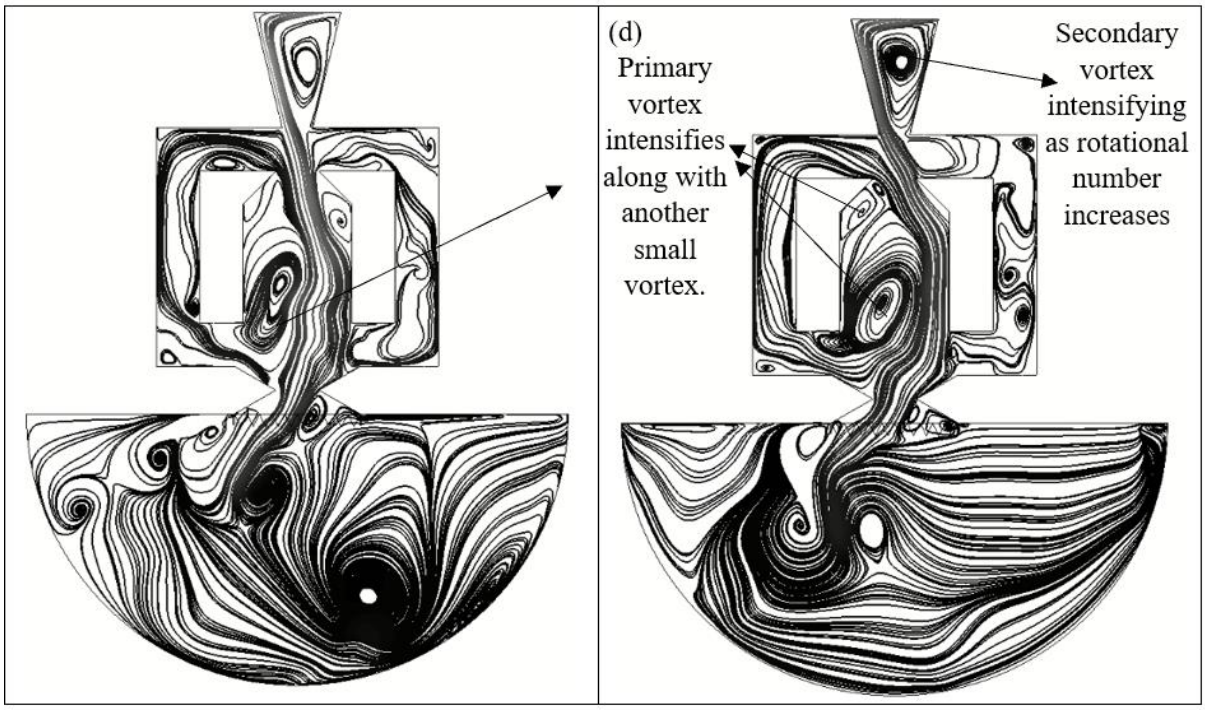

Figure 40: Streamlines depicting primary and secondary vortex of internal flow in Chevroned Sweeping jet at (a) Stationary condition (b) 3000 RPM (c) 10000 RPM (d) 15000 RPM (Continued)

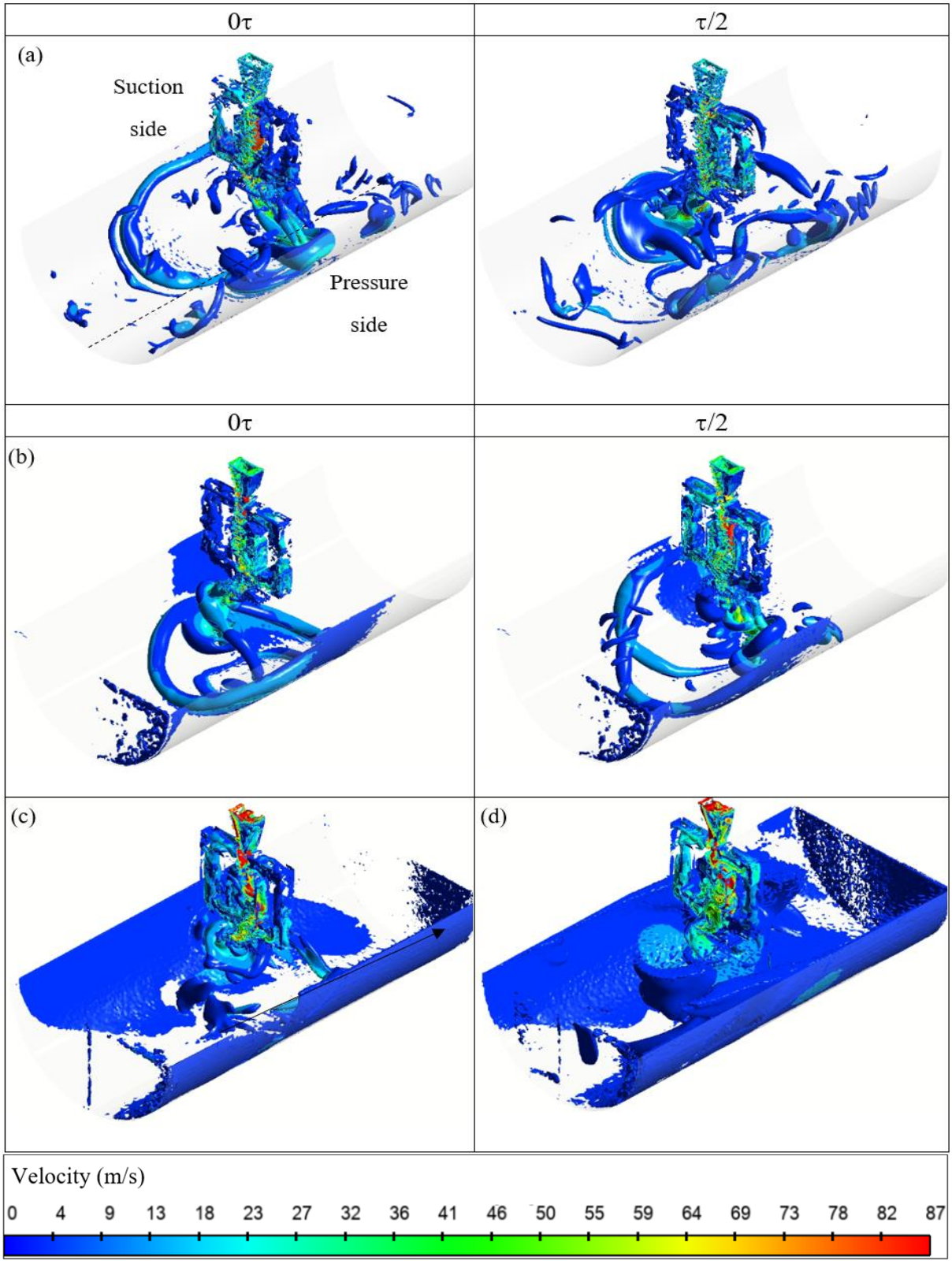

Figure 41: Iso-surface with Q-criterion at $7x10^6$ $1/s^2$ for velocity contours related to Chevroned Sweeping jet at (a) Stationary condition (b) 3000 RPM (c) 10000 RPM (d) 15000 RPM

3.4 Heat transfer performance at Stationary condition

It is well established that chaotic flow induced by turbulence aids in better heat removal and improves mixing. From the abovementioned literature, it is evident that intrinsic oscillations of a sweeping jet results is an efficient method of spreading the coolant over the target surface enhancing heat removal at a given coolant mass flow rate. One of the intents of this study is appending more disturbances, by addition of chevrons, to the already oscillating turbulent flow of sweeping jet to achieve even higher heat removal and to establish a comparative study of flow disturbance with other potential jets.

Figure 42 compared time averaged temperature contours for all the jets. All contours are plotted corresponding to jet hydraulic Reynolds number of sweeping jet at 12000. Also, all the legends of these contours are set to a fixed range resulting in such distribution of temperature and Nusselt contours. A quick glance at these contours shows that chevrons undoubtedly increase the heat transfer performance owing to increased turbulence levels of the impinging flow as described by Nichols et al. [82]. The effect of target section distance is not studied here since it is well known that the heat removal performance will drop as the jet-to-target distance increases as reported in literature Tu et al. [89]. As expected, all the contours show that the coolest temperature occurs at the location where jet strikes the target surface which is since the target surface encounters the highest velocity with thinnest boundary layer thickness near that location. This allows better heat removal from the surface and that is shown by the lowest temperature region as shown in Figure 42. It can be observed that the temperature distribution of steady jet is broader than swirling jet however the Nusselt number is relatively higher than any jet along the hot spot edges i.e., extremes of the blade as observed from Figure 42 (a) and Figure 42 (c) which was reported by Xu et al. [91] as well.

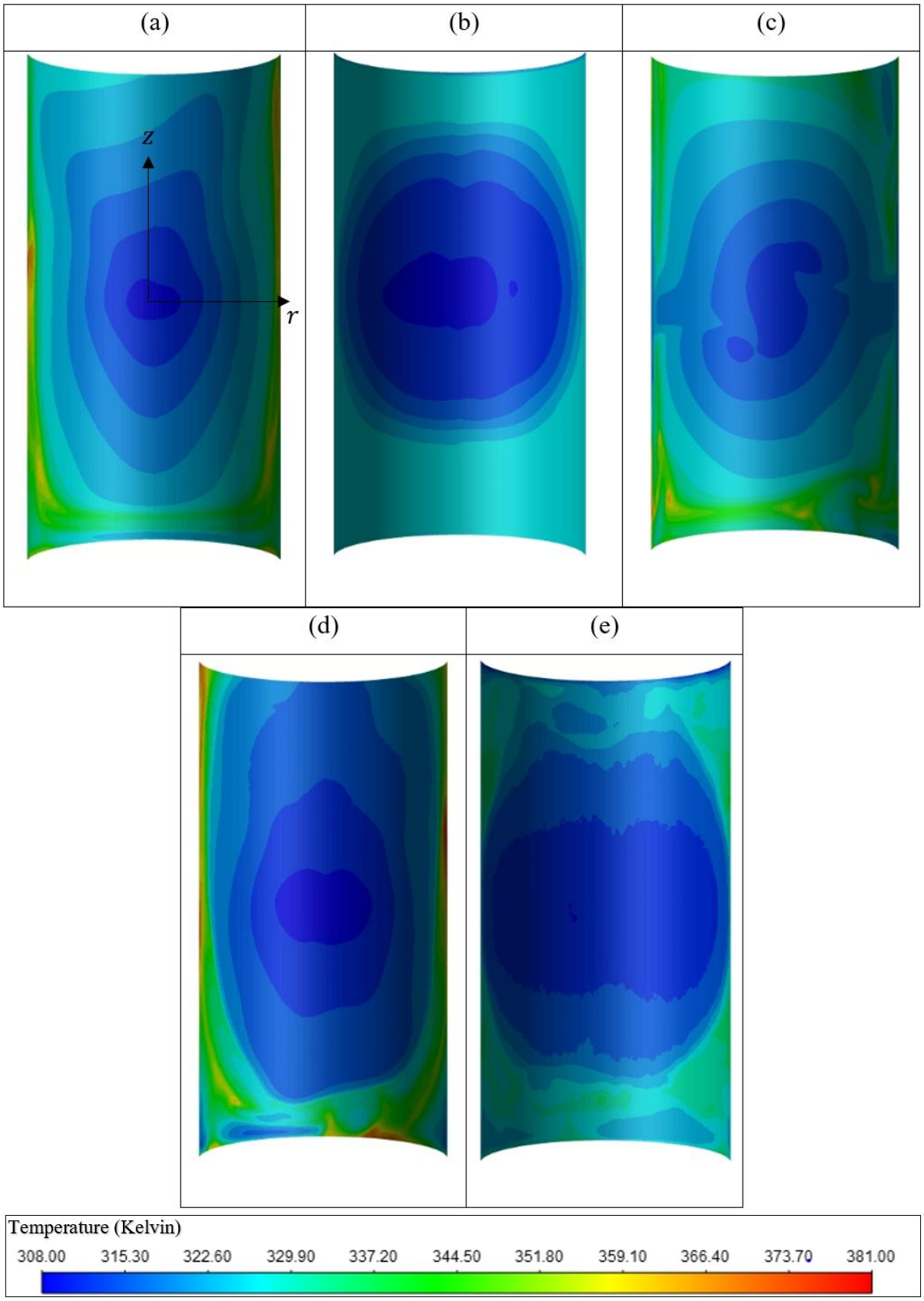

Figure 42: Time Averaged temperature contours for (a) Steady jet (b) Sweeping jet (c) Swirling jet (d) Steady jet with chevrons (e) Sweeping jet with chevrons

Figure 43 and Figure 44 show the time averaged local Nusselt number and time averaged local temperature, respectively, over a line falling on the semi-circular target surface where the jet strikes the surface (see Figure 13). Figure 44 shows almost the same minimum temperature is reached by all type of jets flow, however the Chevroned Sweeping jet and sweeping jet shows wider region of low temperature. This is because oscillating nature allows better spreading of the coolant while the chevron prompts higher chaotic motion. Hence, such behavior leads to better heat removal. As expected, the Nusselt number will produce similar behavior but with inverted curves shape since the highest Nusselt number is achieved at the lowest temperature as shown in Figure 40. Along the curved surface illustrated in Figure 43 'Nu' value was highest for Chevroned Steady jet while the Chevroned Sweeping jet exhibited a uniform Nu value over the span of leading-edge blade. The usual "double peaks" pattern was observed for both Chevroned Steady and steady jet in vicinity of $-0.01 < r/d < 0.01$. However, their patterns differed due to the presence of chevron, and it is noted that chevrons increased these double-peaks Nu value as well. For the sweeping jet and Chevroned Sweeping jet no such peaks are reported along the curvature like the study of Tu et al. [89], the 'Nu' distribution along the curvature shifts from peaking at the stagnation point for sweeping jet due to the Coanda effect. This effect causes sweeping jet to produce a more uniform cooling over target surface owing to oscillating output. When Chevroned Sweeping jet is compared to sweeping jet, the disturbance created by zig-zag trailing edge geometry i.e., chevron nozzles served the purpose of enhancing the mixing between adjacent streams of fluid. This can be illustrated by observing the Nu value along the curvature in region beyond $-0.02 < r/D < 0.02$ which is referred to as hotspots of leading-edge blade. The longitudinal vortices produced by the chevrons alter the course of large-scale turbulence of fluid stream resulting in better mixing of fluid over the span of leading-edge blade as compared to the sweeping jet, where the Nu value sharply drops over these hotspots of leading-edge blade. At these hotspot regions, swirling jet outperform every other jet (minimum temperature observed at hotspots of 317 K) owing to high tangential velocity linked to wider spreading of coolant over the curved surface observed from Figure 44 but at the cost of low axial velocity resulting in lowest heat transfer rate at the center of curvature i.e., at $r/D = 0$ as observed from Figure 43. The

steady jets both with and without chevrons are incapable of cooling down the hotspots where the temperature rises to values of 355 K and 340 K for Chevroned Steady jet and steady jet respectively. The steady jets exhibited a relatively narrow high-Nu-number zone, the maximum Nu number of Chevroned Steady jet and steady jet near the stagnation impinging region was nearly the same and higher than Chevroned Sweeping and sweeping jet. But the overall heat transfer performance of the sweeping jets didn't die out along the curvature unlike the steady jets. This can be demonstrated by more uniform temperature and Nu contours produced by Chevroned Sweeping jet and sweeping jet respectively as shown in Figure 43 and 44 The difference between these two jets when observed carefully again breaks down in area of curvature region beyond $-0.02 < r/d < 0.02$ where the Chevroned Sweeping jet purely dominates any other jet in terms of cooling.

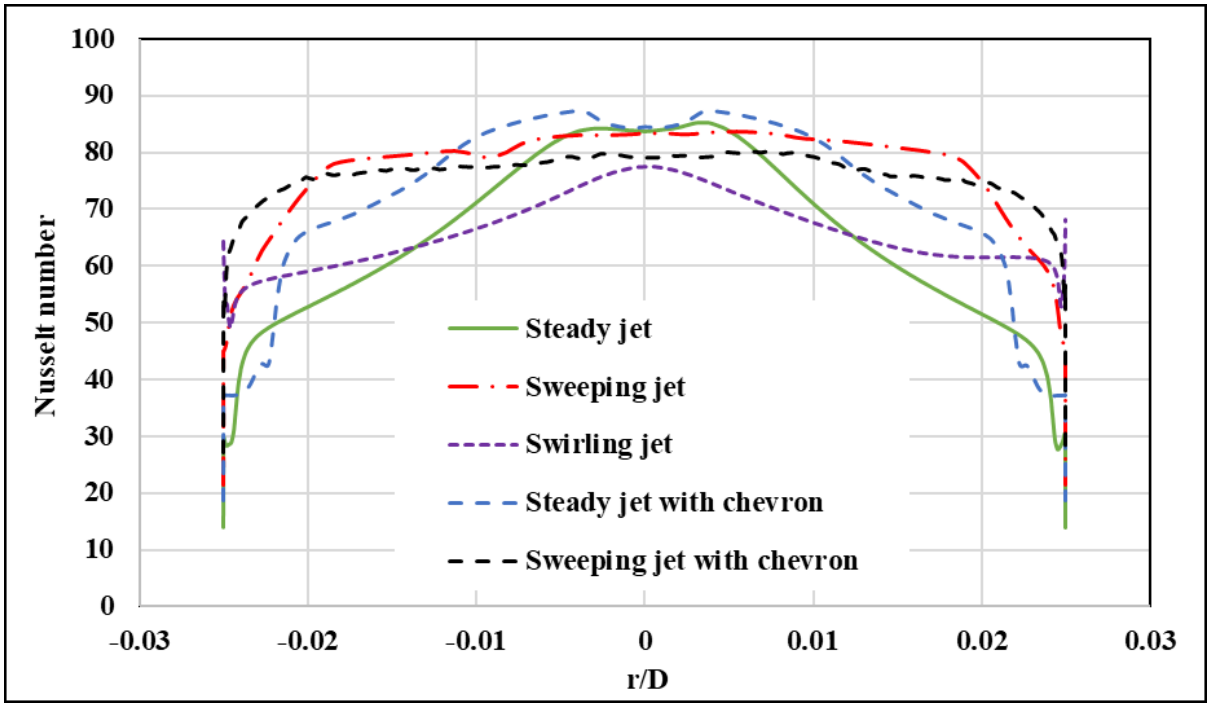

Figure 43: Time Averaged Nusselt number values along the curved line for (a) Steady jet (b) Sweeping jet (c) Swirling jet (d) Steady jet with chevrons (e) Sweeping jet with chevrons

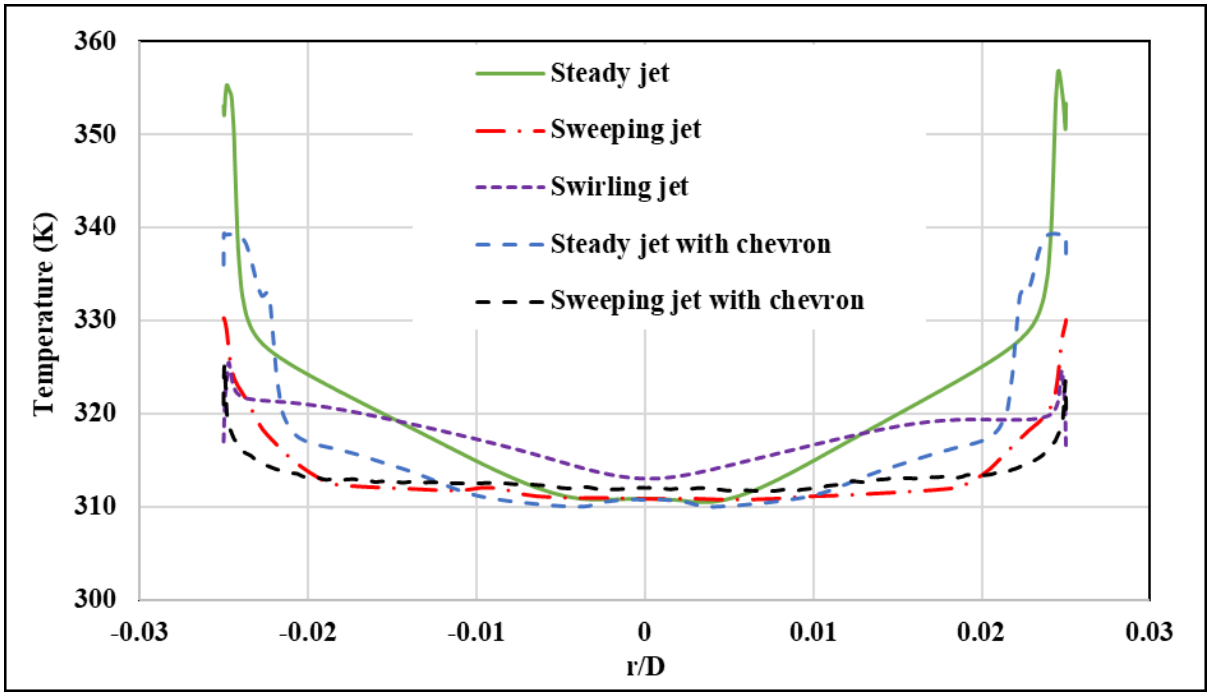

Figure 44: Time Averaged temperature number values along the curved line for (a) Steady jet (b) Sweeping jet (c) Swirling jet (d) Steady jet with chevrons (e) Sweeping jet with chevrons

The heat transfer performance was maximum for Chevroned Sweeping jet which increased by 16.13% compared to steady jet, 15.42% more than swirling jet, increased by 9.0% compared to Chevroned Steady jet and 2.73% more than sweeping jet as shown in Figure 45. The swirling jet as discussed in above text has great cooling capacity over the hotspot edges, but due to poor axial velocity it loses its cooling performance near the bottom edge of leading-edge blade as observed in temperature contours in Figure 39 (c), this is responsible for high temperatures near the bottom edge of the blade as high as 363.8 K when compared to steady jet and Chevroned Steady jet that has maximum temperatures near the curved edges of the blade at 381.23 K and 340.56 K respectively. The Chevroned Sweeping jet created a chaotic flow disturbance that efficiently spread over the curved area, but this hindered its performance over the top and bottom edges of the blade as compared to sweeping jet that spread the cooling fluid uniformly throughout the surface of the blade as observed from Figure 42 (b) and Figure 42 (d). This led to a higher maximum point of temperature for Chevroned Sweeping jet as compared to sweeping jet observed which could be readily solved by using array of impinging jets.

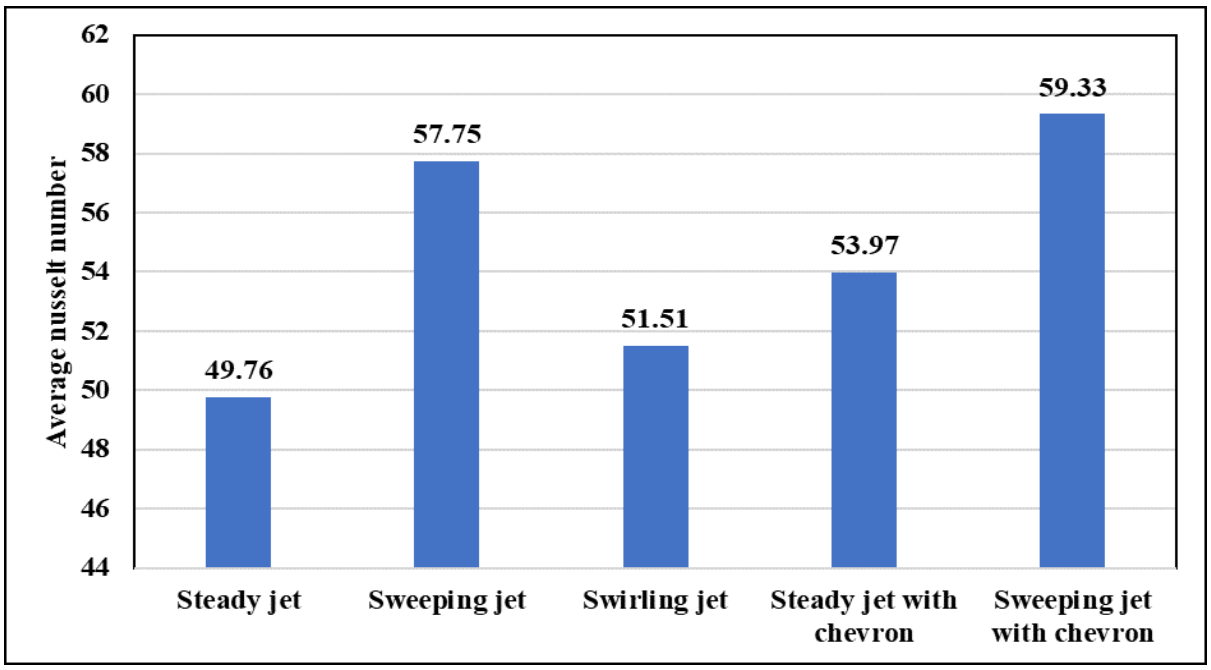

Figure 45: Time averaged Nusselt number values over leading-edge blade for (a) Steady jet (b) Sweeping jet (c) Swirling jet (d) Steady jet with chevrons (e) Sweeping jet with chevron

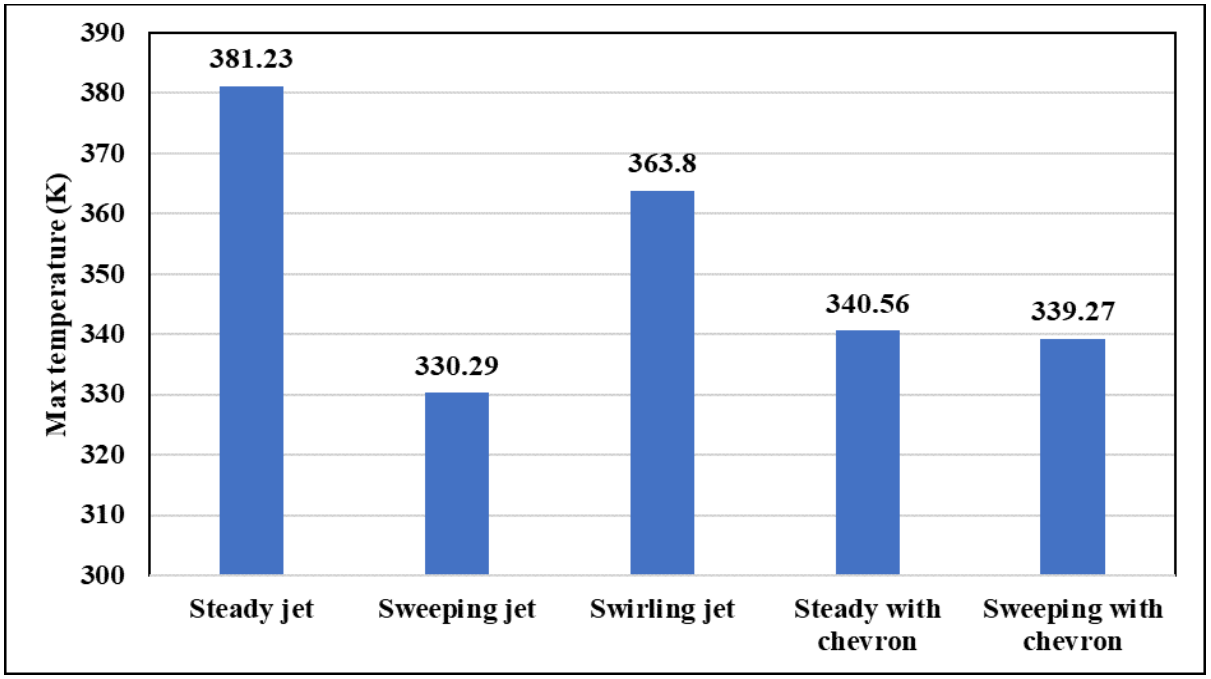

Figure 46: Time averaged maximum temperature values over leading-edge blade for (a) Steady jet (b) Sweeping jet (c) Swirling jet (d) Steady jet with chevrons (e) Sweeping jet with chevrons

3.5 Heat transfer performance at Rotatory condition

The trend observed for each potential jets upon raising the rotational condition was alike i.e., the overall averaged Nusselt number value decreased at 3000 RPM and increased as the rotational condition was increased to 15000 RPM. This incrementation of Nusselt number as rotational number was raised is due to the increase in peak velocity of the jet followed by strong squeezing of Coriolis force in form of recirculation region over the main internal flow. In the figures represented below along curved line $-0.025 \leq r/D < 0$ represents the pressure side and $0 < r/D \leq 0.025$ represents suction side of leading-edge blade.

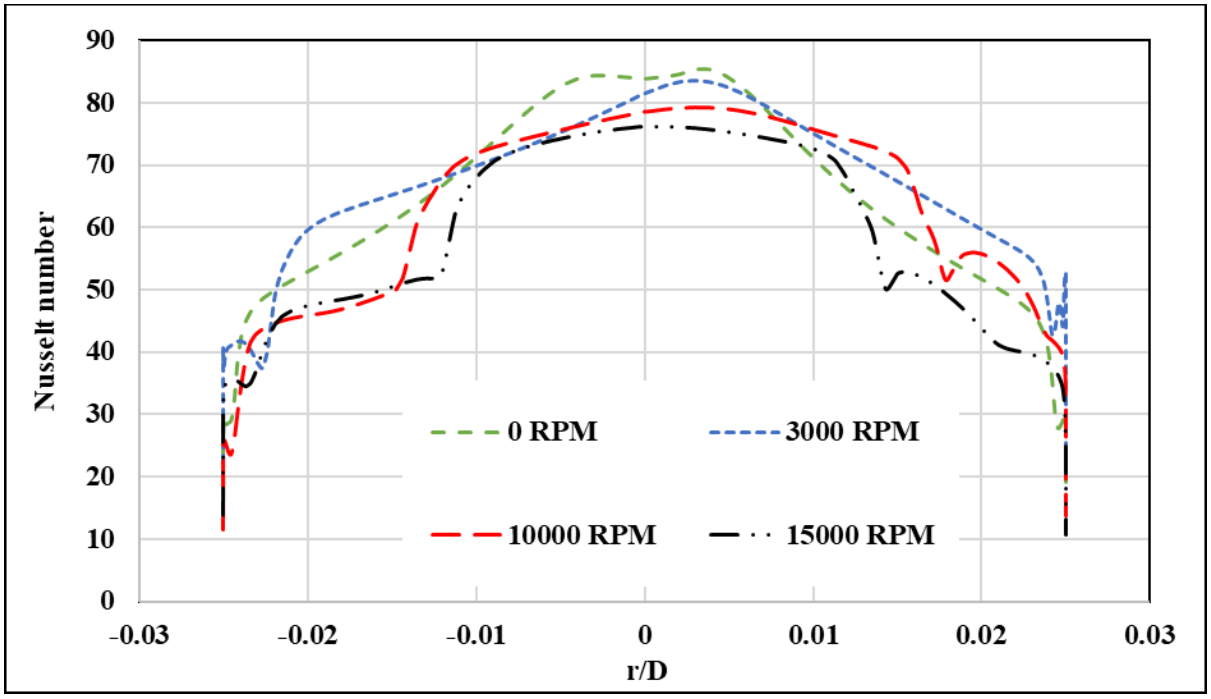

Figure 47: Nusselt number values along the curved line for Steady jet at (a) 0 RPM (b) 3000 RPM (c) 10000 RPM (d) 15000 RPM

The heat removal performance for steady jet over the curved area at 3000 RPM remains close to its performance at stationary condition with a slight inclination of curve towards suction side. As the rotational condition is increased the curve shifts more towards the pressure side as the recirculation region is much stronger now and squeezes the internal flow of jet towards the pressure side as observed in flow structure section and similar pattern can be observed in Figure 47.

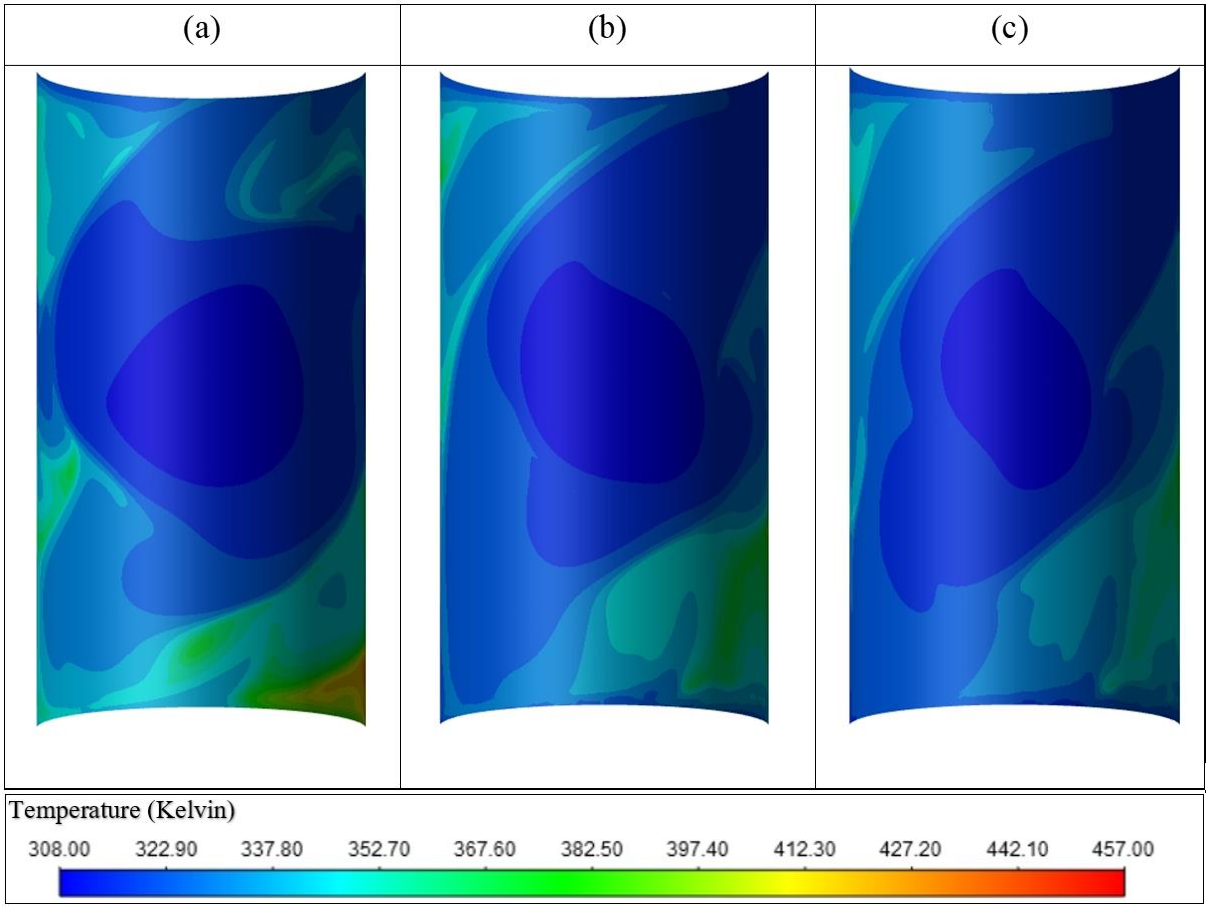

Figure 48: Temperature contours for Steady jet at (a) 3000 RPM (b) 10000 RPM (c) 15000 RPM

With shift of impingement towards the center and pressure side as rotational condition is raised from 3000 to 15000 RPM, the temperature contours for steady jet as shown in Figure 48 have lesser hotspots i.e., decrease in maximum temperature values is observed in Figure 49. This is due to more even cooling and higher peak velocity from the exit of nozzle.

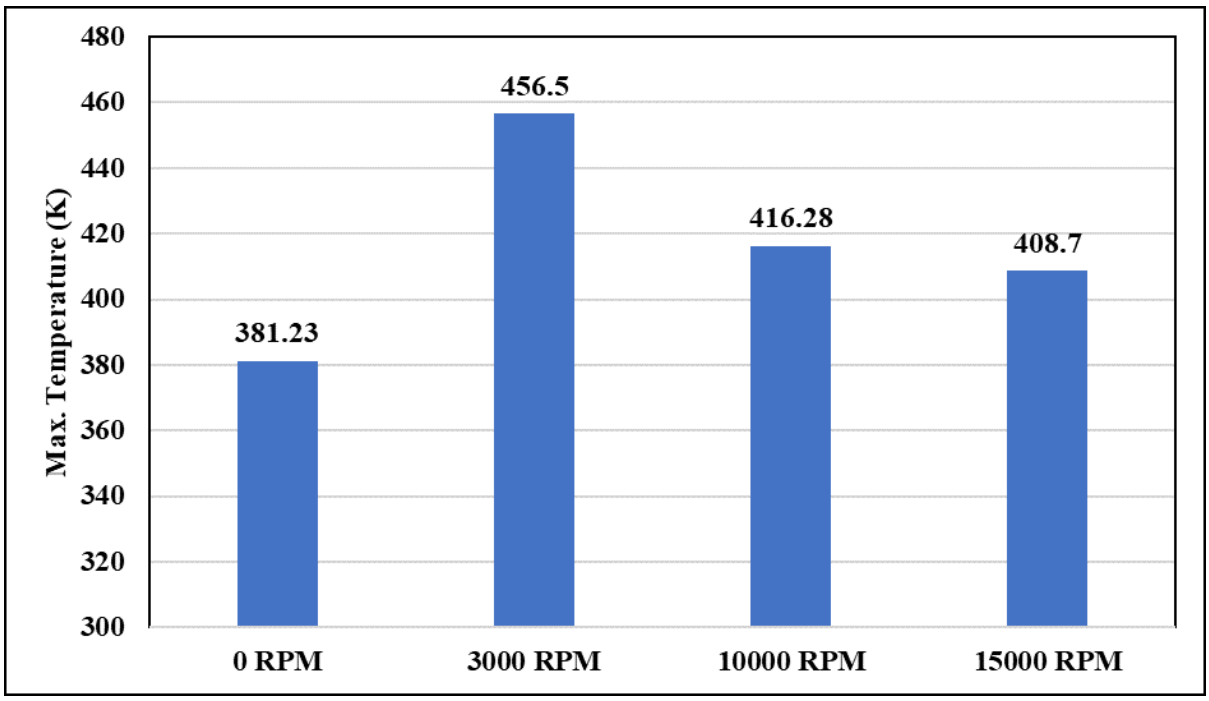

Figure 49: Area averaged maximum temperature values over leading-edge blade for Steady jet at (a) 0 RPM (b) 3000 RPM (c) 10000 RPM (d) 15000 RPM

At 3000 RPM the curved area Nusselt number trend for sweeping jet is close to its performance at stationary condition just like the steady jet. However, the overall averaged heat transfer performance decreases at this rotational condition. This is due to the fact that, yet sweeping/oscillation of fluid occurs at 3000 RPM but at the cost of decreased frequency as shown in Figure 33. As indicated previously higher RPM's for sweeping jet leads to flow pushed towards suction as shown in Figure 50, reducing the span coverage due to secondary vortex intensification, this nevertheless increased the frequency due to reduced covering area and increased peak velocity. This is attributed as the major reason along with it flow behavior as tangential/side impinging jet. This behavior is observed as the flow is directed towards one end of the leading-edge which exits from angled end of sweeping jet nozzle resulting in increment of overall averaged Nusselt number value for sweeping jet as rotational condition is increased from 3000 RPM vividly depicted in Figure 62. As for the hotspots i.e., the maximum temperature values decrease from 3000 to 10000 RPM but increases at 15000 RPM. This could be inferred from Figure 51 and 52 owing to sweeping jet shifting more towards the suction side with hotspots forming at pressure side at 15000 RPM.

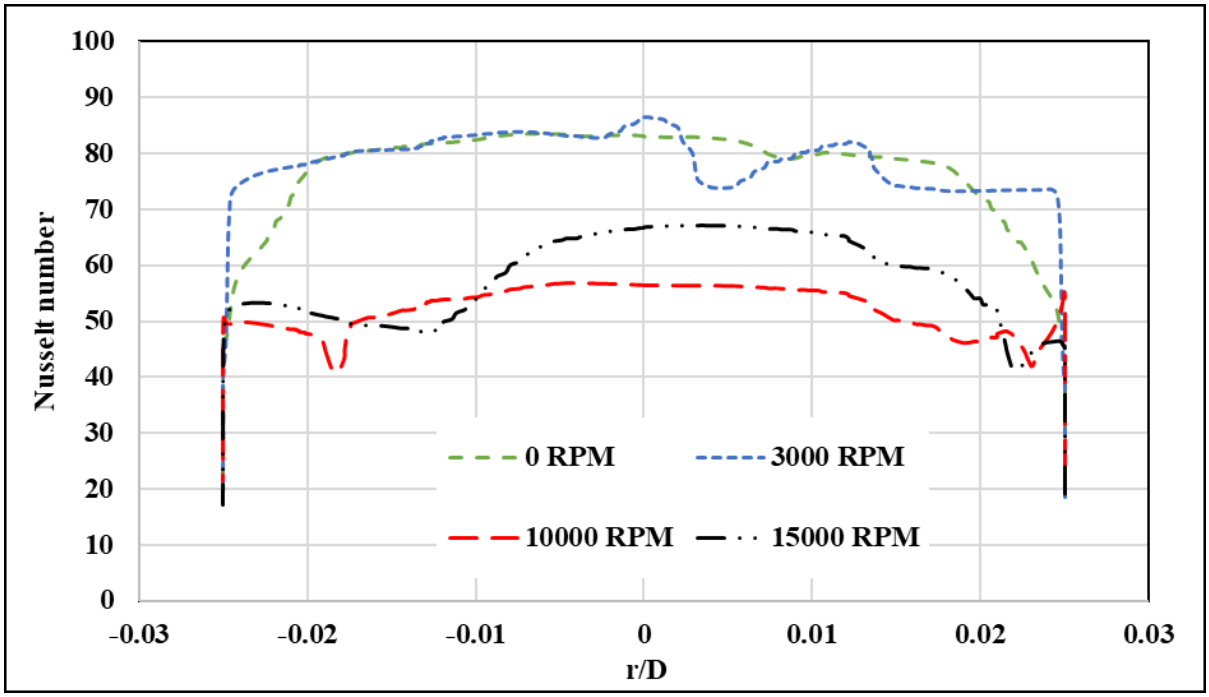

Figure 50: Nusselt number values along the curved line for Sweeping jet at (a) 0 RPM (b) 3000 RPM (c) 10000 RPM (d) 15000 RPM

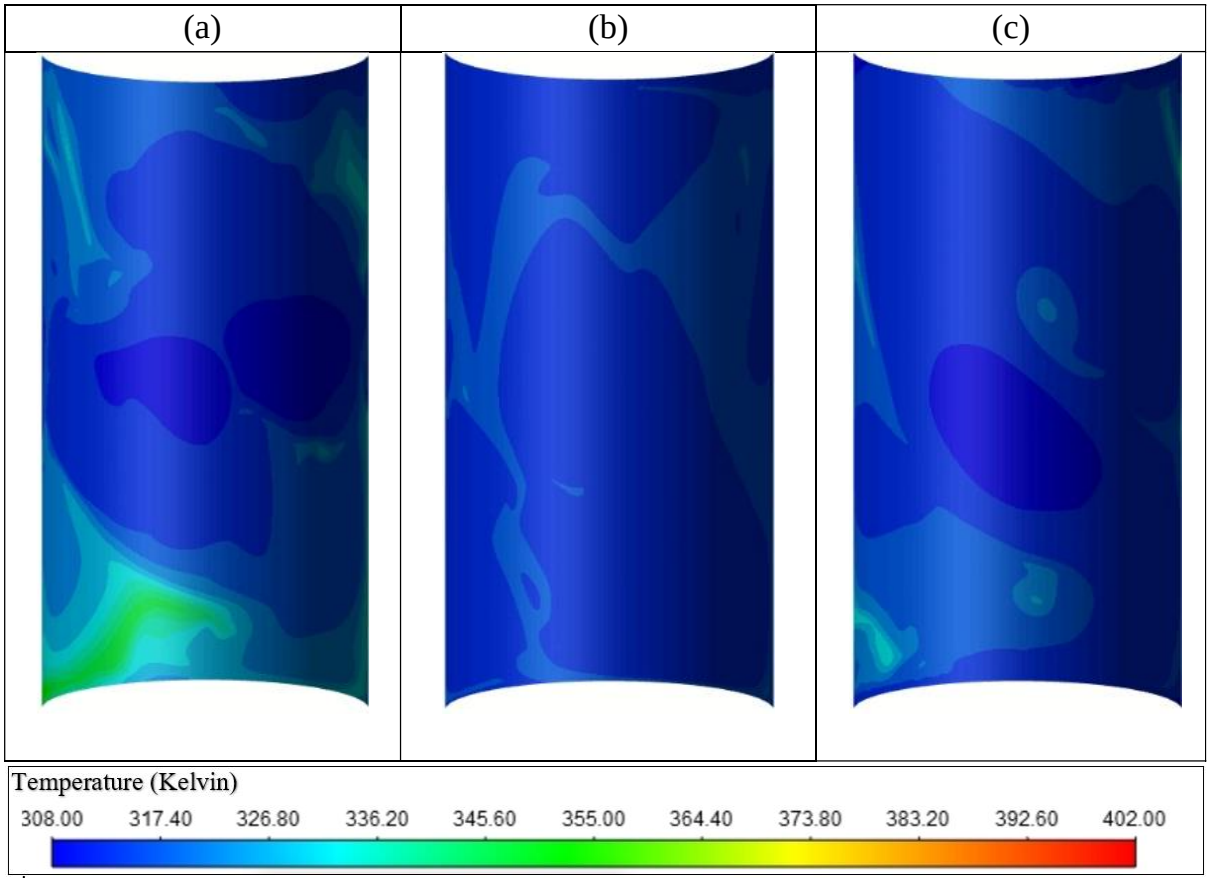

Figure 51: Temperature contours for Sweeping jet at (a) 3000 RPM (b) 10000 RPM (c) 15000 RPM

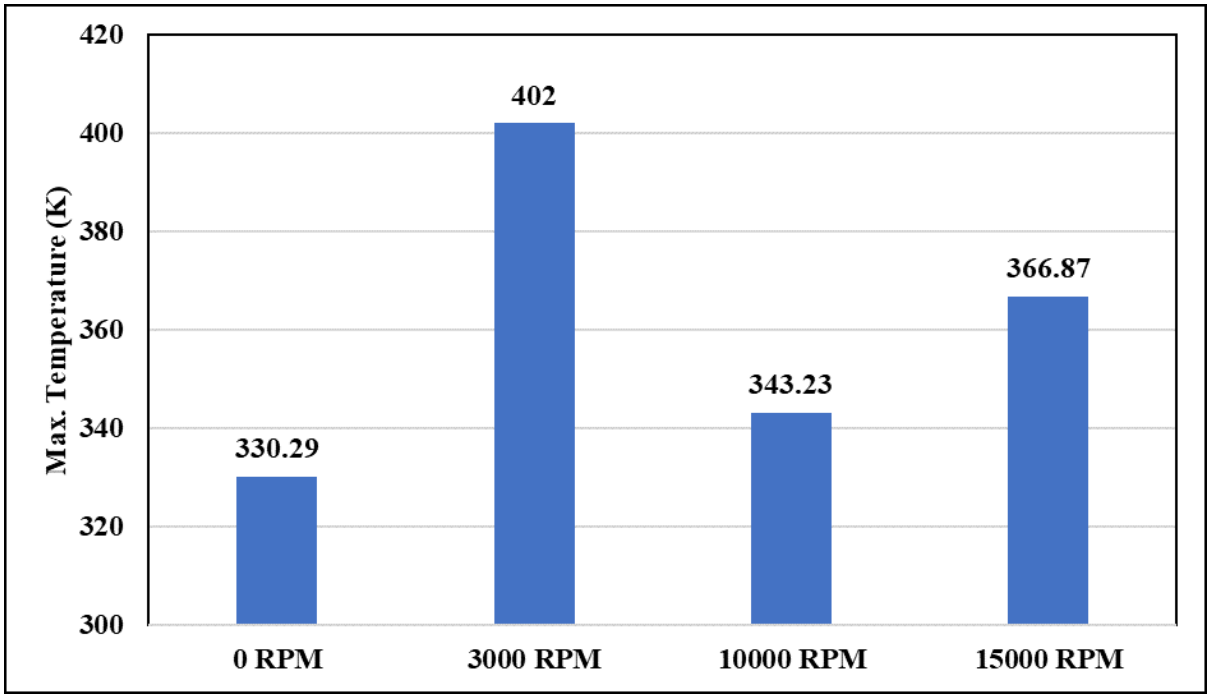

Figure 52: Area averaged maximum temperature values over leading-edge blade for Sweeping jet at (a) 0 RPM (b) 3000 RPM (c) 10000 RPM (d) 15000 RPM

As mentioned in flow structure, performance of swirling jet deteriorates sharply as rotational condition was applied. The swirling strength was weakened when rotation was applied. These swirls were major reason for increase in heat transfer performance at stationary conditions when compared to steady jet. It can be concluded that axial jet strength is much rigid when compared to swirling strength at rotational conditions as steady jet performs better when compared to swirling jet at rotational conditions. A trend however remains similar for all jets i.e., increment of average Nusselt number value and decrease of hotspot is observed for swirling jet as rotational condition is raised observed in Figures 53-55.

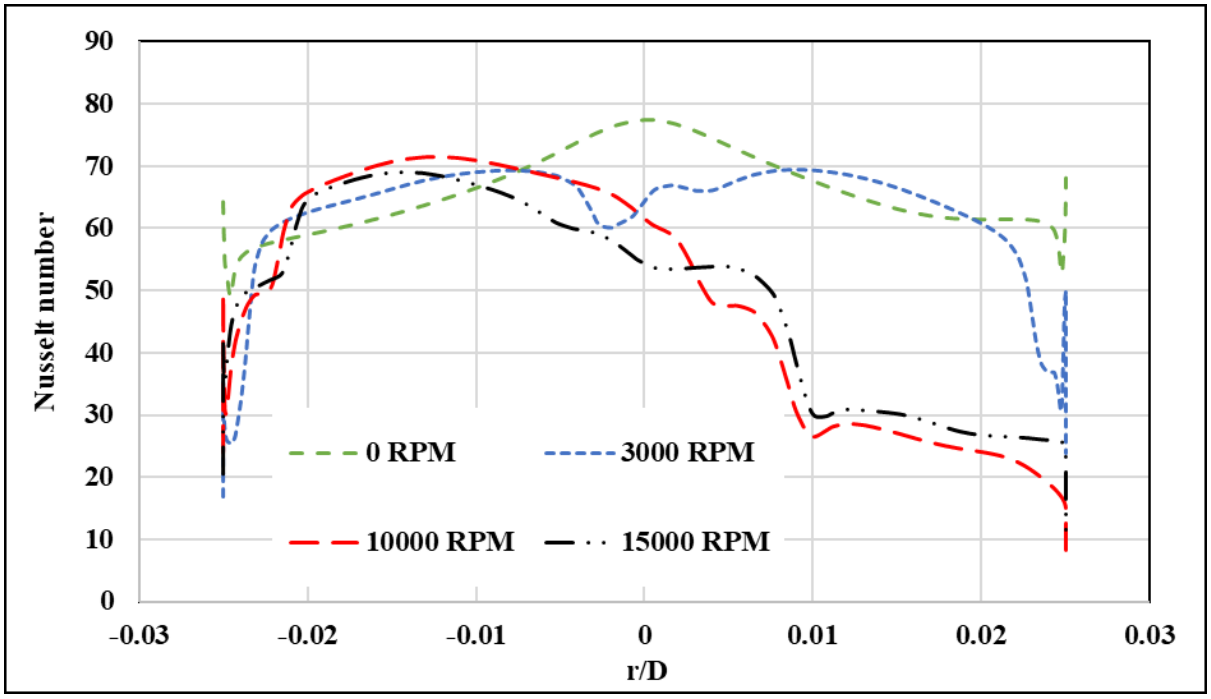

Figure 53: Nusselt number values along the curved line for Swirling jet at (a) 0 RPM (b) 3000 RPM (c) 10000 RPM (d) 15000 RPM

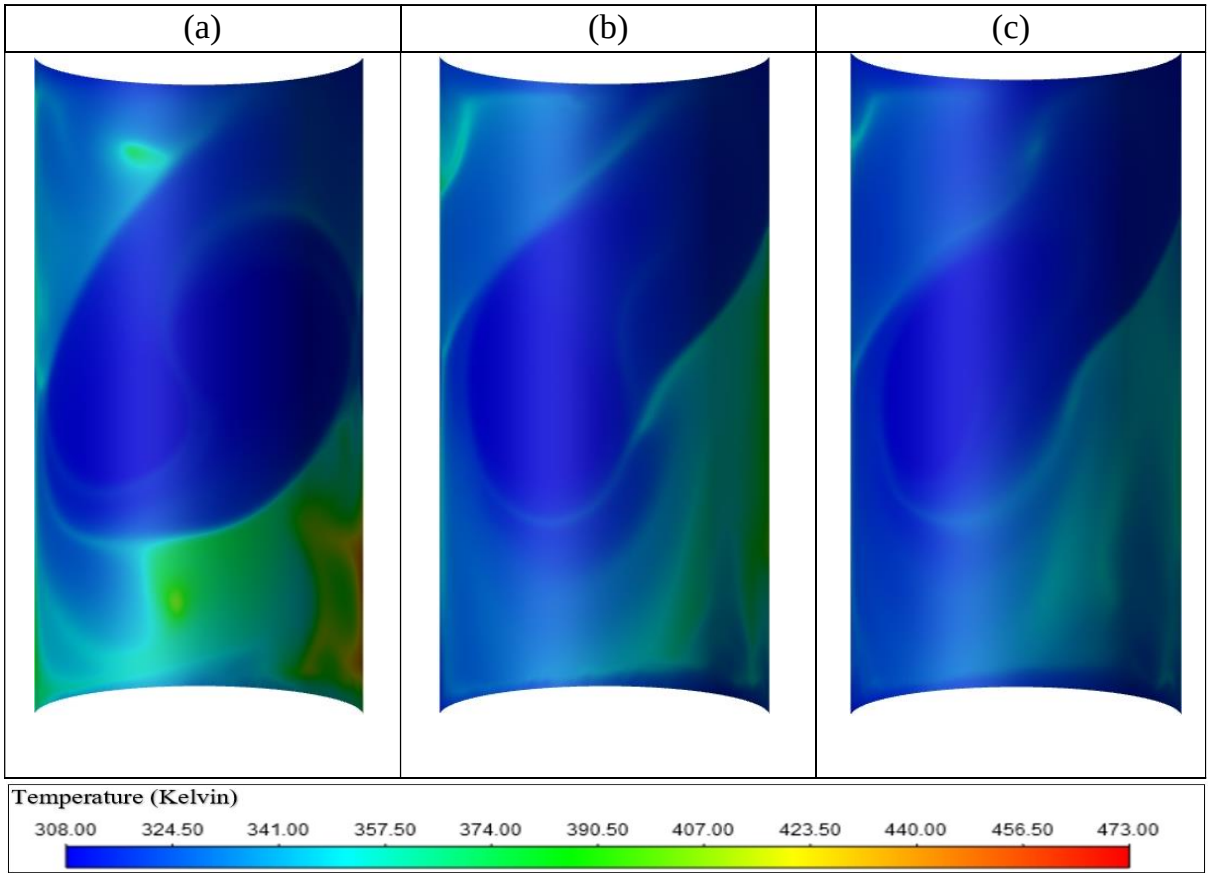

Figure 54: Temperature contours for Swirling jet at (a) 3000 RPM (b) 10000 RPM (c) 15000 RPM

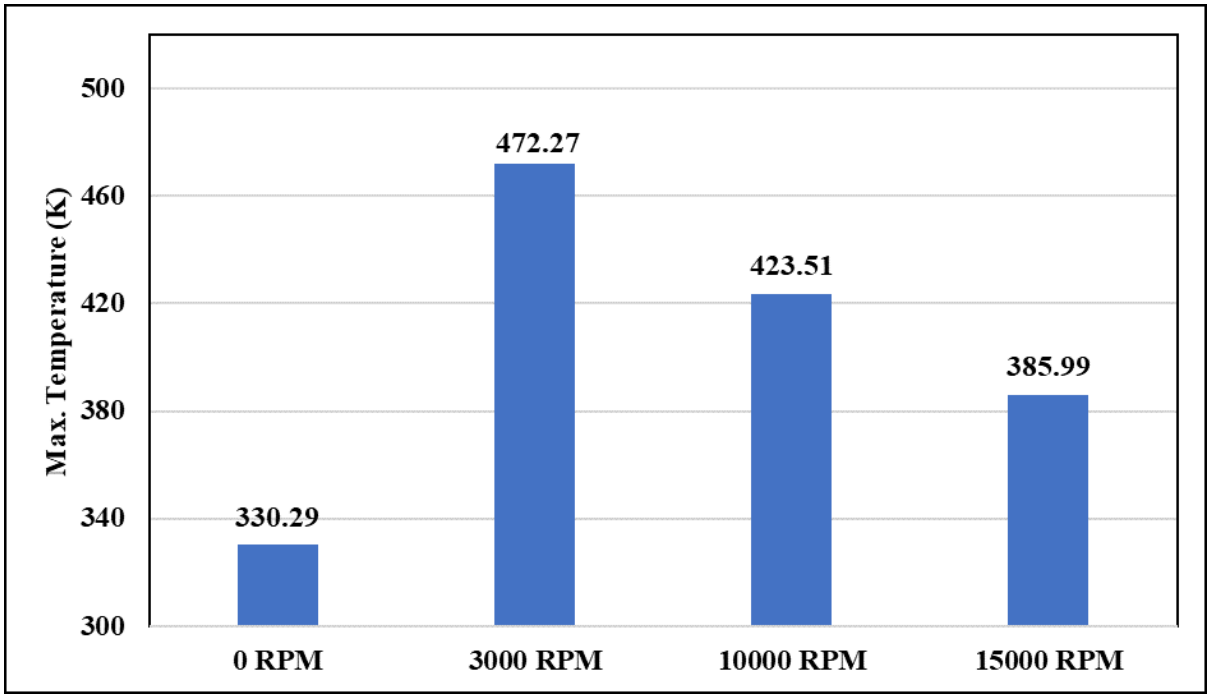

Figure 55: Area averaged maximum temperature values over leading-edge blade for Swirling jet at (a) 0 RPM (b) 3000 RPM (c) 10000 RPM (d) 15000 RPM

The performance behaviour for Chevroned Steady jet isn't augmented as rotational condition is applied. A brief in flow structure section was already highlighted that disturbance created by chevrons are aggravated much more as rotational condition is increased. This leads to formation of strong vortex regions in the vicinity of impinging regions. For Chevroned Steady jets this aggravation isn't as high as compared to Chevroned Sweeping jet. This is why heat transfer performance of Chevroned Steady jet is slightly more that of steady jet at rotational conditions can be compared in Figures 47-49 along with Figures 56-58. Whereas for Chevroned Sweeping jet due to oscillating nature clubbed with chevrons along with rotational swirls leads to aggravated recirculation regions that hinder the spread of coolant over the leading-edge blade resulting in lower heat transfer performance and higher maximum temperatures of hotspots as compared to sweeping jet at rotational conditions. This could be observed in Figures 50-52 along with Figures 59-61 for comparative performance between sweeping jet and Chevroned Sweeping jet at rotational conditions.

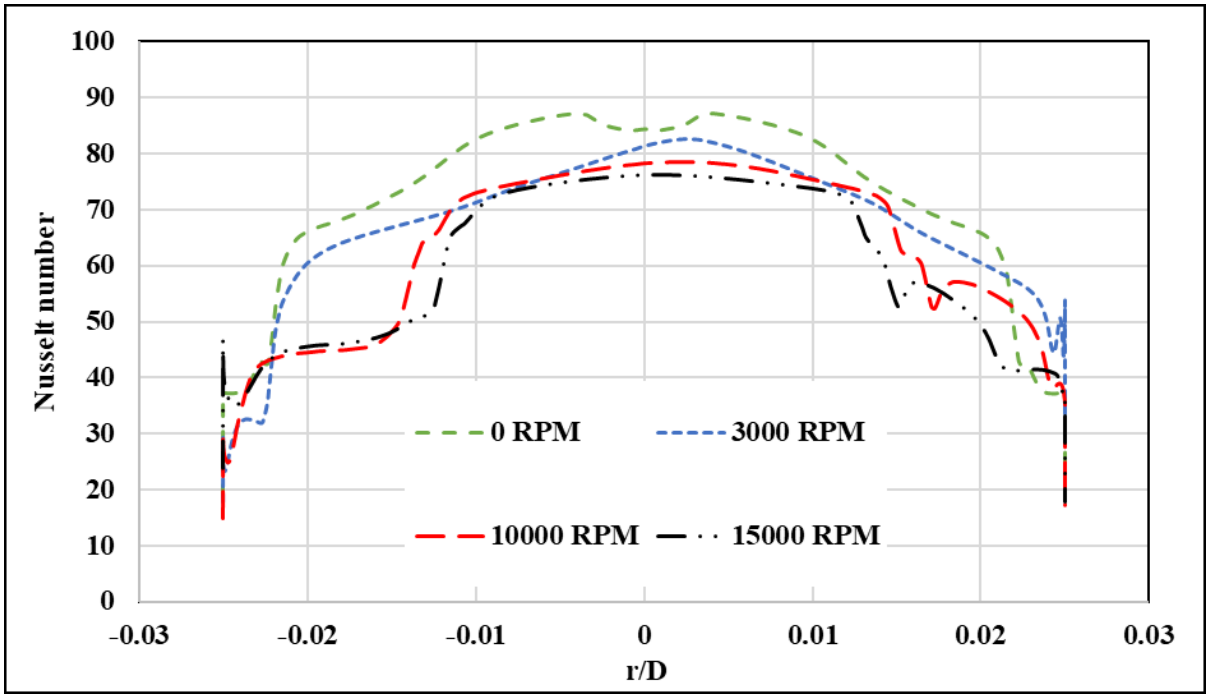

Figure 56: Nusselt number values along the curved line for Chevroned Steady jet at (a) 0 RPM (b) 3000 RPM (c) 10000 RPM (d) 15000 RPM

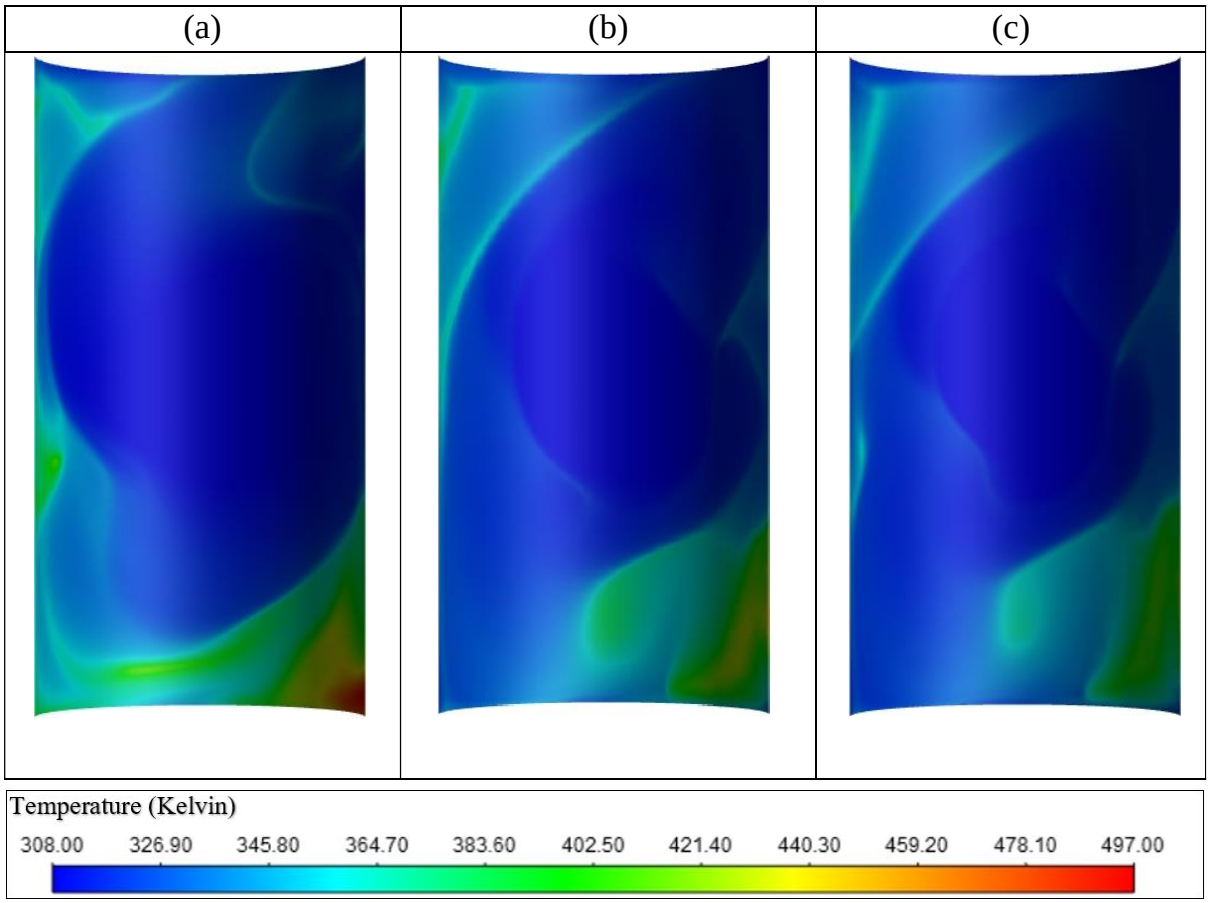

Figure 57: Temperature contours for Chevroned Steady jet at (a) 3000 RPM (b) 10000 RPM (c) 15000 RPM

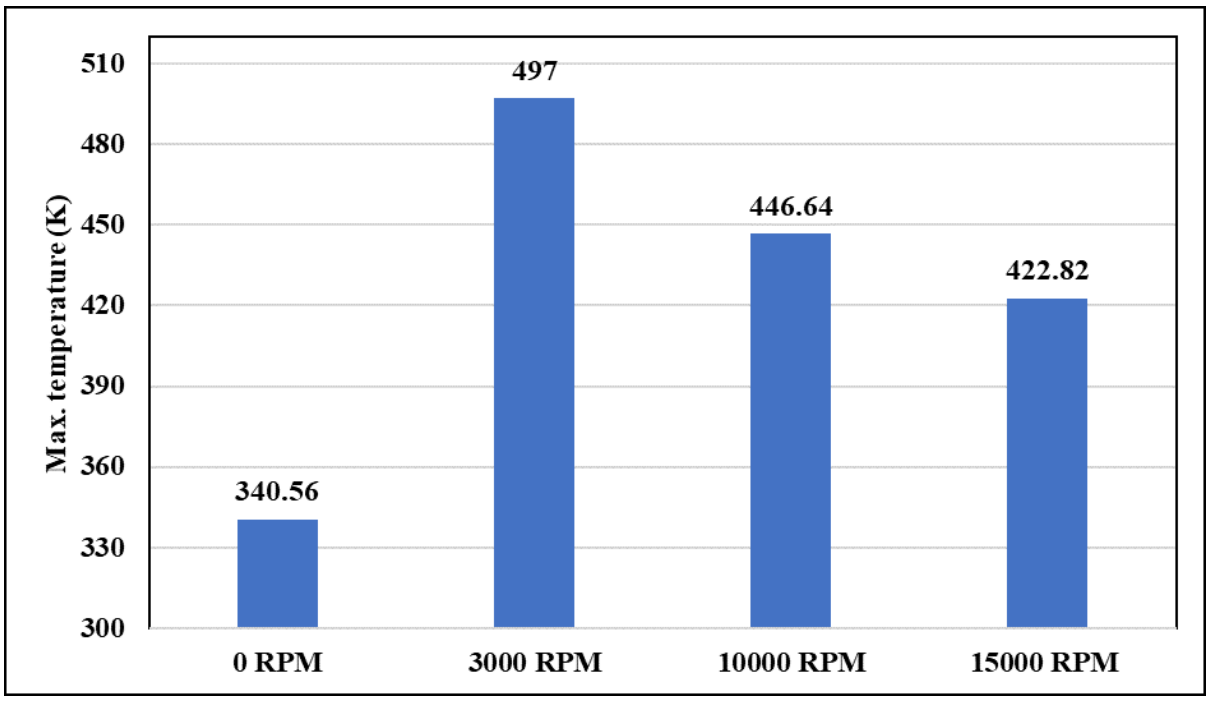

Figure 58: Area averaged maximum temperature values over leading-edge blade for Chevroned Steady jet at (a) 0 RPM (b) 3000 RPM (c) 10000 RPM (d) 15000 RPM

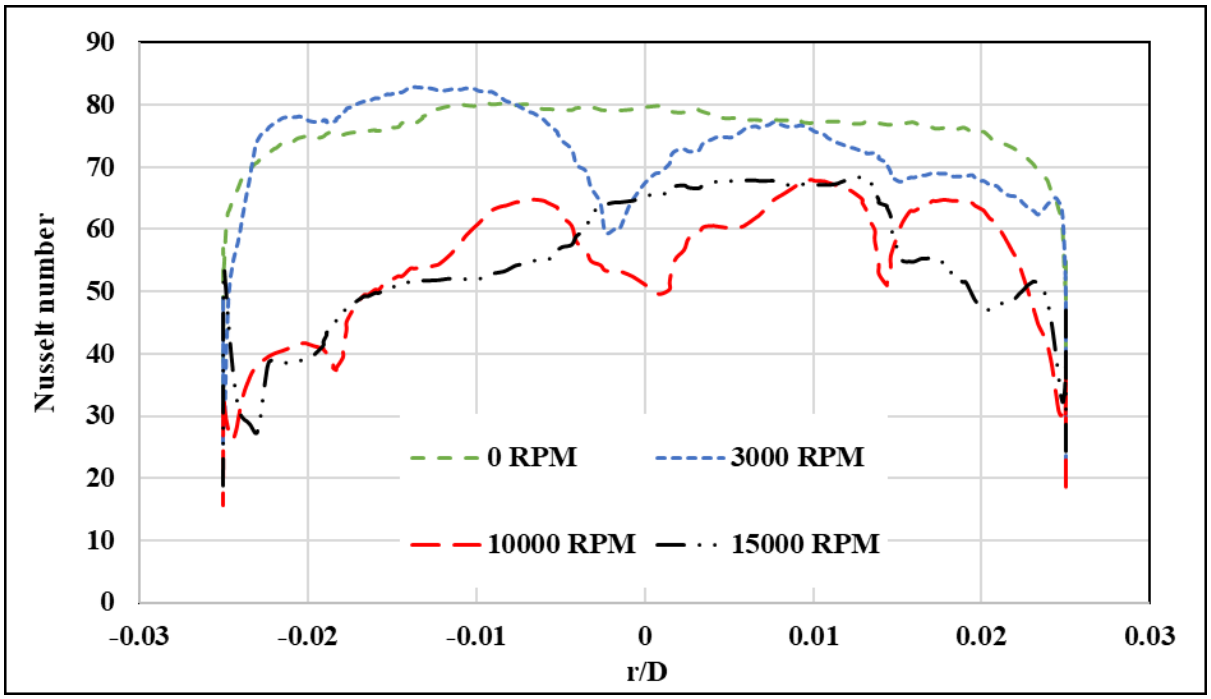

Figure 59: Nusselt number values along the curved line for Chevroned Sweeping jet at (a) 0 RPM (b) 3000 RPM (c) 10000 RPM (d) 15000 RPM

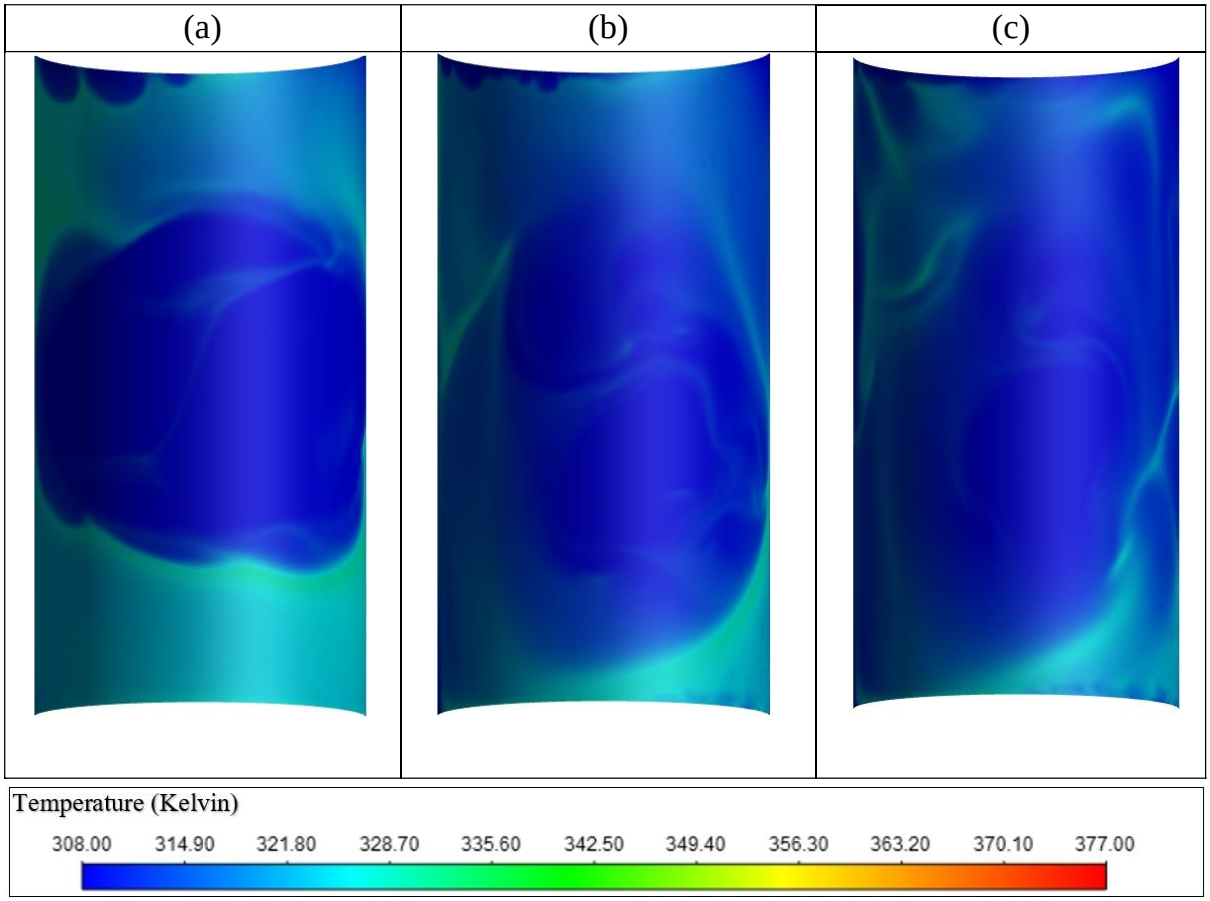

Figure 60: Temperature contours for Chevroned Sweeping jet at (a) 3000 RPM (b) 10000 RPM (c) 15000 RPM

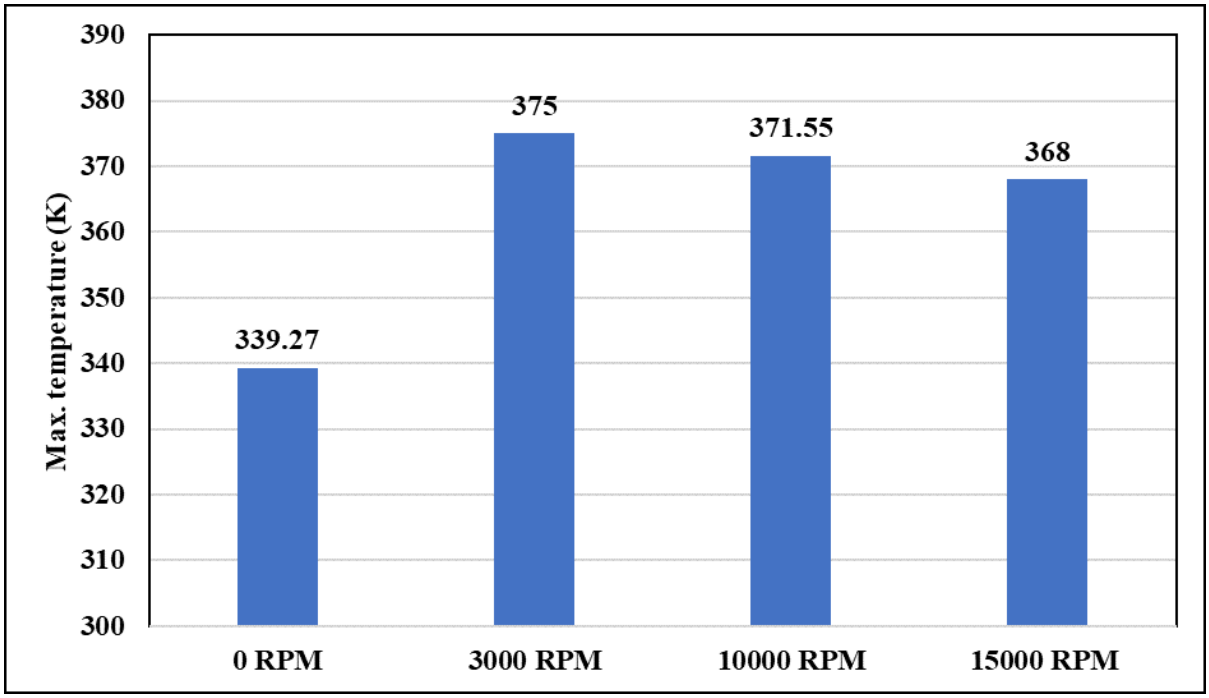

Figure 61: Area averaged maximum temperature values over leading-edge blade for Chevroned Sweeping jet at (a) 0 RPM (b) 3000 RPM (c) 10000 RPM (d) 15000 RPM

In Figure 62 all the averaged surface Nusselt number for different rotational conditions is shown. It is vivid that sweeping jet dominates over other potential jets when rotational conditions are applied. In fact, at higher rotational values it surpasses Chevroned Sweeping jet heat performance removal by 13% value even when the span of sweeping is restricted due to secondary vortex conditions. It outperforms steady jet and swirling jet at any given condition. The chevrons due to their augmented chaotic nature provide a negative impact on heat transfer performance for Chevroned Sweeping jet, while performance of steady jet isn't much increased upon addition of chevrons at rotational conditions.

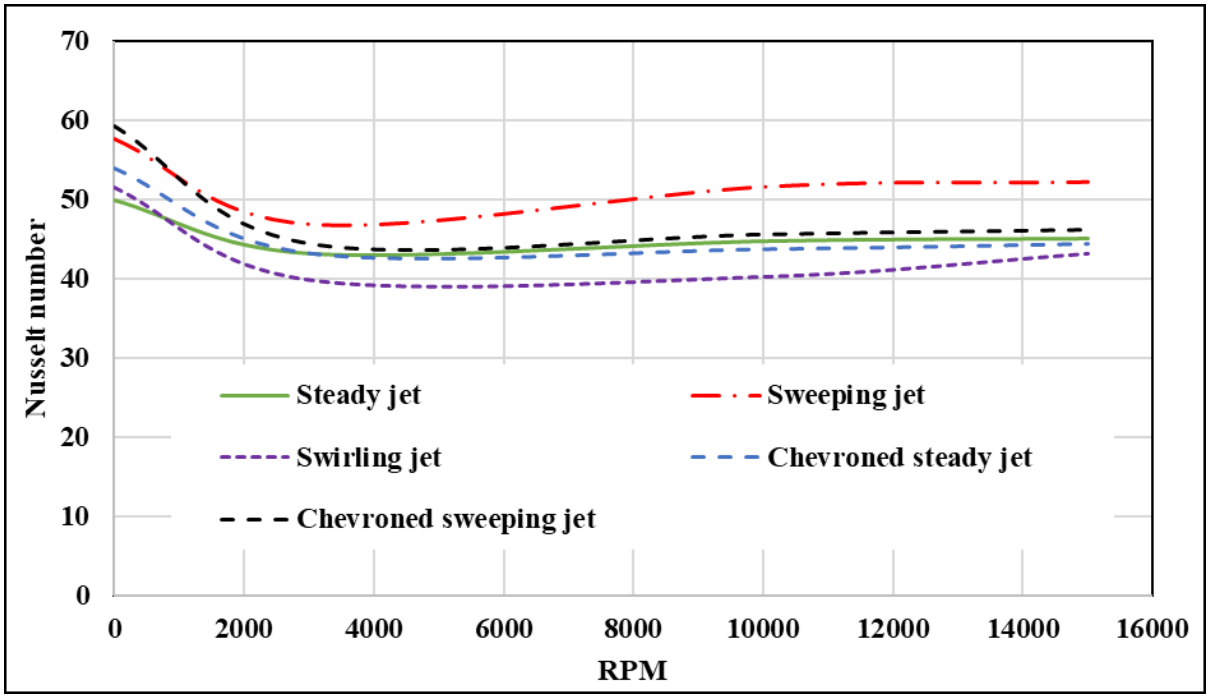

Figure 62: Averaged surface area Nusselt number value for leading-edge blade for (a) Steady jet (b) Sweeping jet (c) Swirling jet (d) Steady jet with chevrons (e) Sweeping jet with chevrons at different RPM

Chapter 4: Conclusion

4.1 Conclusion

In this study, the author used the URANS k–ω SST model to better understand the structure of flow and heat transfer-related performance of a steady jet, a sweeping jet, a swirling jet, a Chevroned Steady jet, and a Chevroned Sweeping jet when they impinged over a semi-circular surface. The novelty of this research lay in the comparing the heat transfer performance run under similar operating conditions tested for stationary and rotatory condition along with use of distinctive design of Chevroned Sweeping jet to cool the leading edge of the blades of a gas turbine. The conclusions are as follows:

1. The addition of chevrons played a significant role in enhancing the turbulence of the cooling fluid. Regular toroidal structures were observed once the fluid had left the nozzle in case of both the sweeping jet and the steady jet. However, this changed significantly when chevrons were added to the sweeping jet in comparison with the steady jet. A mushroom-shaped vortical structure with hairpin vortices was observed in case of the Chevroned Sweeping jet, while an elliptical vortical structure was observed in case of the sweeping jet.
2. In comparison to a steady jet, the swirling jet's spiral channel generates vortices with a higher degree of intensity, which, coupled with axial flow, expel from the nozzle to form a chaotic vortical structure that effectively accelerates heat transfer under stationary conditions.
3. The temporal distributions of the turbulent kinetic energy of the sweeping jet and the Chevroned Sweeping jet in the region along the curvature of the surface were higher, and were not concentrated over the region of stagnation, as was the case when the steady and the Chevroned Steady jets were used. The high intensity of turbulence along the entire region of the curvature of the surface compensated for its lower intensity along the axial direction, with the chevrons increasing the TKE of both the sweeping and the steady jets.
4. The oscillations of the sweeping jet led to the fluid cooling a wider area of the target surface than the steady jet. Past work has shown that the Nusselt number

of the steady jet exhibits a double-peak pattern along the curvature of the leading edge of the blade, while that of the sweeping jet shows a flat pattern. When chevrons were added, these double-peak patterns of the Nusselt number increased in the region ($-0.01 < r/D < 0.01$) for the steady jet, while their addition to the sweeping jet led to more evenly distributed cooling, especially in hotspots, i.e., beyond the region ($-0.02 < r/D < 0.02$).

5. The results show that the addition of chevrons reduced the overall temperature in case of both the sweeping and the steady jets. The Chevroned Sweeping jet yielded a 19.23% increase in the Nusselt number over that of the conventional steady jet. While the addition of chevrons resulted in an increase of 2.73% for sweeping in the time averaged Nusselt number, it (chevrons) increased the Nusselt number of the steady jets by 8.46%, while an increase of 3.51% in Nusselt number was observed as spirals/swirls were added to the steady jet. The Chevroned Sweeping jet outperformed all the other jets by attaining uniform heat transfer throughout the curvature of the surface and yielded the lowest time-averaged temperature of the leading edge of the blade of the turbine at stationary condition.
6. A considerable flow change is seen in all the jets upon implication of rotational conditions because of the interaction between the pressured downstream flow and strong Coriolis force is the jet deflection or bending. For sweeping and Chevroned Sweeping jet along with primary vortex a secondary vortex was developed. Its strength dictated the flow direction of sweeping jet. For steady and Chevroned Steady jet a similar vortex was formed near the inlet of the jet which was primary one. The strength of this primary vortex determined the direction of flow for both jets. It was observed that steady and sweeping jets had opposite flow direction when subjected to rotation.
7. For rotational cases neither chevrons/tabs nor swirls/spirals could aid in augmentation of the heat transfer. As recirculation region was intensified for chevrons that elevated hot-spots due to stagnation regions. Upon implementation of rotation over swirling jets, the swirling strength was reduced i.e., the axial velocity component is weakened and swirls are carried away in direction of

rotation. When compared to a steady jet, these swirls were the primary cause of the improvement in heat transfer performance in stationary conditions.

4.2 Managerial Implications

This investigation involved analysis of capable jets discussed under stationary and rotatory conditions. It is recommended that future research examine parameters that were not covered in the study and may impact the performance of the potential jets. Following is:

- The influence of the higher Reynolds number on the rotational conditions over the performance of the potential jets at both stationary and rotatory conditions.
- The influence of introducing array of these potential jets implicated over the leading-edge blade.
- The influence of distance between these arrays of jets particularly for Chevroned Sweeping jet as it performs excellent along the curved area but
- The influence of distance between jet exit and leading-edge blade on performance of potential jets at both stationary and rotatory conditions.

4.3 Research Implications

The study of the potential impinging jets has significant implications for diverse research fields. Understanding the flow structure behavior of these jets is crucial as it has implications in fields such as aerospace, combustion, noise control etc. Depending on the research area, its operating conditions vary and alter its flow structure. The study will assist the scholars and researchers in the same area in understanding the heat transfer performance of each jet according to their needs. In summary, research on impinging jets has wide-ranging implications in various fields, from fundamental fluid dynamics to practical engineering applications. Understanding the intricacies of impinging jets can lead to innovations that improve efficiency, performance, and sustainability across numerous industries.

References

[1] H. Li and H. Deng, “Heat transfer in a rotating impingement cooling channel with concave target surface,” *International Journal of Heat and Mass Transfer*, vol. 216, pp. 124559, 2023. doi:10.1016/j.ijheatmasstransfer.2023.124559

[2] Thrust from a convergent nozzle - ANSYS innovation courses, https://courses.ansys.com/index.php/courses/cfd-in-aero/lessons/commercial-aircraft-propulsion-thrust-from-a-convergent-nozzle/ (accessed Sep. 1, 2023).

[3] K. Yeranee and Y. Rao, “A review of recent studies on rotating internal cooling for gas turbine blades,” *Chinese Journal of Aeronautics*, vol. 34, no. 7, pp. 85–113, 2021. doi:10.1016/j.cja.2020.12.035

[4] J.-C. Han, “Recent studies in Turbine Blade Cooling,” *International Journal of Rotating Machinery*, vol. 10, no. 6, pp. 443–457, 2004. doi:10.1155/s1023621x04000442

[5] P. Narato, M. Wae-hayee, M. Z. Abdullah, and C. Nuntadusit, “Effect of pin inclination angle on flow and heat transfer characteristics for a row of pins in a flow channel,” *International Communications in Heat and Mass Transfer*, vol. 110, pp. 104396, 2020. doi:10.1016/j.icheatmasstransfer.2019.104396

[6] P. M. Ligrani, M. M. Oliveira, and T. Blaskovich, “Comparison of heat transfer augmentation techniques,” *AIAA Journal*, vol. 41, no. 3, pp. 337–362, 2003. doi:10.2514/2.1964

[7] J.-C. Han and H.-C. Chen, “Turbine blade internal cooling passages with Rib Turbulators,” *Journal of Propulsion and Power*, vol. 22, no. 2, pp. 226–248, 2006. doi:10.2514/1.12793

[8] S. C. Lau, R. T. Kukreja, and R. D. Mcmillin, “Effects of V-shaped rib arrays on turbulent heat transfer and friction of fully developed flow in a square channel,” *International Journal of Heat and Mass Transfer*, vol. 34, no. 7, pp. 1605–1616, 1991. doi:10.1016/0017-9310(91)90140-a

[9] X. Gao and B. Sundén, “Heat transfer and pressure drop measurements in rib-roughened rectangular ducts,” *Experimental Thermal and Fluid Science*, vol. 24, no. 1–2, pp. 25–34, 2001. doi:10.1016/s0894-1777(00)00054-6

[10] P. Ajersch, “Detailed measurements on a row of jets in a crossflow: With applications,” dissertation, University of British Columbia, Vancouver, 1995 .

[11] X. Guo, W. Schröder, and M. Meinke, “Large-eddy simulations of film cooling flows,” *Computers andamp; Fluids*, vol. 35, no. 6, pp. 587–606, 2006. doi:10.1016/j.compfluid.2005.02.007

[12] M. Metka and J. W. Gregory, “Drag reduction on the 25-deg Ahmed model using fluidic oscillators,” *Journal of Fluids Engineering*, vol. 137, no. 5, pp. 051108 (1-8), 2015. doi:10.1115/1.4029535

[13] T. I. Khan, A. R. Tajik, and V. Parezanovic, “Drag reduction of a generic transport vehicle model using a fluidic oscillator,” *International Journal of Thermofluids*, vol. 15, pp. 100180, 2022. doi:10.1016/j.ijft.2022.100180

[14] G. Raman and S. Raghu, “Miniature Fluidic Oscillators for flow and Noise Control - transitioning from macro to Micro Fluidics,” *Fluids 2000 Conference and Exhibit*, pp. 1-6, 2000. doi:10.2514/6.2000-2554

[15] S. Ghanami and M. Farhadi. Fluidic oscillators’ applications, structures and mechanisms–a review. *Challenges in Nano and Micro Scale Science and Technology*, vol. *7*(1), pp. 9-27, 2019. doi: 10.22111/tpnms.2018.25051.1153

[16] J. Gregory and M. N. Tomac, “A review of Fluidic oscillator development and application for Flow Control,” *43rd Fluid Dynamics Conference*, pp. 1-17, 2013. doi:10.2514/6.2013-2474

[17] M. Sieber, F. Ostermann, R. Woszidlo, K. Oberleithner, and C. O. Paschereit, “Lagrangian coherent structures in the flow field of a fluidic oscillator,” *Physical Review Fluids*, vol. 1, no. 5, pp. 050509 (1-2), 2016. doi:10.1103/physrevfluids.1.050509

[18] K. B. Zaman, M. F. Reeder, and M. Samimy, “Control of an axisymmetric jet using vortex generators,” *Physics of Fluids*, vol. 6, no. 2, pp. 778–793, 1994. doi:10.1063/1.868316

[19] B. Heberling, “Numerical investigation of a shielded Chevron nozzle,” *AIAA Scitech 2019 Forum*, pp. 1-19, 2019. doi:10.2514/6.2019-0254

[20] M. F. Reeder and M. Samimy, “The evolution of a jet with vortex-generating tabs: Real-time visualization and quantitative measurements,” *Journal of Fluid Mechanics*, vol. 311, no. 1, pp. 73, 1996. doi:10.1017/s0022112096002510

[21] A. Ianiro, K. P. Lynch, D. Violato, G. Cardone, and F. Scarano, “Three-dimensional organization and dynamics of vortices in multichannel swirling jets,” *Journal of Fluid Mechanics*, vol. 843, pp. 180–210, 2018. doi:10.1017/jfm.2018.140

[22] A. Safi, M. O. Hamdan, and E. Elnajjar, “Numerical investigation on the effect of rotation on impingement cooling of the gas turbine leading edge,” *Alexandria Engineering Journal*, vol. 59, no. 5, pp. 3781–3797, 2020. doi:10.1016/j.aej.2020.06.035

[23] D. E. Metzger, T. Yamashita, and C. W. Jenkins, “Impingement cooling of concave surfaces with lines of circular Air Jets,” *Journal of Engineering for Power*, vol. 91, no. 3, pp. 149–155, 1969. doi:10.1115/1.3574713

[24] R. E. Chupp, H. E. Helms, P. W. Mcfadden and T. R. Brown, “Evaluation of internal heat-transfer coefficients for impingement-cooled turbine airfoils,” *Journal of Aircraft*, vol. 6, no. 3, pp. 203–208, 1969. doi:10.2514/3.44036

[25] W. Tabakoff and W. Clevenger, “Gas turbine blade heat transfer augmentation by impingement of Air Jets having various configurations,” *Journal of Engineering for Power*, vol. 94, no. 1, pp. 51–58, 1972. doi:10.1115/1.3445620

[26] G. Yang, M. Choi, and J. S. Lee, “An experimental study of slot jet impingement cooling on concave surface: Effects of nozzle configuration and curvature,” *International Journal of Heat and Mass Transfer*, vol. 42, no. 12, pp. 2199–2209, 1999. doi:10.1016/s0017-9310(98)00337-8

[27] B. Han and R. J. Goldstein, “Jet-impingement heat transfer in gas turbine systems,” *Annals of the New York Academy of Sciences*, vol. 934, no. 1, pp. 147–161, 2006. doi:10.1111/j.1749-6632.2001.tb05849.x

[28] M. E. Taslim, L. Setayeshgar, and S. D. Spring, “An experimental evaluation of advanced leading edge impingement cooling concepts,” *Journal of Turbomachinery*, vol. 123, no. 1, pp. 147–153, 2000. doi:10.1115/1.1331537

[29] E. Elnajjar, M. Hamdan, Y. Haik, “Experimental investigation of internal channel cooling via jet impingement,” *FDMP: Fluid Dynamics and Materials Processing*, vol. *9*(1), pp. 77-89, 2013. doi:10.3970/fdmp.2013.009.077

[30] E. Elnajjar, M. Hamdan, Y. Haik, “Experimental investigation of impinging jet flow on a heated curved surface,” In *6th International Conference on Thermal Engineering*, pp. 1-4, 2012.

[31] N. Kayansayan and S. Küçüka, “Impingement cooling of a semi-cylindrical concave channel by confined slot-air-jet,” *Experimental Thermal and Fluid Science*, vol. 25, no. 6, pp. 383–396, 2001. doi:10.1016/s0894-1777(01)00094-2

[32] M. E. Taslim, K. Bakhtari, and H. Liu, “Experimental and numerical investigation of impingement on a rib-roughened leading-edge wall,” *Volume 5: Turbo Expo 2003, Parts A and B*, pp. 31-41, 2003. doi:10.1115/gt2003-38118

[33] R. Jia, M. Rokni, and B. Sundén, “Impingement cooling in a rib-roughened channel with cross-flow,” *International Journal of Numerical Methods for Heat andamp; Fluid Flow*, vol. 11, no. 7, pp. 642–662, 2001. doi:10.1108/09615530110403598

[34] B. V. Kumar and B. V. Prasad, “Computational flow and heat transfer of a row of circular jets impinging on a concave surface,” *Heat and Mass Transfer*, vol. 44, no. 6, pp. 667–678, 2007. doi:10.1007/s00231-007-0274-3

[35] Z. Liu, Z. Feng, and L. Song, “Numerical study of flow and heat transfer of impingement cooling on model of Turbine Blade Leading edge,” *Volume 4: Heat Transfer, Parts A and B*, pp. 657-674 2010. doi:10.1115/gt2010-23711

[36] M. O. Hamdan, E. Elnajjar, and Y. Haik, “Measurement and modeling of confined jet discharged tangentially on a concave semicylindrical hot surface,” *Journal of Heat Transfer*, vol. 133, no. 12, pp. 122203 (1-7), 2011. doi:10.1115/1.4004529

[37] M. A. R. Sharif, “Heat transfer from an isothermally heated flat surface due to twin oblique slot-jet impingement,” *Procedia Engineering*, vol. 56, pp. 544–550, 2013. doi:10.1016/j.proeng.2013.03.158

[38] L. Yang, J. Ren, H. Jiang, and P. Ligrani, “Experimental and numerical investigation of unsteady impingement cooling within a blade leading edge passage,” *International Journal of Heat and Mass Transfer*, vol. 71, pp. 57–68, 2014. doi:10.1016/j.ijheatmasstransfer.2013.12.006

[39] N. Wang, A. F. Chen, M. Zhang, and J.-C. Han, “Turbine blade leading edge cooling with one row of normal or tangential impinging jets,” *Journal of Heat Transfer*, vol. 140, no. 6, 2018. doi:10.1115/1.4038691

[40] S. Ghadi, K. Esmailpour, S. M. Hosseinalipour, and A. Mujumdar, “Experimental study of formation and development of coherent vortical structures in pulsed turbulent impinging jet,” *Experimental Thermal and Fluid Science*, vol. 74, pp. 382–389, 2016. doi:10.1016/j.expthermflusci.2015.12.007

[41] H. M. Maghrabie, “Heat transfer intensification of jet impingement using exciting jets - A comprehensive review,” *Renewable and Sustainable Energy Reviews*, vol. 139, pp. 110684 (1-30), 2021. doi:10.1016/j.rser.2020.110684

[42] S. V. Kalinina, V. I. Terekhov, and K. A. Sharov, “Special features of flow in an annular jet impinging on a barrier,” *Fluid Dynamics*, vol. 50, no. 5, pp. 665–671, 2015. doi:10.1134/s0015462815050087

[43] L. Xu, J. Lan, Y. Ma, J. Gao, and Y. Li, “Numerical study on heat transfer by swirling impinging jets issuing from a screw-thread nozzle,” *International Journal of Heat and Mass Transfer*, vol. 115, pp. 232–237, 2017. doi:10.1016/j.ijheatmasstransfer.2017.07.053

[44] M. S. Khan, M. O. Hamdan, S. A. B. Al-Omari, and E. Elnajjar, “A comparison of oscillating sweeping jet and steady normal jet in cooling gas turbine leading edge: Numerical Analysis,” *International Journal of Heat and Mass Transfer*, vol. 208, pp. 124041, 2023. doi:10.1016/j.ijheatmasstransfer.2023.124041

[45] T. Shakouchi and M. Kito, “Heat transfer enhancement of impinging jet by notched – orifice nozzle,” *An Overview of Heat Transfer Phenomena*, 2012. doi:10.5772/52029

[46] L. A. Brignoni and S. V. Garimella, “Effects of nozzle-inlet chamfering on pressure drop and heat transfer in Confined Air Jet Impingement,” *International Journal of Heat and Mass Transfer*, vol. 43, no. 7, pp. 1133–1139, 2000. doi:10.1016/s0017-9310(99)00207-0

[47] J. Stevens, Y. Pan, and B. W. Webb, “Effect of nozzle configuration on transport in the stagnation zone of axisymmetric, impinging free-surface liquid jets: Part 1—turbulent flow structure,” *Journal of Heat Transfer*, vol. 114, no. 4, pp. 874–879, 1992. doi:10.1115/1.2911895

[48] E. C. Mladin and D. A. Zumbrunnen, “Dependence of heat transfer to a pulsating stagnation flow on pulse characteristics,” *Journal of Thermophysics and Heat Transfer*, vol. 9, no. 1, pp. 181–192, 1995. doi:10.2514/3.645

[49] N. Uddin, B. Weigand, and B. A. Younis, “Comparative study on heat transfer enhancement by turbulent impinging jet under conditions of swirl, active excitations and passive excitations,” *International Communications in Heat and Mass Transfer*, vol. 100, pp. 35–41, 2019. doi:10.1016/j.icheatmasstransfer.2018.12.002

[50] J. Kim, “Active control of impinging jet for modification of mixing,” *Journal of Mechanical Science and Technology*, vol. 28, no. 3, pp. 927–935, 2014. doi:10.1007/s12206-013-1160-1

[51] S. Rakhsha, M. Rajabi Zargarabadi, and S. Saedodin, “Experimental and numerical study of flow and heat transfer from a pulsed jet impinging on a pinned surface,” *Experimental Heat Transfer*, vol. 34, no. 4, pp. 376–391, 2020. doi:10.1080/08916152.2020.1755388

[52] A.V. Bilsky, Y.A. Lozhkin, D.M. Markovich and A.S. Nebuchinov, “The effect of an external excitation on a heat transfer in an impinging jet,”. *HEFAT*, pp. 1059-1063, 2010.

[53] K. Kataoka, M. Suguro, H. Degawa, K. Maruo, and I. Mihata, “The effect of surface renewal due to largescale eddies on jet impingement heat transfer,” *International Journal of Heat and Mass Transfer*, vol. 30, no. 3, pp. 559–567, 1987. doi:10.1016/0017-9310(87)90270-5

[54] P. J. Strange and D. G. Crighton, “Spinning modes on axisymmetric jets. Part 1,” *Journal of Fluid Mechanics*, vol. 134, no. 1, pp. 231-245, 1983. doi:10.1017/s002211208300333x

[55] R. Vinze, S. Chandel, M. D. Limaye, and S. V. Prabhu, “Local heat transfer distribution between smooth flat surface and impinging incompressible air jet from a Chevron nozzle,” *Experimental Thermal and Fluid Science*, vol. 78, pp. 124–136, 2016. doi:10.1016/j.expthermflusci.2016.05.017

[56] D. Violato, A. Ianiro, G. Cardone, and F. Scarano, “Three-dimensional vortex dynamics and convective heat transfer in circular and chevron impinging jets,” *International Journal of Heat and Fluid Flow*, vol. 37, pp. 22–36, 2012. doi:10.1016/j.ijheatfluidflow.2012.06.003

[57] L. Hussain *et al.*, “Heat transfer augmentation through different jet impingement techniques: A state-of-the-art review,” *Energies*, vol. 14, no. 20, p. 6458, 2021. doi:10.3390/en14206458

[58] M. F. Reeder and M. Samimy, “The evolution of a jet with vortex-generating tabs: Real-time visualization and quantitative measurements,” *Journal of Fluid Mechanics*, vol. 311, no. 1, pp. 73-118, 1996. doi:10.1017/s0022112096002510

[59] N. Gao, H. Sun, and D. Ewing, “Heat transfer to impinging round jets with triangular tabs,” *International Journal of Heat and Mass Transfer*, vol. 46, no. 14, pp. 2557–2569, 2003. doi:10.1016/s0017-9310(03)00034-6

[60] Y. Yu, J. Zhang, and H. Xu, “Convective heat transfer by a row of confined air jets from round holes equipped with triangular tabs,” *International Journal of Heat and Mass Transfer*, vol. 72, pp. 222–233, 2014. doi:10.1016/j.ijheatmasstransfer.2014.01.004

[61] Y. Yu, J. Zhang, and Y. Shan, “Convective heat transfer of a row of air jets impingement excited by triangular tabs in a confined Crossflow Channel,” *International Journal of Heat and Mass Transfer*, vol. 80, pp. 126–138, 2015. doi:10.1016/j.ijheatmasstransfer.2014.08.066

[62] T. Guan, J. Zhang, Y. Shan, and J. Hang, “Conjugate heat transfer on leading edge of a conical wall subjected to external cold flow and internal hot jet impingement from Chevron nozzle – Part 1: Experimental analysis,” *International Journal of Heat and Mass Transfer*, vol. 106, pp. 329–338, 2017. doi:10.1016/j.ijheatmasstransfer.2016.06.101

[63] T. Guan, J. Zhang, and Y. Shan, “Conjugate heat transfer on leading edge of a conical wall subjected to external cold flow and internal hot jet impingement from Chevron nozzle – part 2: Numerical analysis,” *International Journal of Heat and Mass Transfer*, vol. 106, pp. 339–355, 2017. doi:10.1016/j.ijheatmasstransfer.2016.10.048

[64] Y. Lyu, J. Zhang, X. Liu, and Y. Shan, “Experimental study of single-row Chevron-jet impingement heat transfer on concave surfaces with different curvatures,” *Chinese Journal of Aeronautics*, vol. 32, no. 10, pp. 2275–2285, 2019. doi:10.1016/j.cja.2019.07.002

[65] Y. Lyu, J. Zhang, Y. Shan, and X. Tan, “The experimental investigation of impinging heat transfer of pulsation jet on the flat plate,” *Journal of Heat Transfer*, vol. 140, no. 12, pp. 122202 (1-18), 2018. doi:10.1115/1.4041183

[66] Y. W. Lyu, Y. D. Zhao, J. Y. Zhang, J. Z. Zhang, Y. Shan, X. Y. Luo, “Large eddy simulation of impinging heat transfer of pulsed chevron jet on a semi-cylindrical concave plate,”. *Physics of Fluids*, vol. 35 (2): pp. 025115 (1-19), 2023. doi:10.1063/5.0130230

[67] J. A. Parsons, J.-C. Han, and C. P. Lee, “Rotation effect on jet impingement heat transfer in smooth rectangular channels with four heated walls and film coolant extraction,” *Volume 5: Turbo Expo 2003, Parts A and B*, pp. 671-680, 2003. doi:10.1115/gt2003-38905

[68] S.-S. Hsieh, H.-H. Tsai, and S.-C. Chan, “Local heat transfer in rotating square-rib-roughened and smooth channels with Jet Impingement,” *International Journal of Heat and Mass Transfer*, vol. 47, no. 12–13, pp. 2769–2784, 2004. doi:10.1016/j.ijheatmasstransfer.2003.10.040

[69] S. K. Hong, D. H. Lee, and H. H. Cho, “Heat/mass transfer measurement on concave surface in rotating jet impingement,” *Journal of Mechanical Science and Technology*, vol. 22, no. 10, pp. 1952–1958, 2008. doi:10.1007/s12206-008-0738-5

[70] C. A. Elston and L. M. Wright, “Leading edge jet impingement under high rotation numbers,” *Journal of Thermal Science and Engineering Applications*, vol. 9, no. 2, pp. 021010 (1-18), 2017. doi:10.1115/1.4035892

[71] L. Yang, K. Tyagi, S. Ekkad, and J. Ren, “Influence of rotation on heat transfer in a two-pass channel with impingement under High Reynolds number,” *Volume 5A: Heat Transfer*, pp. 1-11, 2015. doi:10.1115/gt2015-42871

[72] J. A. Lamont, S. V. Ekkad, and M. A. Alvin, “Effects of rotation on heat transfer for a single row jet impingement array with crossflow,” *Journal of Heat Transfer*, vol. 134, no. 8, pp. 082202 (1-12), 2012. doi:10.1115/1.4006167

[73] P. Singh and S. V. Ekkad, “Detailed heat transfer measurements of jet impingement on dimpled target surface under rotation,” *Journal of Thermal Science and Engineering Applications*, vol. 10, no. 3, pp.1-31, 2018. doi:10.1115/1.4039054

[74] T. J. Craft, H. Iacovides, and N. A. Mostafa, “Numerical modelling of flow and heat transfer from an array of jets impinging onto a concave surface under stationary and rotating conditions,” *Volume 6: Turbomachinery, Parts A, B, and C*, pp. 2435-2444, 2008. doi:10.1115/gt2008-50624

[75] H. Iacovides, D. Kounadis, B. E. Launder, J. Li, and Z. Xu, “Experimental study of the flow and thermal development of a row of cooling jets impinging on a rotating concave surface,” *Journal of Turbomachinery*, vol. 127, no. 1, pp. 222–229, 2005. doi:10.1115/1.1812778

[76] E. Y. Jung *et al.*, “Effect of rotation on heat transfer of a concave surface with array impingement jet,” *Volume 3A: Heat Transfer*, pp. 1-9, 2013. doi:10.1115/gt2013-95443

[77] E. Burberi *et al.*, “Effect of rotation on a gas turbine blade internal cooling system: Numerical Investigation,” *Journal of Turbomachinery*, vol. 139, no. 3, 031005 (1-10), 2016. doi:10.1115/1.4034799

[78] D. Massini *et al.*, “Effect of rotation on a gas turbine blade internal cooling system: Experimental investigation,” *Journal of Engineering for Gas Turbines and Power*, vol. 139, no. 10, pp. 101902 (1-10), 2017. doi:10.1115/1.4036576

[79] M. A. Hossain, A. Ameri, J. W. Gregory, and J. P. Bons, “Effects of rotation on a fluidic actuator,” *AIAA Scitech 2019 Forum*, pp. 0885 (1-19), 2019. doi:10.2514/6.2019-0885

[80] Y. Amini, M. Mokhtari, M. Haghshenasfard, and M. Barzegar Gerdroodbary, “Heat transfer of swirling impinging jets ejected from nozzles with twisted tapes utilizing CFD technique,” *Case Studies in Thermal Engineering*, vol. 6, pp. 104–115, 2015. doi:10.1016/j.csite.2015.08.001

[81] L. Xu *et al.*, “Flow and heat transfer characteristics of a swirling impinging jet issuing from a threaded nozzle,” *Case Studies in Thermal Engineering*, vol. 25, pp. 100970 (1-12), 2021. doi:10.1016/j.csite.2021.100970

[82] J. Nichols *et al.*, “Large-eddy simulation for supersonic rectangular jet noise prediction: Effects of chevrons,” *18th AIAA/CEAS Aeroacoustics Conference (33rd AIAA Aeroacoustics Conference)*, pp. 2212 (1-11), 2012. doi:10.2514/6.2012-2212

[83] K. Zhao, Y. Liang, T. Yue, Y. Wang, and G. J. Bennett, “Rectangular cavity flow noise suppression using chevron treatment to the front edge at subsonic speeds,” *25th AIAA/CEAS Aeroacoustics Conference*, pp. 2693 (1-10), 2019. doi:10.2514/6.2019-2693

[84] A. Arshad, N. Andrew, and I. Blumbergs, “Computational study of noise reduction in CFM56-5B using core nozzle chevrons,” *2020 11th International Conference on Mechanical and Aerospace Engineering (ICMAE)*, pp. 162-167, 2020. doi:10.1109/icmae50897.2020.9178891

[85] K. Zore, S. Shah, J. Stokes, B. Sasanapuri, and P. Sharkey, “Ansys CFD study for High Lift Aircraft Configurations,” *2018 Applied Aerodynamics Conference*, pp. 1-11, 2018. doi:10.2514/6.2018-2844

[86] Y. Wu, S. Yu, and L. Zuo, “Large eddy simulation analysis of the heat transfer enhancement using self-oscillating fluidic oscillators,” *International Journal of Heat and Mass Transfer*, vol. 131, pp. 463–471, 2019. doi:10.1016/j.ijheatmasstransfer.2018.11.070

[87] F. R. Menter, “Review of the shear-stress transport turbulence model experience from an industrial perspective,” *International Journal of Computational Fluid Dynamics*, vol. 23, no. 4, pp. 305–316, 2009. doi:10.1080/10618560902773387

[88] H. Yadav, A. Agrawal, and A. Srivastava, “Mixing and entrainment characteristics of a pulse jet,” *International Journal of Heat and Fluid Flow*, vol. 61, pp. 749–761, 2016. doi:10.1016/j.ijheatfluidflow.2016.08.006

[89] T. Tu, S. Chen, Y. Shi, and W. Li, “Flow mechanism and heat transfer characteristic of sweeping jet impinging on confined concave surfaces,” *Physics of Fluids*, vol. 35, no. 1, pp. 0151471 (1-15), 2023. doi:10.1063/5.0136661

[90] H. Deng, Z. Wang, J. Wang, and H. Li, “Flow and heat transfer in a rotating channel with impingement cooling and film extraction,” *International Journal of Heat and Mass Transfer*, vol. 180, pp. 121751 (1-16), 2021. doi:10.1016/j.ijheatmasstransfer.2021.121751

[91] L. Xu *et al.*, “Flow and heat transfer characteristics of a swirling impinging jet issuing from a threaded nozzle of 45 degrees,” *Energies*, vol. 14, no. 24, pp. 8412 (1-26), 2021. doi:10.3390/en14248412

List of Publications

M.S. Khan, M.O. Hamdan, S.A. Al-Omari and E. Elnajjar. “A comparison of oscillating sweeping jet and steady normal jet in cooling gas turbine leading edge: Numerical analysis,” *International Journal of Heat and Mass Transfer*, vol. 208, pp. 124041, 2023. (Published in International Journal of Heat and Mass Transfer). Impact Factor 5.43. doi:10.1016/j.ijheatmasstransfer.2023.124041

UAE UNIVERSITY MASTER THESIS NO. 2023: 65

A numerical investigation of the potential impinging jets over the leading-edge blade of gas turbine upon subjected to stationary and rotatory conditions is evaluated.

Mohammed Sami Uddin Khan received his Master of Science in Mechanical Engineering from the Department of Mechanical and Aerospace Engineering, College of Engineering at UAE University, UAE. He received his Bachelor of Science in Mechanical Engineering from the College of Engineering, Osmania University, India.